The University of Manitoba

CHARACTERISTICS OF LOOP YAGI ARRAYS WITH LOADED ELEMENTS AND THEIR APPLICATION TO SHORT BACKFIRE ANTENNAS

By

ALIREZA SHOAMANESH

A Thesis
Submitted to the Faculty Of Graduate Studies
In Partial Fulfillment Of the Requirements For The
Degree Of Doctor Of Philosophy

DEPARTMENT OF ELECTRICAL ENGINEERING

Winnipeg, Manitoba
Canada

JUNE 1979

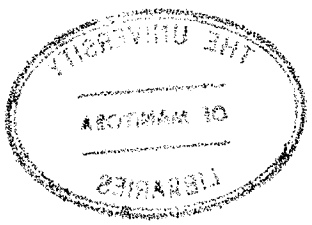

CHARACTERISTICS OF LOOP YAGI ARRAYS WITH LOADED ELEMENTS AND THEIR APPLICATION TO SHORT BACKFIRE ANTENNAS

BY

ALIREZA SHOAMANESH

A dissertation submitted to the Faculty of Graduate Studies of the University of Manitoba in partial fulfillment of the requirements of the degree of

DOCTOR OF PHILOSOPHY

ABSTRACT

An analysis of wave propagation along an infinitely long array of single or two concentric loaded circular loops is presented. The travelling wave idea is applied to derive a relationship for the propagation constant along the structure. The analysis is based on a "circuit theory" method and gives the dispersion relation in terms of the mutual impedances between a reference and the other elements, in the array. In addition, Flouquet's theorem is used to account for the periodicity of the structure. It is found that capacitive loading increases the operating frequency range, for a given phase velocity of the travelling wave along the structure, and consequently, increases the bandwidth of the array. Capacitive loading of the inner array in a two concentric loop array, which operates in two passbands separated by a stop-band, increases both the separation of the pass-bands and the bandwidth of the second pass-band.

A study of the excitation problem in finite Yagi arrays shows that for arrays made of two concentric loops the choice of the outer loop as the feeder gives the most superior gain and input admittance characteristics.

As an example of multiple-loadings, the case of a doubly loaded array is considered. It is found that for a relatively smooth variation of the input admittance in a Yagi array, the exciter may be loaded resistively. Extensive investigation has also shown that to improve the gain bandwidth

performance of a Yagi array, its directors and reflector must be loaded by capacitive and inductive loads, respectively. Similar result is also obtained for distributed impedance loadings.

Coaxial planar loops and their application to backfire antenna are also studied. First, a general method is described which enables one to study compact arrays and coaxial planar loop antennas with considerable ease. The technique is then used to investigate the radiation characteristics of coaxial planar loop arrays and backfire antennas constructed entirely with loops. The comparison between this type of backfire antenna and the conventional one with a solid reflector reveals that the optimum sizes of the reflector and the peripheral rim are approximately the same for both kinds of the reflectors. However, the optimum gain of the loop-reflector is found to be about 1dB less than that of the solid reflector aerial. In addition, it is found that as few as 6 loops are sufficient to construct the optimum size of the reflectors and almost the same number of loops are required to form the optimum peripheral rim. The new structure reduces the weight, windage and obstruction of view which accompany solid reflectors. In addition, the new antenna lends itself to exact analytical investigation.

ACKNOWLEDGEMENTS

The author wishes to express his sincere appreciation to Dr. L. Shafai of the Electrical Engineering Department, University of Manitoba, for his guidance, continuous interest and encouragement and constructive criticism throughout all phases of this work.

My special thanks go to my wife, Ziba Kamal, for her help, encouragement and understanding through the years which made this work possible. Her reading of the final manuscript is also acknowledged.

Special acknowledgement is given to my good friend H. Kunkel for his valuable assistance in reading the draft which led to a number of clarifications and other improvements. I would also like to acknowledge my appreciation to a very capable typist, Ms. M. Tyler, for her cheerful and patient efforts in typing the entire manuscript.

The author also expresses his gratitude and appreciation to all those individuals who assisted him in various phases of this work. In particular, extended thanks are due to the following members of the Department of Electrical Engineering, University of Manitoba; Professor E. Bridges, Dr. W. Goddard, my colleagues K. Iskander and A. Ittipiboon for long hours of discussions and helpful suggestions. Secretarial assistance by Mrs. L. Ramsay is also appreciated.

The financial support provided by the National Research Council of Canada (Grant A-7702) and the Department of

Electrical Engineering of the University of Manitoba is gratefully acknowledged.

Last but not least, the author wishes to thank the people of Iran and the Province of Manitoba for providing him an opportunity to study at the University of Tehran and the University of Manitoba. Toward them, I shall remain reverent for years to come.

TABLE OF CONTENTS

LIST OF FIGURES

LIST OF SYMBOLS

Unless otherwise stated, the symbols most commonly used in this thesis have the following meaning:

LATIN ALPHABET:

a	radius of wire cross section
a_i	radius of wire cross section of the ith-element
A	a coefficient
b	radius of loop antenna
b_i	radius of the ith-element in a circular loop array
B	a coefficient
c	velocity of electromagnetic waves in free space
C	a coefficeint
C	lumped capacitance
C_{gi}	gap capacitance of the ith element
C'_{gi}	gap capacitance at $\phi = 0$ of the ith element
C''_{gi}	gap capacitance at $\phi = \pi$ of the ith element
d	spacing between two adjacent elements
d_F	spacing between exciter and disk (or loop) reflector
d_{ij}	distance between the ith and jth-element in an array
d_s	spacing of loop antenna from the ground plane

LATIN ALPHABET:

d_s	skin depth
dB	decibel
D	disk (or loop) reflector diameter
e	base of natural logarithms
E_θ, E_ϕ	θ and ϕ components of electric field
E_ϕ^a	ϕ component of applied electric field
E_ϕ^i	ϕ component of induced electric field
f	frequency
$F(\pi/2, \cdot)$	complete Elliptic integral of the first kind
G_d	directive gain in positive Z-direction
G_r	directive gain in negative Z-direction
$h_m^2(\cdot)$	second kind spherical Hankel function of order m
I	integral associated with complete Elliptic integral of the first kind
$I_i(\phi)$	total current of ith-element
I_i^n	coefficient of the nth element mode of ith-element
Im(·)	imaginary part of a complex number
$J_m(\cdot)$	first kind Bessel function of order m
k	free space wave number
kb_i	size of the ith-loop in an array
kb_M	size of the largest loop in a loop reflector

LATIN ALPHABET:

K_{ij}^{n}, $K_{ij}^{'n}$, $\hat{K}_{ij}^{n}$	nth coefficient in Fourier series expansion of the kernel
ℓ	length of Yagi array
L	lumped inductance
ln(•)	natural logarithm
m_o	an integer number after which the impedance matrix can be considered a diagonal matrix
m!	factorial m
n	mode number
n_i	ratio of loop and wire radii, i.e., b_i/a_i
N	number of elements in an array of circular loops
P_D	dissipated power
P_r	radiated power
r, θ, φ	spherical coordinates
R	resistance
$R_{ij}(\cdot)$	distance between two current components normalized by radius b_i
Re(•)	real part of a complex number
$U_i(\cdot)$, $U_i^0(\cdot)$, $U_i^\pi(\cdot)$	a function equal to unity at the driving-point and zero elsewhere
v	phase velocity of electromagnetic waves
V_i, V_i^0, V_i^π	driving voltage of the ith-element
$W_{ij}(\cdot)$	kernel

Y_{ij}^{n}	element of admittance matrix
Y_i	input admittance of ith-element
Z_i	internal impedance per unit length
Z_L, Z_{Li}, Z_{Li}^{0}, Z_{Li}^{π}	lumped impedance
Z_{ij}^{n}, $Z_{ij}^{'n}$, $\hat{Z}_{ij}^{n}$	element of impedance matrix

GREEK ALPHABET:

α_i	function
α_i	constant in tapered capacitive loading
β	phase constant of travelling wave
β	constant and $\ln(2\beta) = \gamma$
γ	Euler's constant
δ_{ij}	Kronecker delta function
$\delta\phi_i$	gap width of the driving-point of the ith-element
ϵ_0	permittivity of free space
ζ_i, ζ_i'	functions
η_0	characteristic impedance of free space
θ	spherical coordinate
$\bar{\theta}$	coefficient
μ_0	permeability of free space
σ	conductivity
ϕ	spherical coordinate
ϕ_{ij}	element of matrix
ψ	angle in surface current distribution
Ω	thickness parameter
ω	angular velocity

CHAPTER I

INTRODUCTION

The electromagnetic theory of circular loop antennas has received considerable attention in the past due to its advantages over dipole antennas, and its relatively simple geometry. The radiation pattern of a small loop antenna is similar to that of a dipole antenna and shows a figure eight shape in the vertical plane involving the loop axis. However, it tends to become directive in the axial direction as the loop circumference approaches one wavelength [1 - 2]. This fact suggests that a highly directive beam may be obtained if an array of coaxial loops of a proper dimension is utilized. A well suited application of the loop array is to employ loops as elements in a Yagi-Uda array, in which only the second element is excited. However, in contrast to the extensive studies available on dipole Yagi-Uda arrays, the literature on Yagi arrays of loop antenna is scarce. The goal of this thesis is to undertake a detailed investigation of these antennas.

1.1 Literature Review

The first general analysis of a circular loop as a transmitting antenna was carried out by Hallen [3]. He considered the loop antenna excited by a lumped generator, an idealized delta function generator, and obtained a formal solution for the current and the input admittance in the form of Fourier series. However, due to the occurrence of a

singularity in the high order Fourier coefficients, he was unable to obtain numerical results except for loops small compared to the wavelength. Storer [4] reconsidered the problem but avoided the contribution from the higher order terms by approximating the series by an integral and evaluating it using the Caushy's principle value. He provided extensive tables and graphs of the input admittance and current distributions for loops up to a wavelength in circumference and a number of different wire cross sections. Storer also examined the validity of the constant current distribution on a small loop and was led to the conclusion that loops with circumference larger than 0.2 wavelength can not be considered small.

T.T. Wu re-examined the problem of evaluating the Fourier series. He pointed out that, assuming that the current flows along the center of the conductor, the expansion of Hallen and Storer does not converge everywhere on the antenna [5]. He examined the surface current distribution on a perfectly conducting loop and verified that the resulting Fourier series for $I(\phi)$ converges everywhere except at the driving point.

Later King et al. [6] computed the input admittance of a circular loop by taking a partial summation of the infinite series obtained by Wu. They suggested that a Fourier series solution with twenty terms is satisfactory for determining the admittance of thin $(\Omega = 2 \ln 2\pi \frac{b}{a} \geq 10)$ and $kb \leq 2.5$ loops in air and dissipative media. Here k, a,

and b are the free space propagation constant and the wire and loop radii, respectively.

Inagaki et al. by assuming a finite gap at the driving point gave a theoretical basis for determining the required number of terms in the current and admittance computations [7]. They obtained an expression for the driving-point admittance in which the gap capacitance is a lumped representation of the effect of the gap width.

Iizuka et al. have analyzed an array of two identical parallel loop antennas. They have decomposed the voltage and current into symmetric and antisymmetric components. As a result, the simultaneous integral equations for the distribution of the current along the loops have been converted into a single integral equation similar to that of an isolated circular loop antenna which has already been studied [8]. This method, however, is not applicable to antennas with loops of different circumferences. The experimental work of Lindsay [9] is the first published study of relatively large circular loop Yagi arrays. Lindsay reported a gain difference of about 1.8dB in favour of loop arrays in comparison with dipole arrays of the same length. Later, Appel-Hansen reported similar experimental comparison [74] and [10]. He utilized a feeding system which consisted of a circular loop antenna as the exciter and a parasitic loop as reflector. For the director he selected three different configurations, an array of parasitic circular loops made of flat plate loops, a parasitic array of wire loops and a parasitic array of

straight rods. Comparing the experimental gain of these directors, he found that for array lengths less than 2λ all three had similar gain performances, but for large arrays the gain of rod directors was somewhat higher. A similar problem was also examined by Takata and Sekiguchi [11]. Their numerical and experimental results show that for arrays lengths less than 2λ there is a gain difference of about 1 dB in favour of loop arrays over the arrays made of rod elements.

The first theoretical investigation of an array of coaxial circular loop antennas with arbitrary circumferences, has been carried out by Ito et al. [12] using Fourier series expansion, with emphasis on the existence of finite gaps at the driving points. The expression for the current distribution on each loop and the input admittance involve matrices, where the dimension of each matrix is related to the array size. Thus, in the investigation of loop arrays the required computer time and storage capacity increase with the array size and for very large arrays become excessive. To overcome these difficulties, the resonant property of loops was later applied by the author to develop an efficient method for the investigation of Yagi loop arrays [13] . For this method, the exact radiation fields and the current distributions of a finite and relatively large uniform array of circular loops were compared with that obtained using the dominant mode only. The discrepancies between the results of both radiation fields and current distributions were found to be negligible. Later, an approximate method was also utilized

which facilitated the rapid and accurate analysis of large loop arrays [14]. In this method, a large loop array consisting of an arbitrary number of elements, was sub-divided into several small sub-arrays such that the first sub-array contained the active element. Neglecting all sub-arrays except the first two, the resulting two sub-arrays were solved simultaneously to yield loop currents. The results for the first sub-array were retained and were used in simultaneous solution of the second and third sub-arrays. The process was continued until all loop currents were obtained. The travelling wave approach has also been used to study coaxial loop arrays. Shen and Raffoul have applied this method to finite uniform Yagi arrays of equal loops to provide design parameters for a given bandwidth, directivity or array length [15]. Finally, the electrical properties of coaxial Yagi loop arrays were investigated by the author by applying the exact solution and the significance of each array parameter and their effects on antenna characteristics was determined [16]. Based on these works extensive design data for short and medium size arrays were obtained in [17].

In this thesis we extend the investigation of circular loop arrays to arrays with loaded elements. Wave propagation on an infinite structure is investigated and characteristics of finite arrays are studied. The work presented here is based on the Fourier series expansion method. Thus, a brief review of this theory for an array of coaxial circular loops with arbitrary circumferences is given in the next

sections.

Chapter II deals with the phase velocity of wave propagation on a loaded infinite array of circular coaxial loops. A dispersion relation is derived by using the so-called "circuit theory" method and Flouquet's theorem.

It is shown that reactive loading has significant effects on the phase velocity of the propagating wave and the cut-off frequency can be controlled by proper loading. For a finite array, the effect of reactive loading is also studied and by a capacitive loading broad-band antenna characteristics are obtained as well.

Multi-source and loaded arrays are investigated in Chapter III. Initially, the array is excited by arbitrary sources at two symmetrical points with respect to the array axis. The principle of superposition is applied and expressions for the current distribution and the input admittance are obtained. Later, all sources except for those on the qth element which excite the array, are replaced by lumped loads of finite lengths. The properties of these arrays are investigated and broadband characteristics for directive gain and input admittance are reported.

Chapter IV deals with the coaxial loop arrays with distributed impedance loading. It is shown that, in general, a broadband characteristic can be obtained by a distributed impedance loading. The constant resistive loading is studied in more detail since this type of impedance distribution can be fabricated readily and all practical antennas made of

conductive metals fall into this category.

There has been increasing attention on high gain antennas which are generally achievable by compact arrays. In Chapter V, a method is described which enables one to study compact arrays with considerable ease. Then, the method is applied to investigate co-planar arrays and backfire antennas.

The technique given in Chapter V is combined with the analysis of Chapter II in order to investigate the phase velocity of an infinite array of two concentric loops. This kind of structure possesses two distinct pass-bands separated by a stop-band which can be controlled by array geometry and suitable reactive loadings. This is done in chapter VI.

Chapter VII summarizes the results and provides a list of suggested topics for future research.

1.2 Fourier Series Solution of Circular Loop Arrays

Since the Fourier expansion method is used as the basic tool in this work, it is reviewed briefly in this section. Figure (1-1) shows an array of coaxial circular loops composed of N elements with arbitrary circumferences. The center of loops are located on the z-axis and there is a finite gap at their driving-points. The radius of the ith loop, the radius of the conductive wire, and the driving-point voltage are denoted by b_i, a_i and V_i, respectively. It is assumed that $b_i >> a_i$ and $a_i << \lambda$ where λ is the wavelength of the signal in free space. Its finite driving-point gap is denoted by $b_i \delta\phi_i$. The loop current $I_i(\phi_i)$ is assumed to flow uniformly in the ψ direction along the conductor

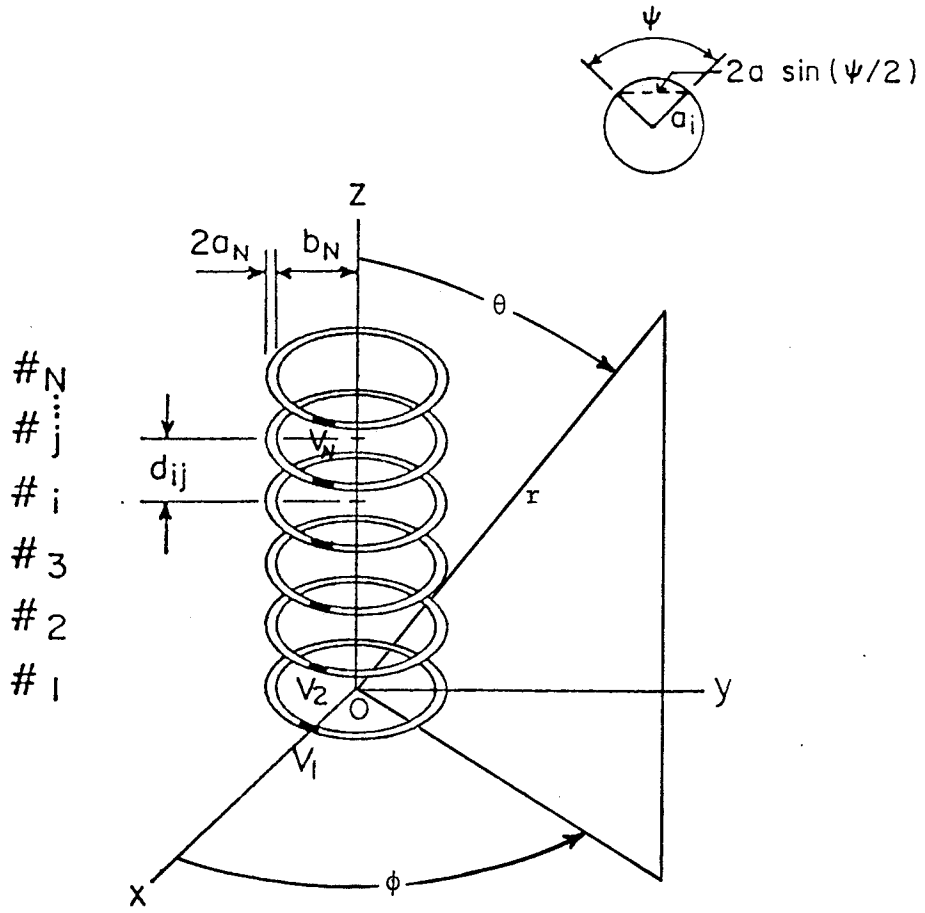

Fig. 1-1: An array of circular coaxial loops

surface. Following the procedure in [3]-[7] for a single loop, the integral equation satisfying the boundary conditions of the electric field on the surfaces of N circular loops may be shown to be [12]

$$\frac{V_i}{b_i \frac{\delta}{\delta\phi_i}} U_i(\phi_i) = \frac{j\eta_o}{4\pi b_i} \sum_{j=1}^{N} \int_0^{2\pi} [kb_i \cos(\phi_i - \phi_j') + \frac{1}{kb_i} \frac{\partial^2}{\partial \phi_i^2}] W_{ij}(\phi_i - \phi_j') I_j(\phi_j') d\phi_j' \quad i = 1, 2, \ldots, N \tag{1.1}$$

where

$$W_{ij}(\phi) = \begin{cases} \frac{1}{2\pi}\int_0^{2\pi} e^{-jkb_i R_{ii}(\phi,\psi)} / R_{ii}(\phi,\psi)\, d\psi & i = j \\ \exp[-jkb_i R_{ij}(\phi)]/R_{ij}(\phi) & i \neq j \end{cases} \tag{1.2}$$

where $I_j(\phi_j)$ is the current on the jth loop, $k = \frac{2\pi}{\lambda}$ is the propagation constant, and $\eta_o = 120\pi\Omega$ is the characteristic impedance of free space. $U_i(\phi_i)$ is equal to 1 within the driving-point gap and is zero elsewhere. The distance R_{ij} between two currents, normalized by the loop radius b_i and for $i = j$ is

$$R_{ii}(\phi,\psi) = [4 \sin^2 \phi/2 + 4(a_i/b_i)^2 \sin^2 \psi/2]^{\frac{1}{2}} \tag{1.3}$$

and when $i \neq j$ and assuming $d_{ij} >> a_i$, it is

$$R_{ij}(\phi) = [4(b_j/b_i)^2 \sin^2 \phi/2 + (\frac{d_{ij}}{b_i})^2 + (\frac{b_j}{b_i} - 1)^2]^{\frac{1}{2}} \tag{1.4}$$

In order to solve the simultaneous integral equations (1.1), the current $I_j(\phi_j)$ and the kernel $W_{ij}(\phi)$ are expanded into Fourier series

$$I_j(\phi_j) = \sum_{n=0}^{\infty} I_j^n \cos n\phi_j \,, \quad (j = 1, 2, \ldots, N) \tag{1.5}$$

$$W_{ij}(\phi) = \sum_{n=-\infty}^{\infty} K_{ij}^{n} \, e^{-jn\phi} \qquad (i,j = 1, 2, \ldots, N) \tag{1.6}$$

where for $i = j$

$$K_{ii}^{n} = K_{ii}^{-n} = \frac{1}{4\pi^2} \int_0^{2\pi} \int_0^{2\pi} \frac{e^{-jkb_i R_{ii}(\phi,\psi)}}{R_{ii}(\phi,\psi)} \, e^{jn\phi} d\phi d\psi \tag{1.7}$$

and for $i \neq j$

$$K_{ij}^{n} = K_{ij}^{-n} = \frac{1}{2\pi} \int_0^{2\pi} \frac{e^{-jkb_i R_{ij}(\phi)}}{R_{ij}(\phi)} \, e^{jn\phi} \, d\phi \tag{1.8}$$

An introduction of (1.5) and (1.6) into the right hand side of equation (1.1), after some manipulation gives

$$\beta_i^n = \frac{\sin n(\delta\phi_i/2)}{n \, \delta\phi_i/2} V_i = \sum_{j=1}^{N} Z_{ij}^{n} \, I_j^{n} \tag{1.9}$$

$$i = 1,2,\ldots,N \; ; \; n \geq 0$$

where

$$Z_{ij}^{n} = \begin{cases} j\pi\eta_o \; kb_j \; K_{ij}^{1} & n = 0 \\ \dfrac{j\pi\eta_o}{2} \left(kb_j \dfrac{K_{ij}^{n+1} + K_{ij}^{n-1}}{2} - \dfrac{n^2}{kb_i} K_{ij}^{n} \right) , & n \geq 1 \end{cases} \tag{1.10}$$

Equation (1.9) in the matrix form is

$$[Z_{ij}^{n}] \; [I_j^{n}] = [\beta_i^{n}] \qquad n \geq 0 \tag{1.11}$$

These simultaneous equations contain a group of Fourier coefficients of the current I_j^n $(j = 1, 2, \ldots, N)$ for the same order n only. The diagonal and off diagonal elements of the matrix Z_{ij}^n represent the generalized self and mutual impedances of the nth order mode of the loop currents, respectively. Z_{ii}^n and Z_{ij}^n correspond to cases where the observation points of the electric field are on the same or

different elements. To calculate Z^n_{ij} and Z^n_{ii} the values of K^n_{ij} and K^n_{ii} should be known. To evaluate K^n_{ii}, the range of integration of equation (1.7) was divided into three regions where in each region an approximation was used. The details of this procedure is given in [7].

The other coefficients K^n_{ij} $(i \neq j)$ are presented in polynomial form in [12]

$$K^n_{ij} = -jkb_i \sum_{n=0}^{\infty} \frac{(y/2Z)^{n+2m}}{m!\,(n+m)!}\, h^2_{n+2m}(Z) \qquad (1.12)$$

$$(i,j = 1,2,\ldots,N \; ; \; n = 0,1,\ldots)$$

where

$$y = kb_i\, kb_j \qquad (1.13)$$

$$Z = [(kb_i)^2 + (kb_j)^2 + (kd_{ij})^2]^{\frac{1}{2}} \qquad (1.14)$$

and $h^2_{n+2m}(Z)$ is the second kind spherical Hankel function of order $(n + 2m)$

1.2.1 Current Distributions and the Admittance

Assuming that (y^n_{ij}) represents the inverse of the matrix (Z^n_{ij}) in equation (1.11), the current $I_i(\phi_i)$ on the ith element is then given by

$$I_i(\phi_i) = \sum_{n=0}^{\infty} \left(\sum_{j=1}^{N} y^n_{ij}\, \beta^n_j \right) \cos n\phi_i \qquad (1.15)$$

The admittance matrix (y^n_{ij}) may be considered a diagonal matrix for n larger than a certain number m_o determined by the magnitudes of b_i, b_j and d_{ij}, [12] and [16]. Thus, equation (1.15) may be reduced to

$$I_i(\phi_i) = \sum_{n=0}^{m_o} \left(\sum_{j=1}^{N} y_{ij}^n \beta_j^n \right) \cos n\phi_i + \sum_{n=m_o+1}^{\infty} \frac{\beta_i^n}{Z_{ii}^n} \cos n\phi_i \tag{1.16}$$

For the values of n for which the approximation

$$Z_{ii}^n = -j \frac{\eta_o n}{4ka_i} \qquad n > n_i = b_i/a_i \tag{1.17}$$

is valid, the second summation in (1.16) will be [12]

$$\sum_{n=n_i+1}^{\infty} \frac{\beta_i^n}{Z_{ii}^n} \cos n\phi_i = -j \frac{4ka_iV_i}{\eta_o \delta\phi_i} \int_{\phi_i-\delta\phi_i/2}^{\phi_i+\delta\phi_i/2} \ln\left(2 \sin \frac{|t|}{2}\right) dt -$$

$$- \frac{j4ka_iV_i}{\eta_o} \sum_{n=1}^{n_i} \frac{\sin(n\,\delta\phi_i/2)}{n\,\delta\phi_i/2} \cdot \frac{\cos n\phi_i}{n} \tag{1.18}$$

where $n_i \geq m_o$. For small values of ϕ_i the integral in (1.18) can be evaluated approximately in the form

$$-j \frac{4ka_iV_i}{\eta_o \delta\phi_i} \int \simeq -j \frac{4ka_iV_i}{\eta_o} \left[\frac{\phi_i + \delta\phi_i/2}{\delta\phi_i} \cdot \ln(\phi_i + \delta\phi_i/2) \right.$$

$$\left. - \frac{\phi_i - \delta\phi_i/2}{\delta\phi_i} \cdot \ln |\phi_i - \delta\phi_i/2| - 1 \right] \tag{1.19}$$

when $\phi_i = \delta\phi_i/2$, equation (1.16) represents the driving-point current. Using the relation $\sin(n\delta\phi_i/2)/(n\delta\phi_i/2) \simeq 1$ for $n \leq n_i = b_i/a_i$, the input current $I_i (i = 1, 2, \ldots N)$ may be written as

$$I_i = \sum_{n=0}^{m_o} \sum_{j=1}^{N} y_{ij}^n V_j + \sum_{n=m_o+1}^{n_i} \frac{V_i}{Z_{ii}^n} + j4\omega\varepsilon_o a_i V_i \ln \frac{a_i e}{2\beta b_i \delta\phi_i} \tag{1.20}$$

where $b_i\delta\phi_i$ represents the gap width and hence the third term is related to the gap capacitance, $\ln 2\beta = \gamma$ and

$\gamma = 0.5772$ is Euler's constant. Because in derivation of (1.20) the magnetic current has been neglected, the gap capacitance is twice as large [7],

$$C_{gi} = 2\varepsilon_o a_i \ln \frac{a_i e}{2\beta b_i \delta\phi_i} \tag{1.21}$$

and therefore,

$$I_i = \sum_{n=0}^{m_o} \sum_{j=1}^{N} y_{ij}^n V_j + \left(\sum_{n=m_o+1}^{n_i} \frac{1}{Z_{ii}^n} + j\,\omega C_{gi} \right) V_i \tag{1.22}$$

The contribution of the magnetic current was omitted in equation (1.1), because the effect of the gap capacitance is limited to the vicinity of the driving point. The current distribution on an antenna element is not significantly affected by this omission, and hence can be expressed by

$$I_i(\phi_i) = \sum_{n=0}^{m_o} \sum_{j=1}^{N} y_{ij}^n V_j \cos n\phi_i + V_i \sum_{n=m_o+1}^{n_i} \frac{1}{Z_{ii}^n} \cos n\phi_i \tag{1.23}$$

The admittance matrix Y_{ij} of the array is given by

$$Y_{ij} = \begin{cases} \sum_{n=0}^{m_o} y_{ii}^n + \sum_{n=m_o+1}^{n_i} \frac{1}{Z_{ii}^n} + j\,\omega C_{gi} & , \quad i = j \\ \sum_{n=o}^{m_o} y_{ij}^n & \quad i \neq j \end{cases} \tag{1.24}$$

1.2.2 The Radiation Field and Directive Gain

In terms of spherical coordinates r, θ, ϕ, that have their origin at the center of the first loop in Figure (1.1), the radiation field can be expressed by

$$\begin{bmatrix} E_\theta \\ E_\phi \end{bmatrix} = -\frac{\eta_o}{4r} \exp(-jkr) \begin{bmatrix} \cos\theta \\ 1 \end{bmatrix} \sum_{i=1}^{N} [kb_i \exp(jkd_{i1} \cos\theta] \sum_{n=0}^{\infty} j^n I_i^n [J_{n-1}(x_i) \pm J_{n+1}(x_i)] \cdot \begin{bmatrix} \sin n\phi \\ \cos n\phi \end{bmatrix} \quad (1.25)$$

where $x_i = kb_i \sin\theta$, $J_n(x_i)$ is the Bessel function of the first kind of order n, and d_{i1} represents the spacing between the ith and the first elements.

Using equation (1.25) and the definition of the directive gain, the directive gain with respect to the direction of the z-axis is given by

$$G_{d,r} = \frac{\pi\eta_o}{4} \cdot \frac{\left| \sum_{i=1}^{N} kb_i \exp(\pm jkd_{i1}) \cdot I_i^1 \right|^2}{\sum_{i=1}^{N} \mathrm{Re}(Y_i) |V_i|^2} \quad (1.26)$$

where the plus sign is for the positive z-direction, and the negative sign is for G_r, the gain in the negative direction.

The material covered in the last few pages summarizes the major steps required in developing the theory of loop antennas and their arrays using the Fourier expansion method. This method will be utilized in the next chapter to develop further the theory of loop arrays and to investigate the loading effects on the array characteristics. Both arrays of infinite and finite lengths are studied. To study the characteristics of finite Yagi arrays of circular loops with different number of elements, several different sizes of array are selected whenever possible. The types of structure studied in this thesis are listed below:

i) infinite loaded arrays

ii) finite loaded arrays

iii) multiply loaded arrays

iv) constant distributed resistive loaded arrays

v) tapered distributed capacitive loaded loop antennas

vi) planar arrays of concentric loops

vii) a single and a 2-element loop antenna above the ground plane

viii) a circular loop antenna in front of a solid disk reflector

ix) short backfire antennas with peripheral rim

x) a circular loop antenna in front of a planar array of concentric loops

xi) a circular loop antenna in front of a planar array of concentric loops with peripheral rim

xii) infinite arrays of two concentric loops with loaded elements

xiii) finite arrays of two concentric loops

CHAPTER II

INFINITE AND FINITE LOADED LOOP ARRAYS

2.1 Introduction

Generally, the loading of an antenna by a lumped or distributed impedance modifies its current distribution and affects its radiation characteristics. Thus, by a proper selection of the type, size and the location of the load, the performance of the antenna can usually be improved.

The idea of tuning a radiating structure to control its current and hence its radiation properties, dates from the earliest antennas and was commonly used in the design of broadcast antennas in the 1920's [18]. There has been extensive progress in the techniques of antenna impedance loading during the last twenty years and very interesting results have already been reported for single dipoles and arrays of dipole antennas [19]-[23]. The single loaded circular loop antenna has also been studied in [24]-[26] and a broad frequency characteristic was reported. Here, the work is extended to arrays of circular coaxial loops which are loaded at $\phi = 0$. Attention is specifically focussed on Yagi type arrays in which only one of the elements is excited and the rest are parasitics. These kinds of antennas enjoy the simplicity of feed systems and are very inexpensive to fabricate. Furthermore, these antennas have very high directivity.

2.2 The Reasons for Investigation

Antennas with high directivity are necessary to obtain good sensitivity and selectivity in most communication systems. With the development of radio-astronomical research during the past decades, such antennas have become more and more important, and moreover, the requirements on the directional properties of antennas for radio-astronomy have become more stringent than those for ordinary engineering applications. Antennas for radio-astronomy should have radiation patterns with the narrowest possible main beams and lowest possible side-lobe levels. In the microwave range of frequencies such a high directivity is usually achieved by using the large parabolic dish type of antennas. But in the lower frequency range, the size of the parabolic antenna and consequently, its cost become enormously large. The usual practice in such a range of frequencies is to combine some simple types of antennas in the form of an array in order to obtain the required directional properties. Furthermore, for minimum cost and ease of steering the direction of the main antenna beam, the number of elements in the array should be small. Yagi-Uda antennas are one of the very few types that may be used for such a purpose. In infinite form, this structure may be used as an open waveguide. Shen has given a list of possible applications of this structure in [27].

In spite of many investigations on Yagi arrays of dipoles, reports on circular loop Yagi arrays are scarce. Although they are directive antennas, their 3dB bandwidth

is relatively small which is a major drawback associated with this structure. In this chapter it is shown that the bandwidth of the array can be improved with proper loading of the elements. To do so, the travelling wave idea is applied on an infinite loaded circular loop array in order to obtain an expression for the propagation constant along the structure. Recent theoretical and experimental investigations [28]-[30] have shown that a periodic array of infinite length can support a travelling wave along its structure. This seems to explain why a section of the structure with properly matched ends can yield a rather directional end-fire radiation pattern. The application of the travelling wave idea to the Yagi antenna dates back to 1950 when R.A. Smith [31] suggested that the phsyical action of the directors in the Yagi array is to reduce the phase velocity of the wave travelling along the axis of the Yagi. This is equivalent to saying that the wave radiated by the driven element travels through a region with refractive index greater than unity.

In the next few sections we will derive an approximate expression for the phase velocity of the travelling wave along a loaded loop array. The array extends to infinity in both directions along the z-axis, figure (2-1), and consists of equal coaxial loops of radius b which are separated by a distance d and are loaded with identical loads of finite length $b\delta\phi$ at $\phi = 0$. Therefore, the load impedance can be represented by $Z_L U(\phi)$, where $U(\phi)$ is equal to unity at the load and zero elsewhere. The analysis is based on

the classical method and a dispersion relation is derived in terms of the mutual impedances between the zeroth element (the element on xy plane) and other elements in the array. In addition, Flouquet's theorem [32] is also used to account for the periodicity of the structure. The effects of loading on the finite array is also investigated.

2.3 A Relation for Phase Velocity

Let β be the propagation constant of the travelling wave on the infinite array of figure (2-1), with a time factor $\exp(j\omega t)$. Thus, for the propagation along the positive z-direction (assuming the wave is propagated without attenuation) the current distribution I_m on the mth loop is related to I_0, that of the reference loop by the relation

$$I_m(\phi) = I_0(\phi) \exp(-j\beta md) \qquad (2.1)$$

The investigation of the finite arrays by using the integral equation method has shown [16] that for a properly designed array the above assumption of a constant current magnitude and phase change along the directors is approximately valid. Equation (2.1) may also be recognized as the usual Flouquet type of phase variation used in periodic structure analysis.

This type of phase variation is based on Flouquet's theorem which states that in any medium having a special periodicity d, the fields are multiplied only by some complex constants if one moves down the strucutre by a distance d. This is obvious since if the structure is displaced along the z-axis by an amount d, it coincides with itself and

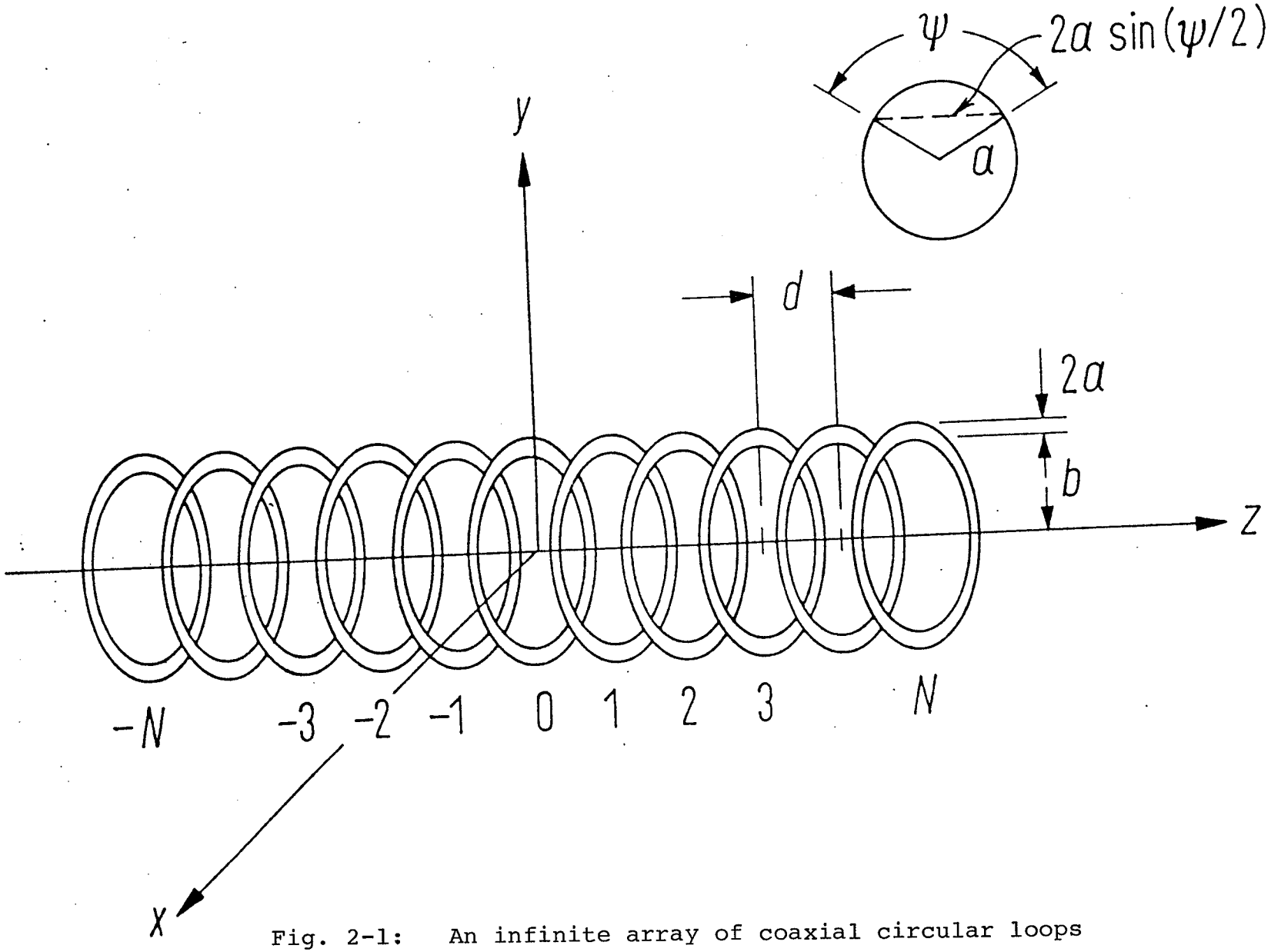

Fig. 2-1: An infinite array of coaxial circular loops

the new field can differ from the previous one only by a constant factor.

For the current distribution $I_0(\phi)$ in equation (2.1) the form $I_0\cos\phi$ is adopted. This assumption for antenna current has already been confirmed in [13] and [16]. Furthermore this form of the current (n = 1 mode) is assumed due to the fact that we are interested in the first passband of the array and within this band the array is an endfire antenna [15].

In order to apply the boundary conditions on the element surface, each load is replaced by a constant voltage generator. This is made possible by applying the compensation theorem, which states that an impedance Z_L in which a current I is flowing can be replaced by a potential difference equal to $-IZ_L$ without changing the electrical behaviour of the network.

Now the application of the boundary condition can be carried out in a similar manner to the case of the unloaded arrays discussed in the previous chapter. The resultant matrix equation (1.11) for $n = 1$ is of the form

$$[Z^1_{ij}][I_j] = -[Z_L I_i], \qquad -\infty \leq \begin{matrix} i \\ j \end{matrix} \leq \infty \tag{2.2}$$

The ith row of this matrix equation is

$$\sum_{j=-\infty}^{\infty} Z^1_{ij} I_j = -Z_L I_i , \qquad -\infty \leq i \leq \infty \tag{2.3}$$

Since the array is a periodic structure with elements extending from $-\infty$ to $+\infty$, due to symmetry one may, there-

fore write equation (2.3) for the 0th element (reference element) without loss of generality. Thus using equation (2.1), equation (2.3) becomes

$$\sum_{-\infty}^{\infty} Z^1_{0m} I_0 \exp(-jm\beta d) = -Z_L I_0 \tag{2.4}$$

where from Chapter I, the impedance Z^1_{0m} is given by

$$Z^1_{0m} = \frac{j\pi\eta_o}{2} \left[kb \frac{K^2_{0m} + K^0_{0m}}{2} - \frac{1}{kb} K^1_{0m}\right] \tag{2.5}$$

and

$$K^n_{0m} = \frac{1}{2\pi} \int_0^{2\pi} \frac{1}{R_{0m}(\phi)} \exp[-jkb\, R_{0m}(\phi) + jn\phi]d\phi \tag{2.6}$$

with

$$R_{0m} = \frac{|m|d}{b} \left[1 + \left(\frac{2b}{md}\right)^2 \sin^2 \phi/2\right]^{\frac{1}{2}} \quad \text{for} \quad m > 0 \tag{2.7}$$

R_{00} and K^n_{00} are as defined in (1.3) and (1.7). The infinite summation in equation (2.4) is a transcendental equation. In order to solve this equation, we will use a technique which was employed first by Serracchiolli and Levis [33] for dipole arrays. This procedure is based on obtaining an asymptotic formula for the Z^1_{0m} function and summing an infinite series at finite M while replacing the truncated terms by their asymptotic equivalent. The magnitude of M depends on the geometry of the array and will be discussed in more detail later. The steps involved in the above procedure are discussed in detail in the next section.

2.4 Evaluation of the Infinite Series (2.4)

The infinite summation in equation (2.4) can be subdivided into three summations in the following way

$$\left[\sum_{-\infty}^{-(M+1)} + \sum_{-M}^{M} + \sum_{M+1}^{\infty}\right] Z^1_{0m} \exp(-j\beta md) = -Z_L \qquad (2.8)$$

where M is an integer such that $\frac{Md}{2b} >> 1$. With this condition the infinite summations of (2.8) can be evaluated approximately. The finite summation should, however, be evaluated exactly by using equation (2.5).

When condition $\frac{Md}{2b} >> 1$ is satisfied, equation (2.7) for R_{0m} can be approximated by two terms of its binomial expansion. The result is given by

$$R_{0m} \simeq |m| \frac{d}{b}\left[1 + \frac{1}{2}\left(\frac{2b}{md}\right)^2 \sin^2 \phi/2\right] = |m| \frac{d}{b} + \frac{b}{|m|d}\left[1 - \cos\phi\right] \qquad (2.9)$$

Introducing this expression into equation (2.6) gives (for $\frac{md}{2b} >> 1$)

$$K^n_{0m} \simeq \frac{b\, e^{-jk|m|d}}{\pi |m| d} \int_0^{\pi} e^{\frac{jkb^2}{|m|d} \cdot \cos\phi} \cdot \cos n\phi \, d\phi \qquad (2.10)$$

The integral in (2.10) is related to the Sommerfield representation of the Bessel function. Thus, one can find

$$K^n_{0m} = \frac{bj^n}{d} \frac{\exp(-jk|m|d)}{|m|} J_n(x), \text{ with } x = \frac{kb^2}{|m|d} \qquad (2.11)$$

Therefore, equation (2.5) modifies to the form

$$Z^1_{0m} = \frac{j\pi\eta_0 b}{2d}\left[kb \frac{J_0(x) - J_2(x)}{2} - \frac{j}{kb} J_1(x)\right] \frac{\exp(-jk|m|d)}{|m|} \qquad (2.12)$$

Now, for the above range of m, and $kb \lesssim 1$, the argument x is small and the small argument approximation for the Bessel functions can be used. Thus, for

$$J_n(x) \xrightarrow[x \to 0]{} \frac{1}{n!} \left(\frac{x}{2}\right)^n \tag{2.13}$$

the result is

$$Z^1_{0m} \simeq \frac{j\pi\eta_o b}{2d} \left[\frac{kb}{2} - \frac{jb}{2d|m|} - \frac{k^3 b^5}{16 d^2 |m|}\right] e^{-jk|m|d}/|m| \tag{2.14}$$

Introducing Z^1_{0m} from equation (2.14) into equation (2.8) gives

$$\sum_{-M}^{M} Z^1_{0m} e^{-j\beta md} + \left[\sum_{-\infty}^{-(M+1)} + \sum_{M+1}^{\infty}\right] \left(A + \frac{B}{|m|} + \frac{C}{|m|^2}\right) \frac{\exp(-jk|m|d + j\beta md)}{|m|} = -Z_L \tag{2.15}$$

where

$$\begin{aligned} A &= \frac{j\pi\eta_o kb^2}{4d} \\ B &= \frac{\pi\eta_o b^2}{4d^2} \\ C &= -j\frac{\pi\eta_o k^3 b^6}{32 d^3} \end{aligned} \tag{2.16}$$

The infinite summations of (2.15) are of the form

$$f_i(\beta) = \left[\sum_{-\infty}^{-(M+1)} + \sum_{M+1}^{\infty}\right] \frac{\exp(-jk|m|d + j\beta md)}{|m|^i} \tag{2.17}$$

with $i = 1$, 2, and 3. Now we will consider (2.17) for each i separately.

(i) Summation for $f_1(\beta)$

Relation (2.17) for $i = 1$ is

$$f_1(\beta) = \sum_{-\infty}^{-(M+1)} \frac{\exp(-jk|m|d+j\beta md)}{|m|} + \sum_{M+1}^{\infty} \frac{\exp(-jk|m|d+j\beta md)}{|m|} =$$

$$\sum_{m=M+1}^{\infty} \frac{e^{(-jkmd-j\beta md)}}{m} + \sum_{m=M+1}^{\infty} \frac{e^{-jkmd+j\beta md}}{m} =$$

$$\left[\sum_{m=1}^{\infty} - \sum_{m=1}^{M}\right] \left[\frac{e^{-jmd(k-\beta)} + e^{-jmd(k+\beta)}}{m}\right] \qquad (2.18)$$

The infinite summation in (2.18) is known and is given in reference [34]

$$\sum_{m=1}^{\infty} \frac{e^{\pm jmx}}{m} = -\ln(2 \sin x/2) \pm j \frac{\pi-x}{2}, \quad 0 < x < 2\pi \qquad (2.19)$$

Utilizing (2.19), the infinite summation of (2.18) gives

$$\sum_{m=1}^{\infty} \frac{e^{-jmd(k+\beta)} + e^{-jmd(k-\beta)}}{m} = -\ln[2 \sin \frac{d(k+\beta)}{2}] -$$

$$-j \frac{\pi-d(k+\beta)}{2} - \ln[2 \sin \frac{d(\beta-k)}{2}] + j \frac{\pi-d(\beta-k)}{2} =$$

$$-\ln 2(\cos kd - \cos \beta d) + jkd \qquad (2.20)$$

Substituting (2.20) into (2.18) gives the final result for $f_1(\beta)$,

$$f_1(\beta) = -\ln 2(\cos kd - \cos \beta d) + jkd - 2 \sum_{m=1}^{M} e^{-jkmd} \cos \beta md \qquad (2.21)$$

(ii) Summation for $f_2(\beta)$

We can find a relation similar to (2.18) for $f_2(\beta)$

$$f_2(\beta) = \left[\sum_{m=1}^{\infty} - \sum_{m=1}^{M}\right] \frac{e^{-jmd(k-\beta)} + e^{-jmd(k+\beta)}}{m^2} \qquad (2.22)$$

Again, referring to [34] we have

$$\sum_{m=1}^{\infty} \frac{e^{\pm jmx}}{m^2} = \frac{\pi^2}{6} - \frac{x}{4}(2\pi - x) \pm j\left(x\ln x - x - \frac{x^3}{72} - \frac{x^5}{14{,}400} - \ldots.\right) \qquad 0 < n < 2\pi \tag{2.23}$$

So that

$$f_2(\beta) = \frac{\pi^2}{3} - \pi\beta d + \frac{(kd)^2 + (\beta d)^2}{2} + j\beta d \ln\left(\frac{\gamma_2}{\gamma_1}\right) + jkd \ln(\gamma_1\gamma_2) - 2jkd + j\left[\frac{\gamma_1^3 - \gamma_2^3}{72} + \frac{\gamma_1^5 - \gamma_2^5}{14400}\right] - 2\sum_{m=1}^{N} \frac{\exp(-jmkd)}{m^2} \cos \beta md \tag{2.24}$$

where

$$\gamma_1 = (\beta - k)d \qquad \gamma_2 = (\beta + k)d \tag{2.25}$$

(iii) Summation for $f_3(\beta)$

Following the procedure for $f_1(\beta)$, we will have

$$f_3(\beta) = \left[\sum_{m=1}^{\infty} - \sum_{m=1}^{M}\right] \frac{e^{-jmd(k-\beta)} + e^{-jmd(k+\beta)}}{m^3} \tag{2.26}$$

It is shown in [34] that

$$\sum_{m=1}^{\infty} \frac{e^{\pm jmx}}{m^3} = \left(\frac{x^2}{2}\ln x - \frac{3x^2}{4} - \frac{x^4}{288} \ldots\right) + \sum_{m}^{\infty} \frac{1}{m^3} \pm j\left(\frac{\pi^2 x}{6} - \frac{\pi x^2}{4} + \frac{x^3}{12}\right) \quad , \quad 0 < x < 2\pi \tag{2.27}$$

Substituting (2.27) into (2.26) yields

$$f_3(\phi) = \frac{(\beta d)^2 + (kd)^2}{2} + \ln(\gamma_1\gamma_2) + \beta dkd \ln\frac{\gamma_2}{\gamma_1} - \frac{3}{4}(\gamma_1^3 + \gamma_2^3) - \frac{1}{288}[\gamma_2^4 + \gamma_1^4] + 2\sum_{m=1}^{\infty} \frac{1}{m^3} - j\left[\frac{\pi^2 kd}{3} -\right.$$

$$\pi\beta dkd + \frac{1}{2}(\beta d)^2\, kd + \frac{1}{6}(kd)^3 - 2 \sum_{m=1}^{M} \frac{\exp(-jmkd)}{m^3} \cos(\beta md) \qquad (2.28)$$

where γ_1 and γ_2 are as defined in (2.25).

Substituting ((2.21), (2.24) and (2.28) into (2.15) we get

$$Af_1(\beta) + Bf_2(\beta) + Cf_3(\beta) + \sum_{m=-M}^{M} Z_{0m}^{1} \exp(-j\beta md) = -Z_L \qquad (2.29)$$

Equation (2.29) is used to determine the propagation constant β from which the phase velocity of the launched wave can be obtained. The convergence of the solution for the phase constant β in equation (2.29) depends on the condition $M >> \frac{2b}{d}$. For a fixed value of the loop radius b, therefore, the number of terms in the finite summation of (2.29) will increase with decreasing the loop spacing d.

2.5 The Numerical Results for the Phase Velocity

A computer program was developed which determines a numerical solution of the transcendental equation (2.29) for the phase constant β. The method which is used to calculate the phase constant is the central point method [35] as explained below.

When an approximate region of existence of the solution for $g(\beta)$ is known, the lower and upper bounds β_ℓ and β_u satisfying $\beta_\ell < \beta < \beta_u$ are first determined. Then the values of the function at both bounds and the central point β_c between β_ℓ and β_u, namely, $g(\beta_\ell)$, $g(\beta_u)$ and $g(\beta_c)$ are obtained. From the signs of these values we can determine which of the equally divided regions contains the

solution β. By carrying out a series of these procedures we can make the central point arbitrarily close to the true value of β. However, before using this technique, it is necessary to find out the range of values which β can assume.

A condition which one should keep in mind when solving (2.29) is that a Yagi array cannot support a travelling wave when the phase velocity is such that the currents of two adjacent elements are out of phase. This is clear from equation (2.1) which for $\beta d = \pi$, where d is the distance between two adjacent loops, gives the current of each loop equal and opposite in phase to that of the current on the adjacent element. Therefore, one can no longer talk of a direction of propagation and the array cannot support a travelling wave. This sets the upper bound of the propagation constant β, i.e., $\beta d \leq \pi$ [29]. The lower bound of β is determined by the fact that to have a slow wave the smallest value that β can take is k, the free space propagation constant. Therefore,

$$kd \leq \beta d \leq \pi \qquad (2.30)$$

The numerical results presented here are obtained using equations (2.29) and (2.30) for an array with arbitrary dimension.

Figure (2.2) shows the solution of equation (2.29) for an array with $b = d = 21.45$cm and operating at a frequency range of 180 MHz to 290 MHz. This figure gives the variation of the normalized phase velocity v/c as a function of the frequency for various reactive loadings. It is seen that,

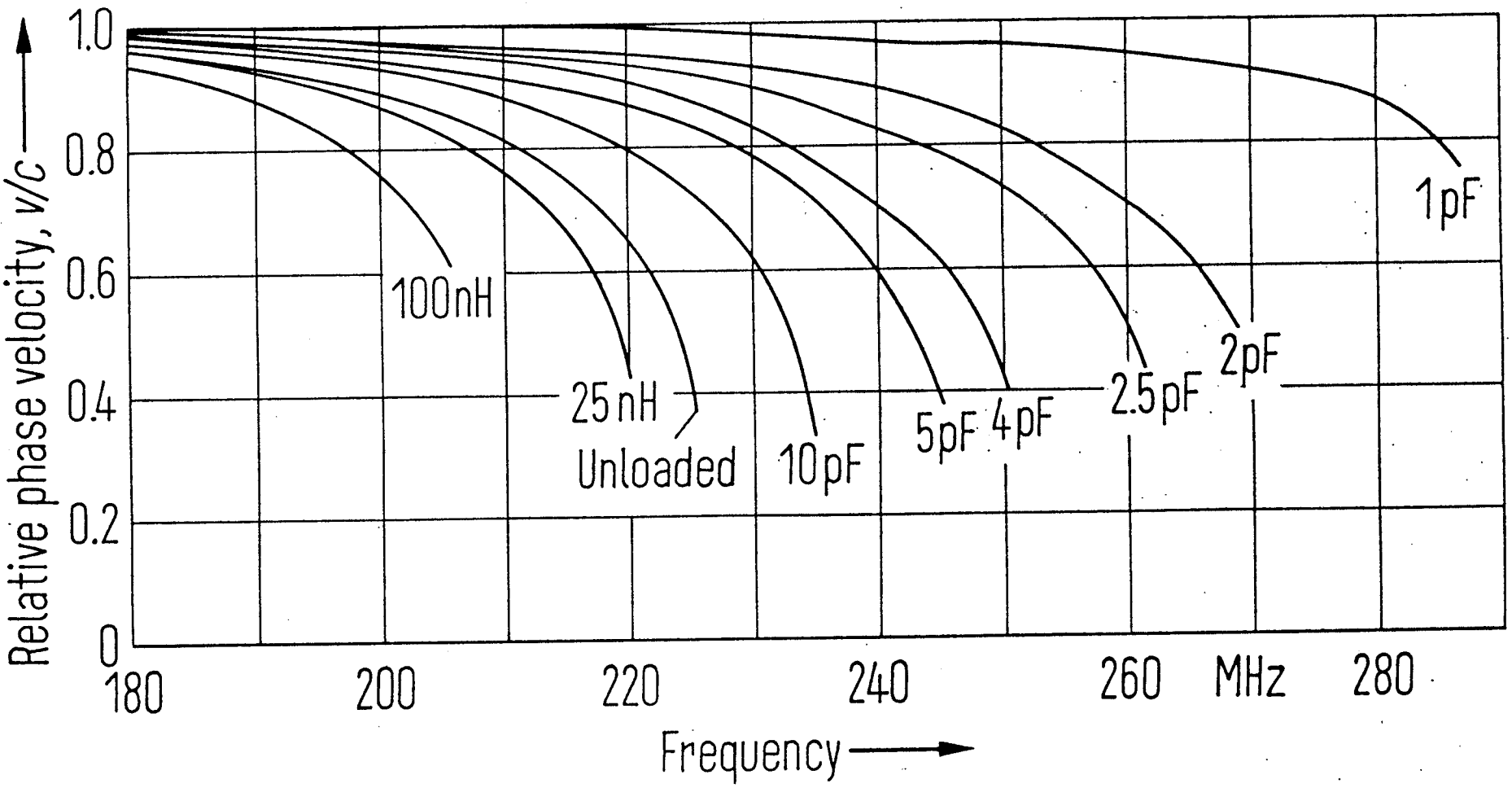

Fig. 2-2: Variation of the relative phase velocity of an infinite array with frequency for various loadings. b = d = 21.4 cm, and b/a = 100

in general, a capacitive loading increases the phase velocity and for a given phase velocity extends the range of the operating frequency. An inductive loading on the other hand, reduces the phase velocity and consequently, reduces the operating frequency range. The reason for an increase (or decrease) in the bandwidth can be understood from the discussion given for the range of β summarized in equation (2.30). For a higher phase velocity we have smaller β and, therefore, the range of frequency at which $\beta d < \pi$ is increased. On the other hand, for inductive loading, the slope of v/c versus frequency is higher and this causes β to increase rapidly until the array stops propagation ($\beta d = \pi$).

2.6 Finite Arrays

The above analysis gives the performance of the loaded infinite arrays. In practice, however, the arrays are finite in extent and cannot generally support travelling waves of a simple nature. The reflections at the array ends cause additional travelling waves which complicate the analysis. If the array is reasonably long these reflections may be neglected and the above analysis can still be used to study approximately the loading effects. However, the summation on the left-hand side of equation (2.8) must be carried out over the array elements. Furthermore, our investigation has shown that equation (2.8) for finite arrays does not have any solution in the real frequency domain. Instead, locating its minima yields solutions which correspond closely to those of the infinite array. As a result, the minima of equation (2.8)

are used to obtain the solution for the finite array case. These solutions, which are in the range of (2.30), represent the frequencies of the slow waves, which can be launched along the finite array.

Figure (2.3) shows the approximate results for the relative phase velocities of 19-element, loaded and unloaded, arrays. Their behaviour is similar to those of the infinite arrays but their initial variation as a function of frequency is somewhat slower. It is interesting to note that the finite structure solution represents also a slow wave along the array. It is obvious that the larger the number of elements in a finite array, the closer its solution is to that of the infinite array solution.

The effects of loading on the directive gain of finite arrays are investigated in the next session.

2.7 Directive Gain of Loaded Arrays

It is known that the relative phase velocity in an optimally designed Yagi antenna of length L must satisfy the Hansen-Woodyard relation [36].

$$v/c = \frac{L/\lambda}{0.5 + L/\lambda} = \frac{2f\lambda}{2fL + c} \qquad (2.31)$$

where f is the frequency of the signal. Differentiation of the above relation with respect to the frequency shows that $d/df(v/c)$ is never negative. This means that for the gain of the array to remain unchanged, the phase velocity in the antenna structure should not decrease with increasing frequency. In addition, the results of the previous section

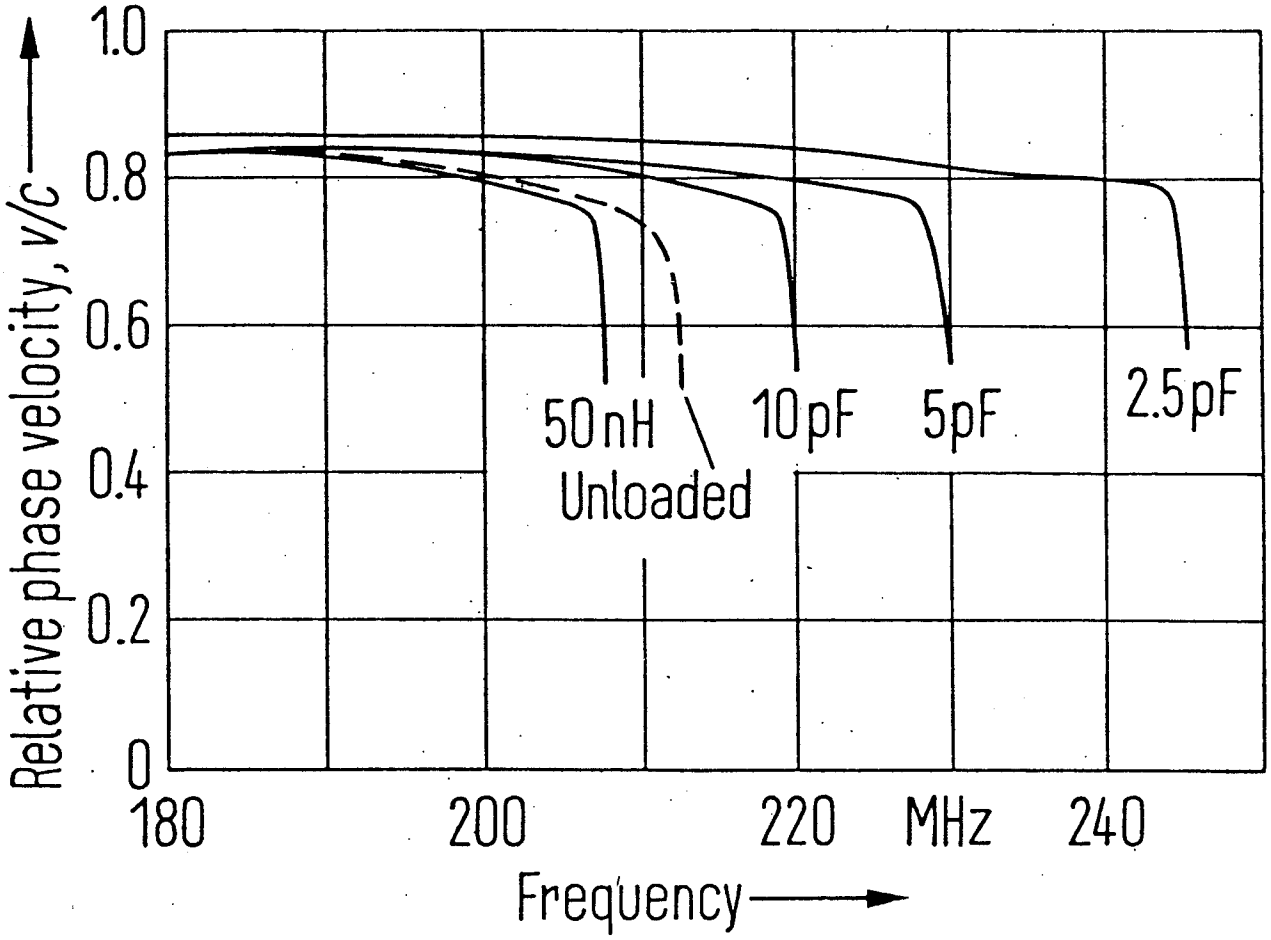

Fig. 2-3: Variation of the relative phase velocity of a 19-element array with frequency for various loadings. b = d = 21.45 cm, b/a = 100

showed that, for a given phase velocity, a capacitive loading of the array increases the operating frequency range and an inductive loading tends to reduce it. Thus from the above discussion and using equation (2.31), one can expect that the gain of the array must also behave in a similar fashion. In practice, however, arrays are finite in size and usually consist of only a few elements. In such cases, the travelling wave along the array is not well established and array currents can be obtained more accurately from equation (2.2). Once these currents are known, other array characteristics can be obtained readily.

As seen in Chapter I, the driving current of the ith element of an N-element array excited at $\phi = 0$ by a voltage $V_i (i = 1, 2, \ldots, N)$ is of the form

$$I_i(0) = \sum_{n=0}^{m_o} \sum_{j=1}^{N} y_{ij}^n V_j + \left(\sum_{n=m_o+1}^{n_i} \frac{1}{Z_{ii}^n} + j\omega C_{gi} \right) V_i \qquad (2.32)$$

where the parameters n_i, m_o are as defined previously.

Equation (2.32) can be used also for the loaded arrays. In this case by using the compensation theorem the load Z_{Li} can be replaced by a generator of voltage $V_i = -Z_{Li} I_i(0)$. Thus, for the Yagi-array in which all the elements are loaded at $\phi = 0$, except for the exciter one (the qth element), the above equation becomes

$$\left[1 + Z_{Li}(1 - \delta_{iq}) \left(\sum_{n=m_o+1}^{n_i} \frac{1}{Z_{ii}^n} + j\omega C_{gi} \right)\right] I_i(0) + \sum_{n=0}^{m_o} \sum_{\substack{j=1 \\ \neq q}}^{N} y_{ij}^n Z_{lj} I_j(0) =$$

$$V_q \sum_{n=0}^{m_o} y_{iq}^n + \delta_{iq} \left(\sum_{m_o+1}^{n_i} \frac{1}{Z_{ii}^n} + j\omega C_{gi} \right) V_i \qquad (2.33)$$

where δ_{iq} is the Kronecker delta function and $i = 1, 2, \ldots, N$. These equations can be modified to a matrix equation of the form

$$[\phi_{ij}][I_j(0)] = [\zeta_i]$$

where $[\phi_{ij}]$ is an $N \times N$ matrix with elements

$$\phi_{ij} = [1 + Z_{Li}(\sum_{n=m_o+1}^{n_i} \frac{1}{Z_{ii}^n} + j\omega C_{gi})]\delta_{ij} + Z_{Li}(1 - \delta_{iq}) \cdot \sum_{n=0}^{m_o} y_{ij}^n$$

$$\zeta_i = V_q \sum_{n=o}^{m_o} y_{iq}^n + \delta_{iq}(\sum_{n=m_o+1}^{n_i} \frac{1}{Z_{ii}^n} + j\omega C_{gi})\, V_i \qquad (2.35)$$

Equation (2.34) is the characteristic equation of the loaded array. Its solution gives the total current of each loop at $\phi = 0$ from which the current modes can be evaluated readily. When only the qth element is excited, i.e., for $j \neq q$ V_j is replaced by $-Z_{Lj}I_j(0)$. The current modes from equation (2.32) take the form

$$I_i^n = y_{iq}^n V_q - \sum_{\substack{j=1 \\ \neq q}}^{N} y_{ij}^n Z_{Lj} I_j(0) \quad \text{for} \quad 0 \leq n \leq m_o \qquad (2.36)$$

and the input admittance becomes

$$Y_{in} = \frac{I_q(0)}{V_q} = \sum_{n=0}^{m_o} y_{qq}^n - \frac{1}{V_q} \sum_{n=0}^{m_o} \sum_{\substack{j=1 \\ \neq q}}^{N} y_{qj}^n Z_{Lj} I_j(0) + \sum_{n=m_o+1}^{n_q} \frac{1}{Z_{qq}^n} + j\omega C_{qq} \qquad (2.37)$$

The gain of such an array can be obtained in a manner similar to that of an unloaded one and in the z-direction it is given by

$$G_{d,r} = \frac{\pi\eta_o}{4} \cdot \frac{\left| \sum_{i=1}^{N} kb_i \exp(\pm jkd_{il}) \cdot I_i^1 \right|^2}{\mathrm{Re}(Y_{in})|V_q|^2 - \sum_{\substack{i=1 \\ \neq q}}^{N} \mathrm{Re}(Z_{Li})|I_i(0)|^2} \qquad (2.38)$$

where I_i^1 is the current mode for $n = 1$.

2.8 Effect of Loading on Directive Gain

Based on the analysis of the previous section, a computer program was developed to investigate the effect of loading on antenna's characteristics. For all arrays discussed here, $q = 2$. The variation with frequency of the gain of a 10-element array in $\theta = 0$ direction is shown in figure (2-4) for various capacitive loads. This figure shows that, as expected, a capacitive loading generally increases the bandwidth of the array and shifts the center frequency upwards. As an example, when the directors are loaded by 1PF capacitors, the 3dB bandwidth is over 55 MHz, which represents an approximate 270% increase over that of the unloaded array. Figure (2-5) shows similar effects for the directive gain of a 14-element Yagi array.

In addition, the effect of reflector loading on the antenna's directive gain is also studied. The computed directive gain in +z-direction ($\theta = 0°$) is shown in figure (2-6). In this figure the array directors are loaded by 2.5PF capacitors. The results show that the loading of the reflector does not affect the high frequency cutoff significantly. However, it has significant effect on the low frequency cutoff of the array. Generally, inductive loading

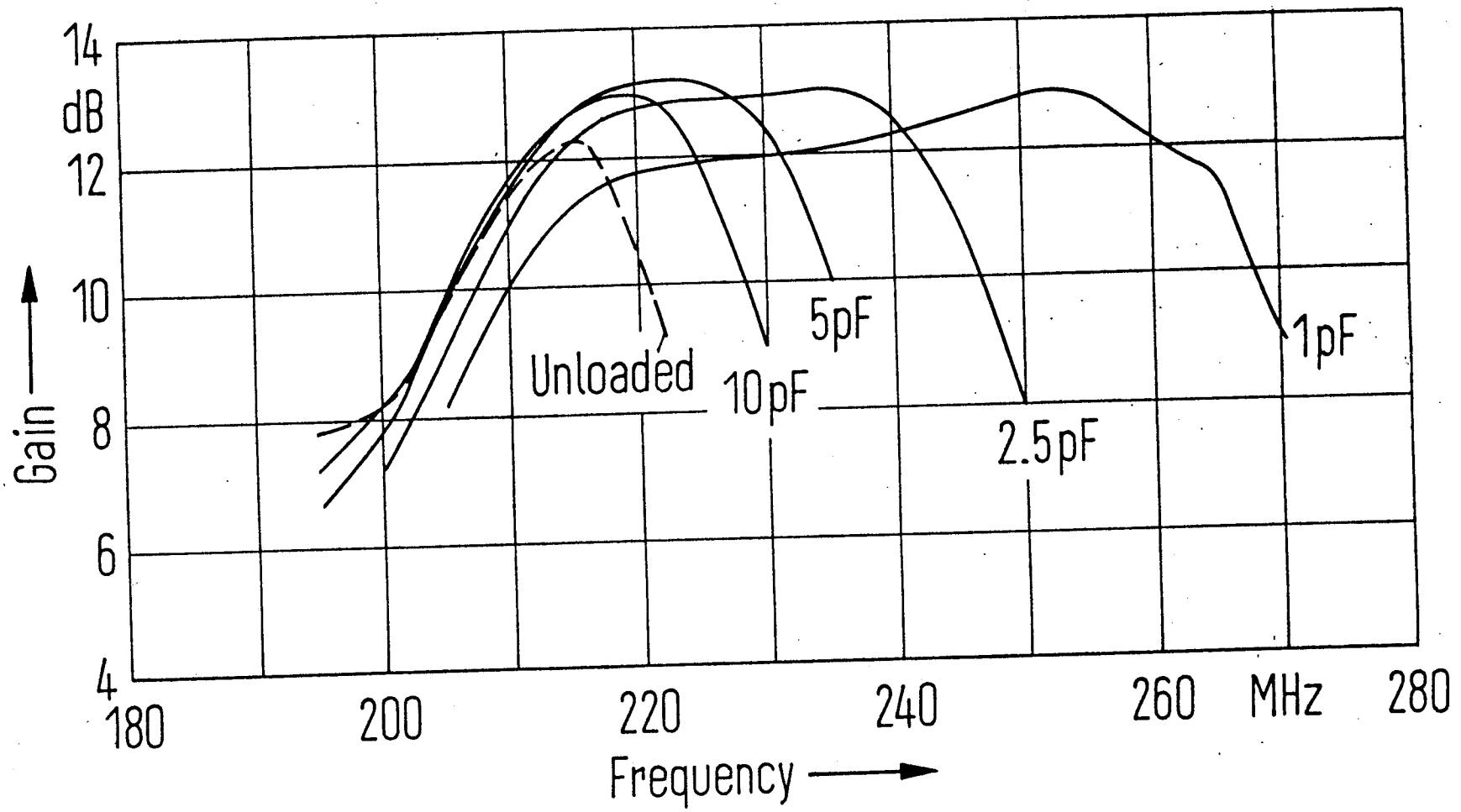

Fig. 2-4: Variation of the directive gain of a 10-element array with frequency for various director loadings. b_1 = 22.75 cm, b_2 = 23.83 cm, b_i = 21.45 cm (i = 3, 4, ... 10), d = 21.45 cm and b_2/a= 82.44

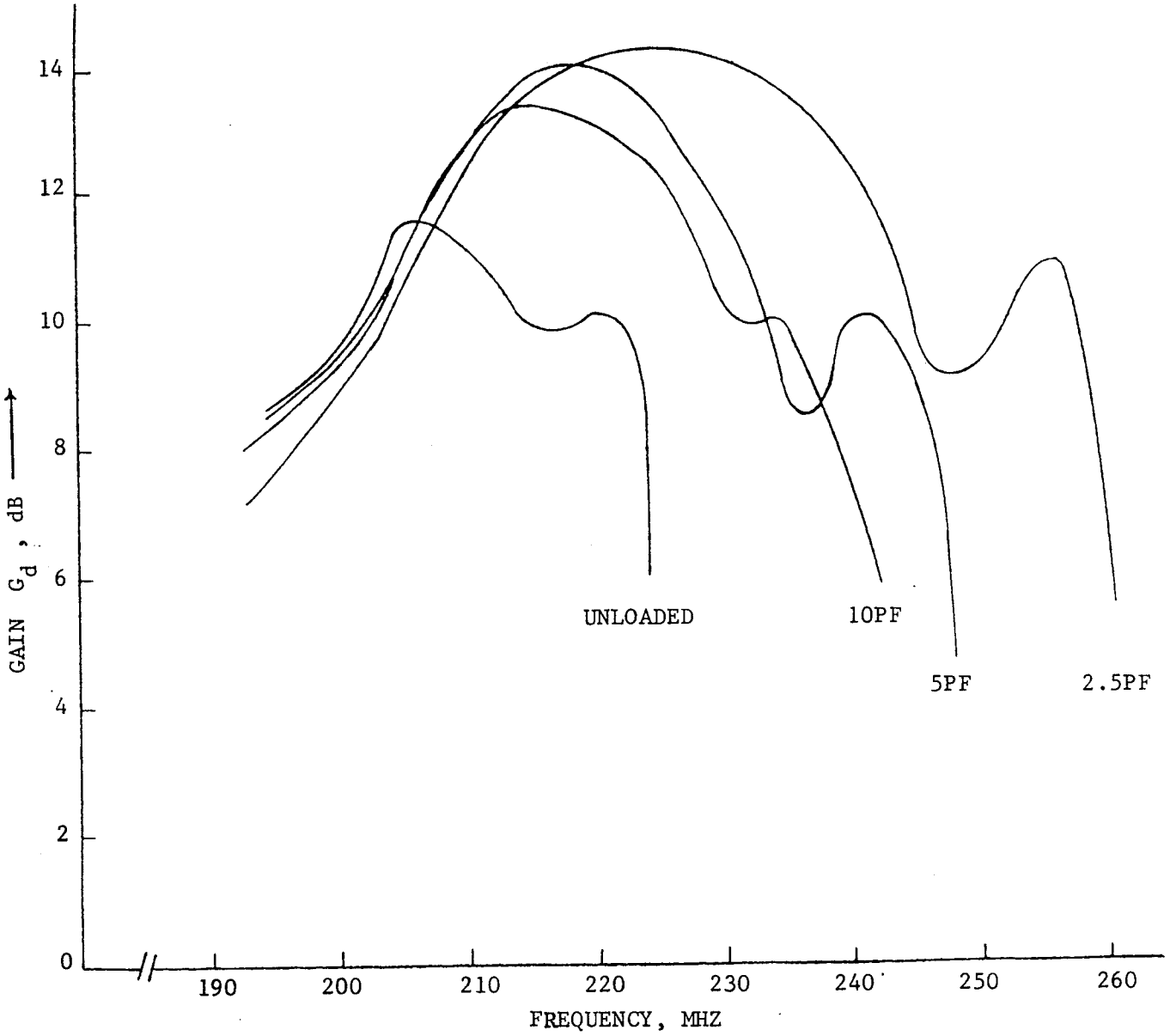

Fig. 2-5: Variation of the directive gain of a 14-element array with frequency for various director loadings. The size and spacing of the loops are the same as figure (2-4)

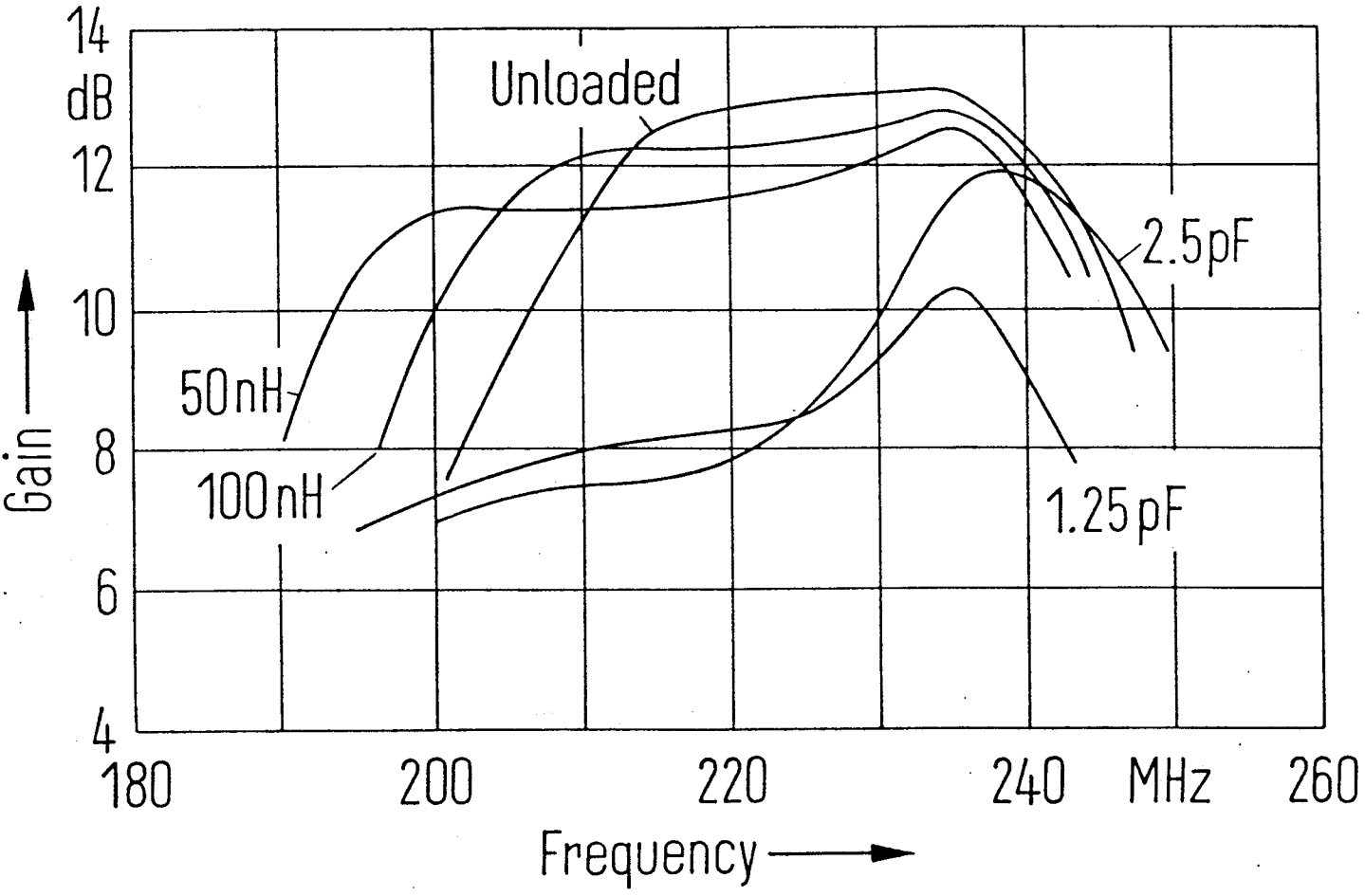

Fig. 2-6: Effect of various reflector loadings on the directive gain of a 10-element array as a function of frequency. Directors are loaded with 2.5 PF capacitor and b_1 = 22.75 cm, b_2 = 23.83 cm, b_i = 21.45 cm (i = 3, 4, ..., 10), b_2/a = 82.44

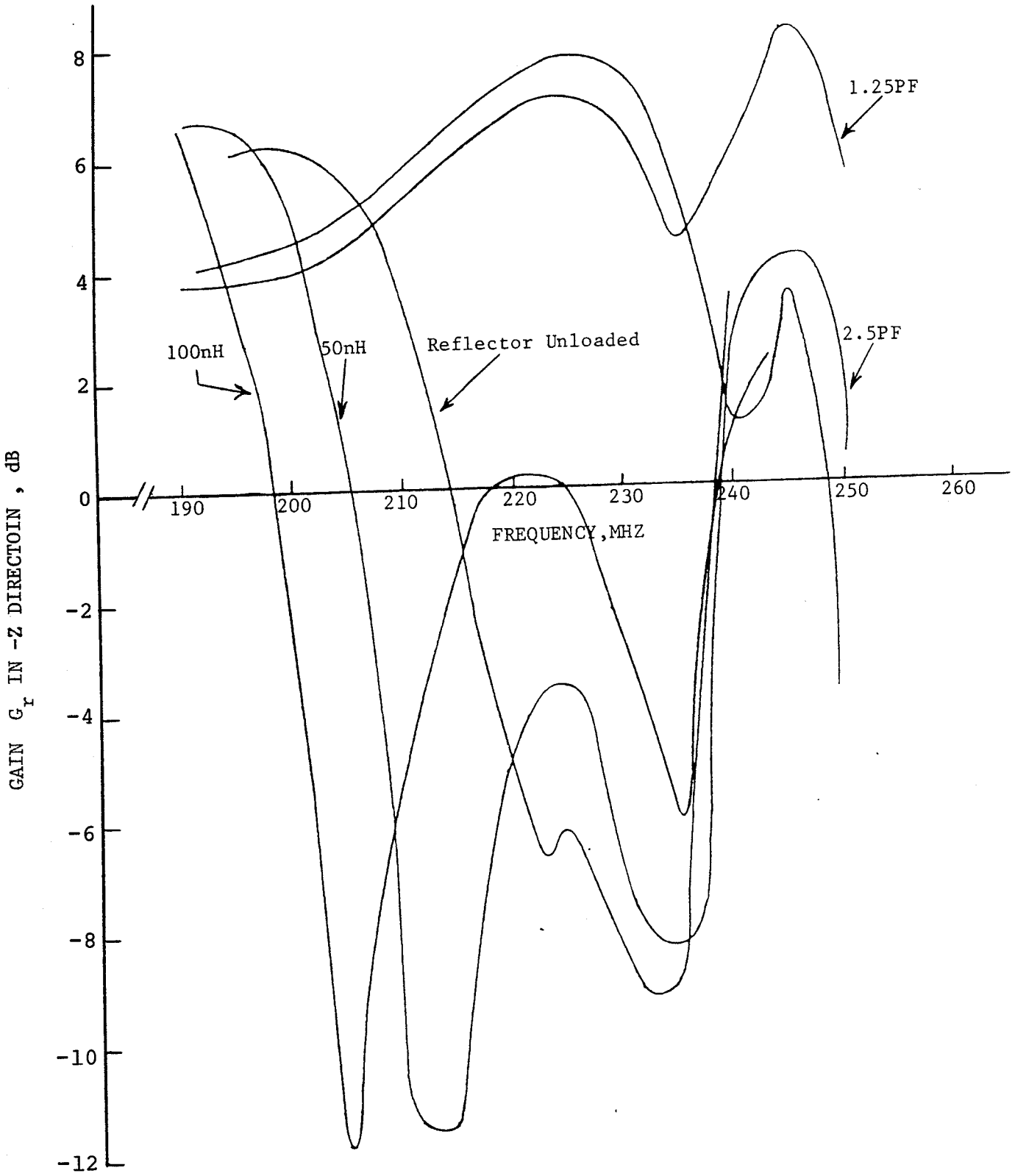

Fig. 2-7: Effect of various reflector loadings on backward gain of a 10-element array as a function of frequency. Directors are loaded with 2.5 PF capacitors. The geometry is the same as figure (2-6)

tends to reduce the low frequency cutoff and consequently increases the bandwidth of the array. In other words, the efficiency of the launching device, i.e., the combination of reflector and exciter, will be increased at lower frequency if the reflector is loaded properly. The reflector loading also reduces the gain of the array. For completeness the effects of reflector loading on backward radiation is studied in figure (2-7) which shows the directive gain of the array of figure (2-6) in -z-direction ($\theta = \pi$). It is seen that the back radiation for the array with its reflector loaded capacitively is comparable with its front directive gain given in figure (2-6). On the other hand, a comparison of figures (2-6) and (2-7) reveals that an inductively loaded reflector decreases the back radiation throughout the major part of the array's bandwidth shown in figure (2-6).

2.9 The Input Impedance

Figures (2-8) and (2-9) show the variation of the input impedance of a loaded Yagi loop array as a function of the frequency. From these figures, it is seen that the oscillations of both the resistance and the reactance of the unloaded array are shifted to higher frequencies as the capacitive loading is increased. The amount of shift is almost inversely proportional to the magnitude of the loading capacitors. The oscillations are also increased by increasing the capacitive loading. It was found that within the 3dB bandwidth the Q of the loaded array is smaller than that of the unloaded one.

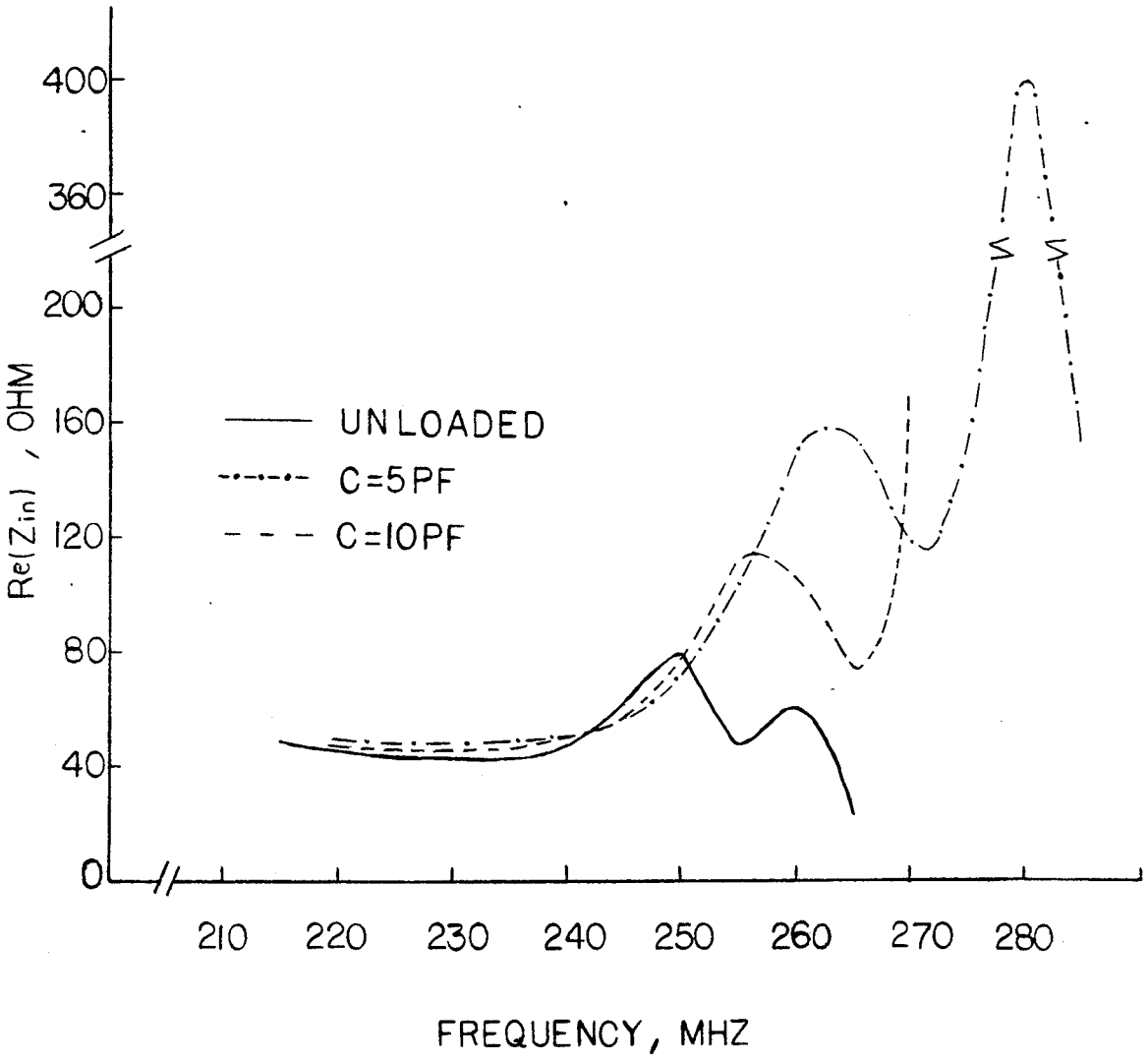

Fig. 2-8: Variation of the real part of the input impedance of an 8-element array with frequency for various director loadings. b_1 = 19.1 cm, b_2 = 20.0 cm, b_i = 18 cm (i = 3, 4, ..., 8), d = 25 cm and b_2/a = 38.94

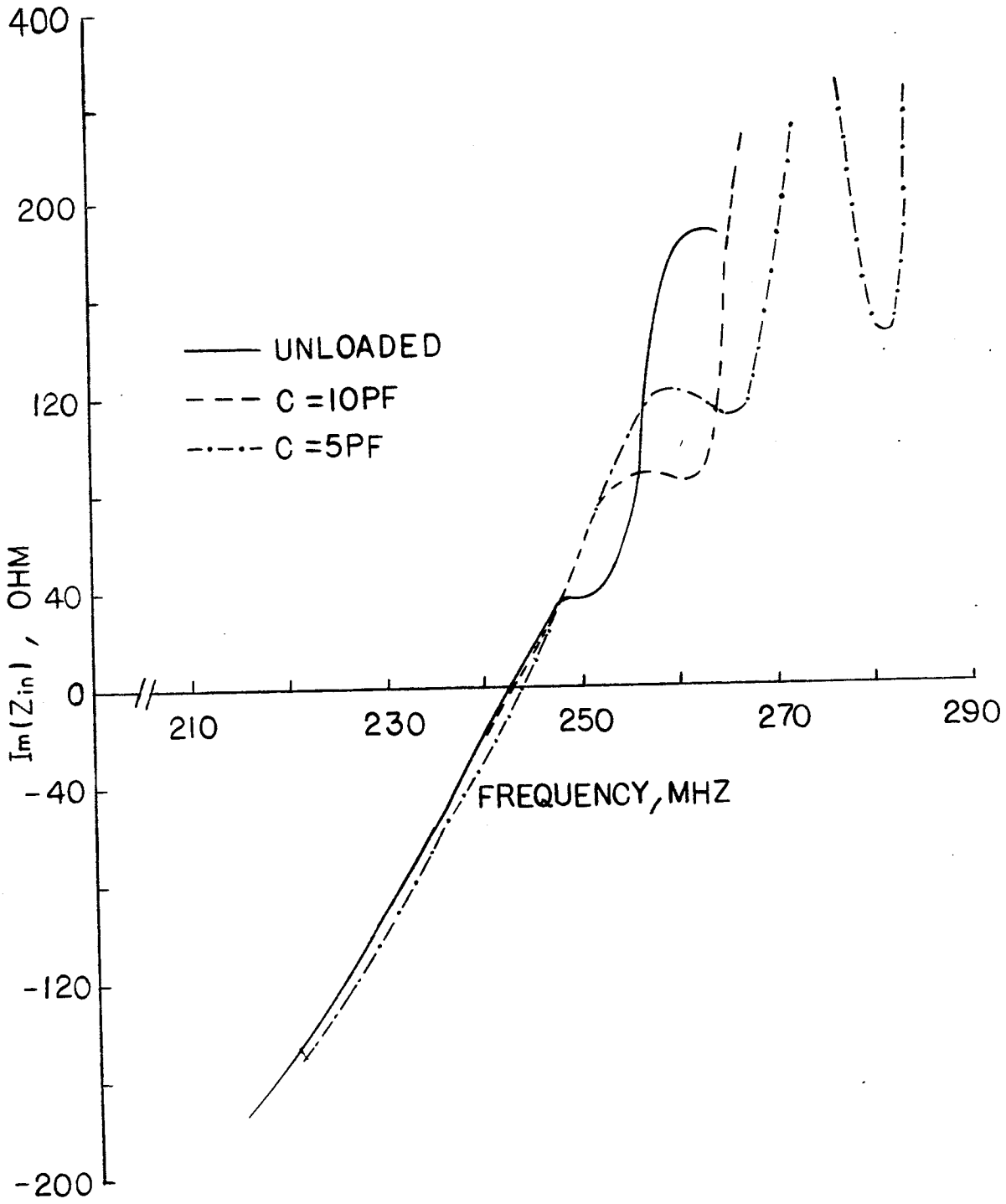

Fig. 2-9: Variation of the imaginary part of the input impedance of the 8-element array given in figure (2-8) with frequency

2.10 The Radiation Field

The radiation field of a loaded Yagi array can readily be found from equation (1.25) when the current distribution of the loaded elements are known [equation (2.36)]. Figure (2-10) compares the H-plane radiation field of a 10-element loaded Yagi array with that of the unloaded one. Only the directors are loaded (C = 2.5 PF) and the frequency of the signal is chosen to be 220 MHz at which the unloaded array is on the verge of cutoff, figure (2-4). It is seen that the radiation field of the unloaded array is deteriorated, but that of the loaded array has good directivity and its side lobe levels are very low. Also, from equation (1.25) it is evident that the E-plane pattern is symmetrical about the xz plane but the H-plane pattern is generally unsymmetrical about the yz plane.

Figure (2-11) compares the radiation field of the unloaded array of figure (2-4) with that of the same array when the reflector is inductively loaded (L = 100 nH). The frequency of the operating signal is 200 MHz and as figure (2-11) indicates, the array with unloaded reflector is outside its 3dB bandwidth. Although the main lobes for both patterns are almost the same, the back radiation of the array with unloaded reflector is in the same order as the main lobe. By adding an inductive load to the reflector, we have increased the efficiency of the launching device, i.e., the combination of the reflector and the exciter, and therefore, a higher gain and lower back lobe is obtained.

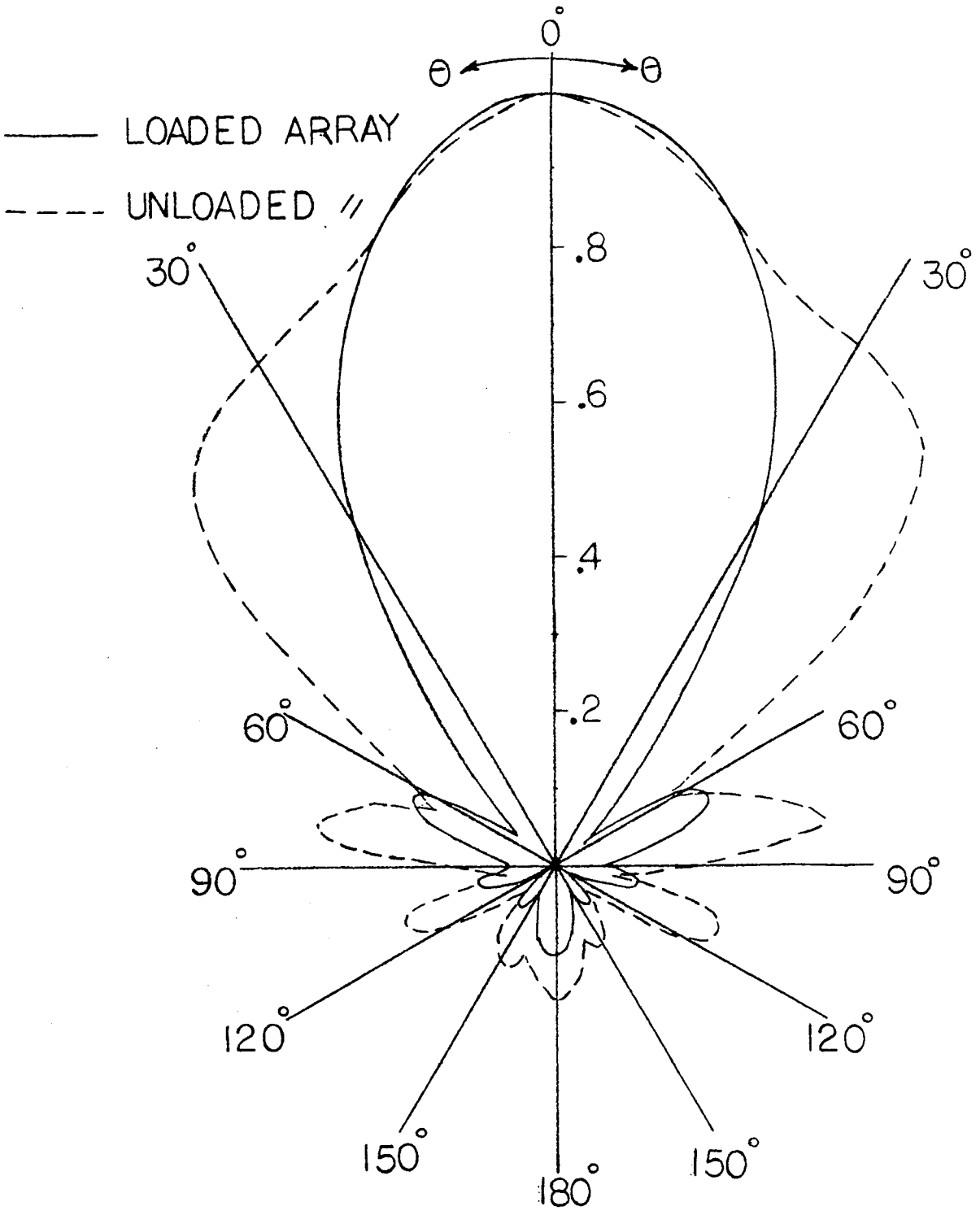

Fig. 2-10: Comparison of the H-plane radiation patterns of a 10-element array with that of unloaded one. The directors are only loaded (C = 2.5 PF), and f = 220 MHz. Geometry is the same as figure (2-4)

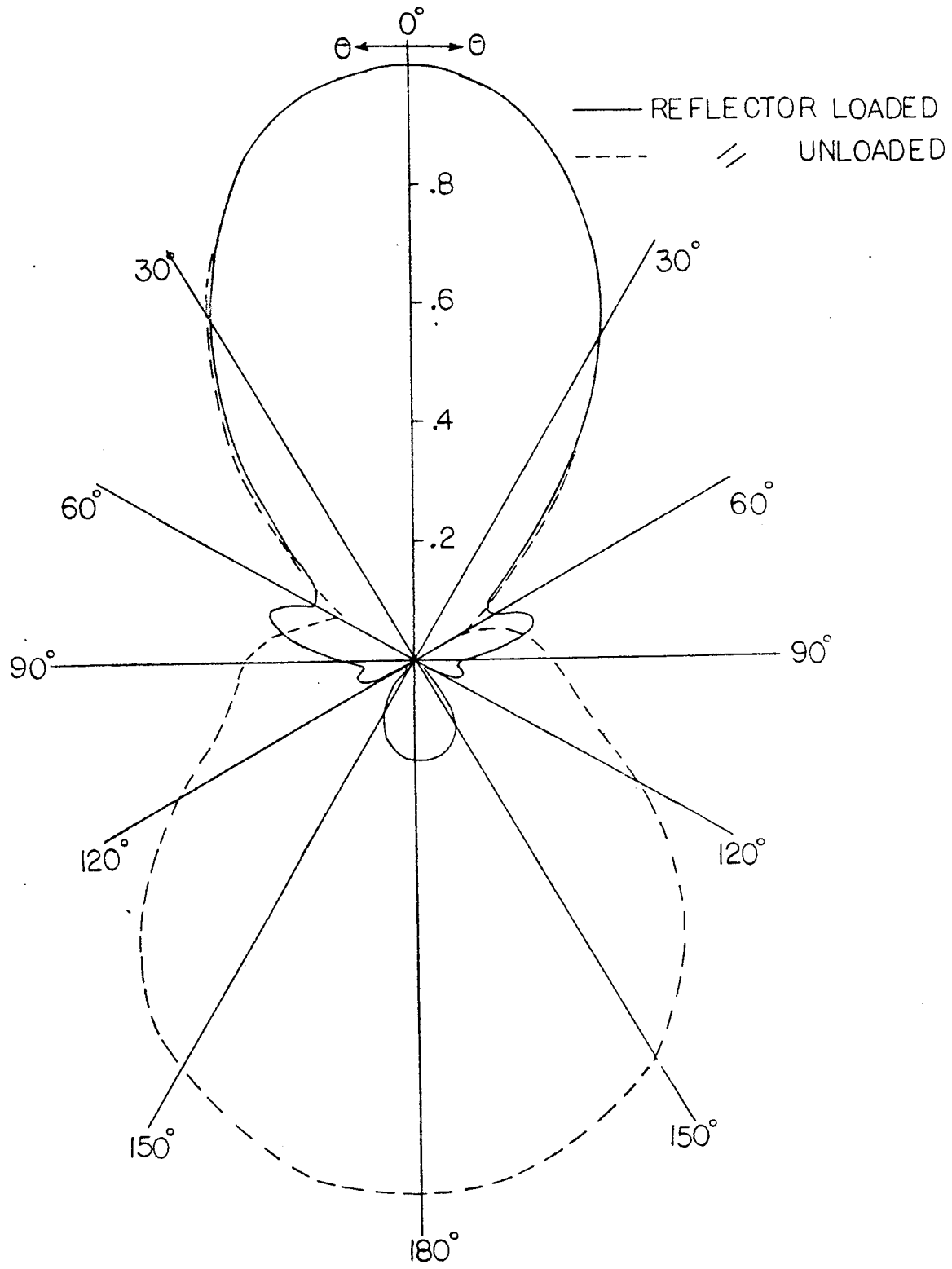

Fig. 2-11: Effect of the reflector loading on the H-plane radiation field of a 10-element array. Directors are loaded with C = 2.5 PF and f = 200 MHz. Geometry is the same as figure (2-4), reflector loading L = 100 nH

2.11 Discussions and Conclusions

The effects of capacitive and inductive loadings on the performance of infinite and finite loop arrays were investigated in this chapter. It was shown that capacitive loading increases the operating frequency range for a given phase velocity of the travelling wave along the structure and consequently increases the bandwidth of the array. A capacitive loading of the directors also increases the maximum gain of a coaxial Yagi loop array. An inductive loading of the directors was found to have opposite effects.

It was shown that the loading of the reflector has negligible effects on the high frequency cutoff of the array, but affects the low frequency cutoff significantly. An inductive loading of the reflector reduces the low frequency cutoff and consequently, further increases the array bandwidth. Thus, to increase the gain bandwidth of a coaxial Yagi-loop array, it is recommended that the directors and the reflector to be loaded by capacitive and inductive loads, respectively.

The results presented in this chapter can be explained physically [37]. An unloaded parasitic reflector, generally, reflects part of the primary field of the driven element, which undergoes a phase change of approximately 180°. However, a reinforcement of the radiation field in the forward direction occurs at reflector to excitor separations smaller than a quarter of a wavelength [16]. This is due to the fact that the antenna induction field also affects the phase distribution. In addition, the phase distribution along the

array may also be adjusted by altering the geometrical dimensions of the parasitic loops. For $kb < 1$ ($kb > 1$) loops are capacitive (inductive) and their currents lead (lag) the excitation voltage. Thus, for a directive antenna, directors (reflector) must be shorter (longer) than one wavelength. In such an array, if the frequency is increased, the directors may become greater than one wavelength in circumference and the array ceases to be directive. However, by a proper series capacitive loading of the loops, their currents can have phase relationships similar to small capacitive loops. In other words, by a proper capacitive loading the loop currents for $kb > 1$ act similar to those of the $kb < 1$ case and the array can support a travelling wave. Therefore, capacitive loading increases the operating bandwidth. In contrast to the optimum bandwidth of an unloaded array, this increase in the bandwidth is not limited as long as we can provide a suitable load. That is, by means of impedance loading, at least theoretically, any bandwidth can be obtained.

CHAPTER III

MULTIPLY-DRIVEN AND LOADED COAXIAL CIRCULAR LOOP ARRAYS

3.1 Introduction

The analysis presented thus far has been restricted to single-loaded or driven coaxial loop arrays. In this chapter multiply-driven and loaded arrays are investigated. Initially, the array loops are excited by arbitrary sources at two symmetrical points with respect to the array axis. The principle of superposition is applied and expressions for the current distributions and the input admittances are obtained. To investigate the loading effects, one of the sources on each loop is replaced by a lumped load of finite length and a new expression for the current distribution is obtained. Finally, all sources except on the qth element, which excites the array, are replaced by lumped loads of small length.

The presentation essentially has the same format as that given in the last two sections. That is, for finite gaps at the driving-points and finite lengths of the loads integral equations for the loop currents are obtained. These integral equations are then reduced to a matrix equation by expanding the currents and the kernel in Fourier series of the azimuthal coordinate. The contribution from each set of sources located at similar points are then treated separately.

3.2 Formulation of the Problem

Consider the array of figure (3-1), which is actually the same array as given in figure (1-1), except that the former is also driven at $\phi = \pi$. The sources at $\phi = 0$ and π are denoted by V_i^0 and V_i^π, respectively. The application of boundary conditions on the surfaces of the loops gives the following integral equations for the currents

$$\frac{V_i^0}{b_i \delta\phi_i} U_i(\Phi_i) + \frac{V_i}{b_i \delta\phi_i} U_i(\phi_i - \pi) = \frac{j\eta_o}{4\pi b_i} \sum_{j=1}^{N} \int_0^{2\pi} \{kb_j \cos(\phi_i - \phi_j') + \frac{1}{kb_i} \frac{\partial^2}{\partial\phi_i^2}\} W_{ij}(\phi_i - \phi_j') I(\phi_j') d\phi_j' \tag{3.1}$$

where all parameters are as defined in Chapter I. It is noted that except for the second term on the left hand side (3.1) is similar to (1.1) and therefore, its solution can be obtained in a similar manner. The Fourier expansion of the currents and kernel $W_{ij}(\phi)$ are substituted in (3.1) and after some manipulation one obtains

$$\beta_i'^n + \beta_i''^n = \sum_{j=1}^{N} Z_{ij}^n I_j^n \quad , \quad \begin{matrix} i = 1, 2, \ldots, N \\ n \geq 0 \end{matrix} \tag{3.2}$$

where

$$\beta_i'^n = V_i^0 \frac{\sin(n\delta\phi_i/2)}{n\delta\phi_i/2} \tag{3.2}'$$

$$\beta_i''^n = V_i^\pi \frac{\sin(n\delta\phi_i/2)}{n\delta\phi_i/2}$$

and Z_{ij}^n is as defined in (1.10). Equation (3.2) can be written in the following matrix form

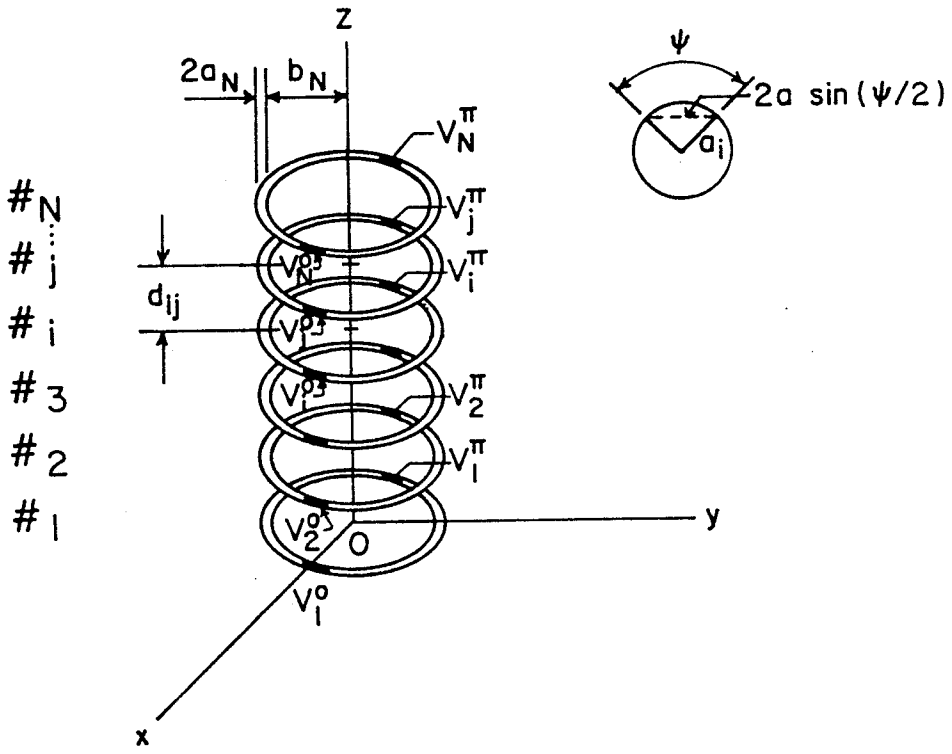

Fig. 3-1: Geometry of the array

$$[Z^n_{ij}][I^n_j] = [\beta_i^{'n}] + [\beta_i^{"n}] \qquad n \geq 0 \qquad (3.3)$$

If (y^n_{ij}) is the inverse of (Z^n_{ij}), then the total current on the ith element may be shown to be

$$I_i(\phi_i) = \sum_{n=0}^{\infty} \sum_{j=1}^{N} y^n_{ij} \beta_i^{'n} \cos n\phi_i + \sum_{n=0}^{\infty} \sum_{j=1}^{N} y^n_{ij} \beta_i^{"n} \cos n\phi_i \qquad (3.4)$$

where the first term on the right hand side of (3.4) is the contribution of the sources at $\phi = 0$, and the second term is due to V_i^{π}. The computation of the currents due to the first term has been discussed previously. We therefore, now consider the simplification of the second term.

3.3 Simplification of the Infinite Series in Equation (3.4)

If m_o is an integer as defined in Chapter I, and (y^n_{ij}) is the inverse of the impedance matrix (Z^n_{ij}), then the second term in (3.4) reduces to

$$\sum_{n=0}^{\infty} \sum_{j=1}^{N} y^n_{ij} \beta_j^{"n} \cos n\phi_i = \sum_{n=0}^{m_o} \sum_{j=1}^{N} y^n_{ij} \beta_j^{"n} \cos n\phi_i +$$

$$\sum_{n=m_o+1}^{\infty} \frac{\beta_i^{"n}}{Z^n_{ii}} \cos n\phi_i \qquad (3.5)$$

for the values of n for which the approximation (1.17) is valid, the infinite summation in (3.5) becomes

$$\sum_{n=m_o+1}^{\infty} \frac{\beta_i^{"n}}{Z^n_{ii}} \cos n\phi_i = \sum_{n=m_o+1}^{n_i} \frac{\beta_i^{"n}}{Z^n_{ii}} \cos n\phi_i +$$

$$\frac{j4ka_i}{\eta_o} \sum_{n=n_i+1}^{\infty} \beta_i^{"n} \frac{\cos n\phi_i}{n} \qquad (3.6)$$

Substituting (3.2)′ into the infinite summation (3.6) simplifies to

$$\sum_{n=n_i+1}^{\infty} \frac{\beta''^n}{n} \cos n\phi_i = \frac{V_i^{\pi}}{\delta\phi_i} \left[\sum_{n=1}^{\infty} \frac{2(-1)^n \sin(n\delta\phi_i/2)\cos n\phi_i}{n^2} - \sum_{n=1}^{n_i} \frac{2(-1)^n \sin(n\delta\phi_i/2)\cos n\phi_i}{n^2} \right] \tag{3.7}$$

The infinite summation in (3.7) may be written as

$$\sum_{n=1}^{\infty} (-1)^n \frac{2\sin(n\delta\phi_i/2)\cos n\phi_i}{n^2} = \sum_{n \text{ even}}^{\infty} \left[\frac{\sin n(\phi_i + \delta\phi_i/2)}{n^2} - \frac{\sin n(\phi_i - \delta\phi_i/2)}{n^2} \right] - \sum_{n \text{ odd}}^{\infty} \left[\frac{\sin n(\phi_i + \delta\phi_i/2)}{n^2} - \frac{\sin n(\phi_i - \delta\phi_i/2)}{n^2} \right] \tag{3.8}$$

The above infinite summations are given in closed form as [33]

$$\sum_{n=1,3,\ldots}^{\infty} \frac{\sin(nx)}{n^2} = -\frac{1}{2}\left(x \ln x/2 - x + x^3/36 + \frac{7x^5}{7200} + \ldots\right) \qquad 0 < x < \pi \tag{3.9}$$

$$\sum_{n=1}^{\infty} \frac{\sin nx}{n^2} = -\left(x \ln x - x - \frac{x^3}{72} - \frac{x^5}{14{,}400} - \ldots\right) \qquad 0 < n < 2\pi \tag{3.10}$$

Therefore, subtracting (3.9) from (3.10) gives

$$\sum_{n=2,4}^{\infty} = \sum_{1}^{\infty} - \sum_{1,3,\ldots}^{\infty} = -\frac{1}{2}\left(x \ln 2x - x - \frac{x^3}{18} - \frac{4x^5}{14{,}400}\right) \tag{3.11}$$

from (3.11) and (3.9) we obtain

$$\sum_{n\ \text{even}}^{\infty} \frac{\sin nx}{n^2} - \sum_{n\ \text{odd}}^{\infty} \frac{\sin nx}{n^2} = -x \ln 2 + \frac{3}{72} x^3 + \frac{15\, x^5}{14{,}400} \cdots \tag{3.12}$$

Substituting (3.12) in (3.8) for $x = \phi_i + \delta\phi_i/2$ and $x = \phi_i - \delta\phi_i/2$ yields

$$\sum_{n=1}^{\infty} (-1)^n \frac{2 \sin(n\ \delta\phi_i/2) \cos n\phi_i}{n^2} = -\delta\phi_i \ln 2 \ldots, \quad \text{for} \quad |\phi_i| << 1 \tag{3.13}$$

Using (3.13) along with the assumption

$$\frac{\sin\ (n\ \delta\phi_i/2)}{n\ \delta\phi_i/2} \simeq 1 \qquad \text{for} \quad n \leq n_i \tag{3.14}$$

reduces (3.5) to

$$\sum_{n=0}^{\infty} \sum_{j=1}^{N} y_{ij}^n\ \beta_j^{"n} \cos(n\phi_i) = \sum_{n=0}^{m_o} \sum_{j=1}^{N} y_{ij}^n\ (-1)^n\ V_j^{\pi} \cos(n\phi_i) +$$

$$+ \sum_{n=m_o+1}^{n_i} \frac{V_i^{\pi}}{Z_{ii}^n} (-1)^n \cos n\phi_i - \frac{j4ka_i}{\eta_o}\ V_i^{\pi} \left[\ln 2 + \sum_{n=1}^{n_i} \frac{(-1)^n}{n} \right] \tag{3.15}$$

Equation (3.15) together with the contribution from V_i^0 in equation (3.3) may be used to obtain the input current at $\phi_i \simeq 0$ (or π) which is given by

$$I_i = \sum_{n=0}^{m_o} \sum_{j=1}^{N} [V_j^0 + (-1)^n\ V_j^{\pi}]\ y_{ij}^n +$$

$$\sum_{n=m_o+1}^{n_i} \frac{[V_i^0 + (-1)^n\ V_i^{\pi}]}{Z_{ii}^n} + j\omega\bar{\theta}\ [C_{gi}'\ V_i^0 - C_{gi}''\ V_i^{\pi}] \tag{3.16}$$

where C_{gi}' is the gap capacitance at $\phi_i = 0$ as defined in (1.21) and C_{gi}'' could be considered as the effect of the

fringe capacitance at $\phi = \pi$ transferred to $\phi = 0$ and is defined as

$$C''_{gi} = 2\,\varepsilon_o a_i \left[\ln 2 + \sum_{n=1}^{n_i} \frac{(-1)^n}{n}\right] \tag{3.17}$$

$\bar{\theta}$ in equation (3.16) is equal to unity for the input current at $\phi = 0$ and is equal to -1 for the input current at $\phi = \pi$. The role and magnitude of C'_{gi} and C''_{gi} are also interchanged when determining the input current at $\phi = \pi$.

Neglecting the third term in (3.16) does not affect the current distribution, since the gap capacitance is confined to the vicinity of the driving point. Hence,

$$I_i(\phi_i) = \sum_{n=0}^{m_o} \sum_{j=1}^{N} y_{ij}^n \left[V_j^0 + (-1)^n V_j^\pi\right] \cos n\phi_i + \sum_{n=m_0+1}^{n_i} \frac{\left[V_i^0 + (-1)^n V_i^\pi\right]}{Z_{ii}^n} \cos n\phi_i \tag{3.18}$$

Notice that when $V_j^0 = V_j^\pi$, all odd modes cancel and the even modes are twice as large as those of a singly driven array. For $V_j^0 = -V_j^\pi$ the situation is reversed. The radiation field and the directive gain of the array can be obtained from similar formula as given in Chapter I.

3.4 Array Excited at $\phi = 0$ and Loaded at $\phi = \pi$

Now that the array current for a doubly-excited array is known, the currents of a loaded array can be obtained by using the compensation theorem. Let each loop in figure (3-1) be loaded by a lumped load Z_{Li}^π at $\phi = \pi$, be excited

by a source V_i^0 at $\phi = 0$, and let $I_i(\phi)$ be the current on the ith element. The current distribution on the loaded array is calculated by applying the compensation theorem. Therefore, each load at $\phi = \pi$ could be replaced by a generator with potential difference equal to $-I_i(\pi)\ Z_{Li}^{\pi}$. With this equivalent representation of the load Z_{Li}^{π}, it is immediately evident that the method developed in the previous section is applicable to this array. An expression for $I_i(\phi_i)$ can be obtained by using $V_j^{\pi} = -Z_{Lj}^{\pi}\ I_j(\pi)$ in equation (3.18) and solving the equation for $I_i(\pi)$, which gives

$$I_i(\pi) = \sum_{n=0}^{m_o} \sum_{j=1}^{N} [(-1)^n\ y_{ij}^n\ V_j^0 - y_{ij}^n\ Z_{Lj}^{\pi}\ I_j(\pi)] + \sum_{n=m_o+1}^{n_i} \frac{1}{Z_{ii}^n} [(-1)^n\ V_i^0 - Z_{Li}^{\pi}\ I_i(\pi)] \quad ; \quad i = 1, 2, \ldots, N \tag{3.19}$$

The above equation can be rearranged as

$$[1 + Z_{Li}^{\pi} \sum_{n=m_o+1}^{n_i} \frac{1}{Z_{ii}^n}]\ I_i(\pi) + \sum_{n=0}^{m_o} \sum_{j=1}^{N} y_{ij}^n\ Z_{Lj}^{\pi}\ I_j(\pi) = \sum_{n=0}^{m_o} \sum_{j=1}^{N} (-1)^n\ y_{ij}^n\ V_j^0 + V_i^0 \sum_{n=m_o+1}^{n_i} \frac{(-1)^n}{Z_{ii}^n}$$

This equation may be used to set up a matrix equation for the currents $I_i(\pi)$ of the form

$$[\phi_{ki}][I_i(\pi)] = [\gamma_k] \tag{3.20}$$

where $[I_i(\pi)]$ and $[\gamma_k]$ are N x 1 column matrices. The elements of $[I_i(\pi)]$ represent the current $I_i(\pi)$ and those of $[\gamma_k]$ are given by

$$\gamma_k = \sum_{n=0}^{m_o} \sum_{j=1}^{N} y_{kj}^n (-1)^n V_j^0 + V_k^0 \sum_{n=m_o+1}^{n_k} \frac{(-1)^n}{Z_{kk}^n} \qquad (3.21)$$

the matrix $[\phi_{ki}]$ is an N x N matrix and its elements are given by

$$\phi_{ki} = (1 - \alpha_i)\delta_{ki} + Z_{Li}^{\pi} \sum_{n=0}^{m_o} y_{ki}^n \qquad (3.22)$$

where

$$\alpha_i = Z_{Li}^{\pi} \sum_{n=m_o+1}^{n_i} \frac{(-1)^n}{Z_{ii}^n} \qquad (3.23)$$

and δ_{ki} is the Kronecker delta function. When $I_i(\pi)$ is known one can readily find the current modes I_i^n from

$$I_i^n = \sum_{j=1}^{N} y_{ij}^n [V_j^0 - (-1)^n Z_{Lj}^{\pi} \cdot I_j(\pi)] \text{ for } n \leq m_o \qquad (3.24)$$

and the remaining antenna characteristics can be found as explained in the previous chapters.

3.5 Yagi Arrays Loaded Both at $\phi = 0$ and $\phi = \pi$

If the array is loaded both at $\phi = 0$ and π, except for the qth element, we will have the familiar Yagi array with loaded elements. Let Z_{Li}^0 and Z_{Li}^{π} be the loads at $\phi = 0$ and π on the ith element. In addition, let the qth element be excited at $\phi = 0$ and loaded at $\phi = \pi$. Following the procedure explained in the last section, equation (3.18) changes to

$$I_i(\phi_i) = \sum_{n=0}^{m_o} y_{iq}^n V_q^0 \cos n\phi_i - \sum_{n=0}^{m_o} \sum_{j=1}^{N} [(1 - \delta_{qj}) Z_{Lj}^0 I_j(0) +$$

$$(-1)^n Z^{\pi}_{Lj} I_j(\pi)] y^n_{ij} \cos n\phi_i + \sum_{n=m_o+1}^{n_i} \frac{-1}{Z^n_{ii}} [(1 - \delta_{qi}) Z^0_{Li} I_i(0) +$$

$$+ (-1)^n Z^{\pi}_{Li} I_i(\pi)] \cos n\phi_i + \delta_{qi} \sum_{m_o+1}^{n_i} \frac{V^0_i}{Z^n_{ii}} \cos n\phi_i \qquad (3.25)$$

To solve the above equation for $I_i(0)$ and $I_i(\pi)$, one may write (3.25) at $\phi = 0$ and π in order to obtain 2N equations for 2N unknown currents $I_i(0)$ and $I_i(\pi)$. In the matrix form, this can be represented as

$$\begin{bmatrix} [f_{ui}] & [\phi_{vi}] \\ [\psi_{uj}] & [g_{vj}] \end{bmatrix} \begin{bmatrix} I_i(0) \\ I_j(\pi) \end{bmatrix} = \begin{bmatrix} [\zeta_i] \\ [\zeta'_j] \end{bmatrix} \qquad (3.26)$$

where $[I_i(0)]$, $[I_j(\pi)]$, $[\zeta_i]$ and $[\zeta'_j]$ are again N x 1 matrices with their elements respectively given by $I_i(0)$, $I_j(\pi)$ for $i,j = 1, 2, \ldots, N$

$$\zeta_i = V^0_q \left[\sum_{n=0}^{m_o} y^n_{iq} + \delta_{iq} \sum_{n=m_o+1}^{n_i} 1/Z^n_{qq} \right]$$

$$\zeta'_j = V^0_q \left[\sum_{n=0}^{m_o} (-1)^n y^n_{jq} + \delta_{jq} \sum_{n=m_o+1}^{n_j} (-1)^n/Z^n_{qq} \right]$$

The submatrices $[f_{uj}]$, $[\phi_{vi}]$, $[\psi_{uj}]$ and $[g_{vj}]$ are N x N matrices and their elements are given by (for $u,v = 1, 2, \ldots, N$)

$$f_{ui} = [1 + \alpha_u (1 - \delta_{uq}) Z^0_{Lu}] \delta_{ui} + Z^0_{Li}(1 - \delta_{iq}) \sum_{n=0}^{m_o} y^n_{ui}$$

$$\psi_{uj} = \gamma_u(1 - \delta_{uq}) Z^0_{Lu} \delta_{uj} + Z^0_{Lj}(1 - \delta_{jq}) \sum_{n=0}^{m_o} y^n_{uj} (-1)^n$$

$$\phi_{vi} = \gamma_v Z^{\pi}_{Lv} \delta_{vi} + Z^{\pi}_{Li} \sum_{n=0}^{m_o} y^n_{vi} (-1)^n$$

$$g_{vj} = (1 + \alpha_v Z^{\pi}_{Lj})\,\delta_{vj} + Z^{\pi}_{Lj} \sum_{n=0}^{m_o} y^n_{vj}$$

where

$$\alpha_v = \sum_{W=m_o+1}^{n_i} 1/Z^W_{vv} \quad , \quad \gamma_v = \sum_{k=m_o+1}^{n_i} \frac{(-1)^k}{Z^k_{vv}}$$

once the currents $I_i(0)$ and $I_i(\pi)$ are known, the current modes I^n_i can readily be determined other antenna characteristics can similarly be obtained.

It may appear simpler to use the N inhomogeneous equations in (3.3) directly to obtain the current modes I^n_i instead of 2N inhomogeneous equations in (3.26), which gives the total currents $I_i(0)$ and $I_i(\pi)$. However, for a given array, equation (3.26) provides the required total current, while equation (3.3) gives only the modal currents I^n_i. Therefore, equation (3.3) must be solved many times in order to find the total array current, which may require extensive computer time. Equation (3.26) may also have time-saving advantages when array characteristics for different loads are being considered. Its solution, however, gives the total current $I_i(0)$ and $I_i(\pi)$. If the modal currents I^n_i are required, such as in field or gain calculations, they can be obtained readily from an equation similar to equation (3.24) by replacing any source V^0_j with $-Z^0_{Lj}\, I_j(0)$, [38].

3.6 Results and Discussions

Based on the theory presented in this chapter, the properties of multiple driven and loaded loop arrays can be investigated. However, the most interesting circular loop array is the well known Yagi-Uda array in which only the second element is excited. For this reason, only the

properties of these types of antennas are reported here.

To investigate the effects of the loading on the antenna characteristics an 8-element array is chosen, where all directors are loaded with equal loads at $\phi = 0$ and π. The exciter and the reflector are assumed to be unloaded. The variation of the directive gain with frequency and for various capacitive loading is shown in figure (3-2). Similar to the array with single loads shown in figure (2.4), a capacitive (inductive) loading generally increases (decreases) the bandwidths of the array. For example, when directors are loaded by 2.5 PF capacitors, the 3dB bandwidth is over 70 MHZ which corresponds to an approximate 350% increase over that of the unloaded array. By loading the array at $\phi = 0$ location, it was found that the frequency dependence of the array gain becomes identical to that of a doubly loaded one, when the loading capacitors are twice as large. This behaviour can readily be understood by using the travelling wave approach explained in the previous chapter. Applying the method to the doubly loaded array, we will have the sum of the loads at $\phi = 0$ and π in the right hand side of equation (2.3). Hence, the frequency range over which the noramlized phase velocity remains almost constant - and, therefore, the gain remains unchanged - is twice as large as that of a single loaded one for $Z_L^0 = Z_L^\pi$ [39]. This has also been proved in Appendix IIIA for finite arrays.

The variation of the input admittance of the above doubly loaded array with frequency is given in figure (3-3).

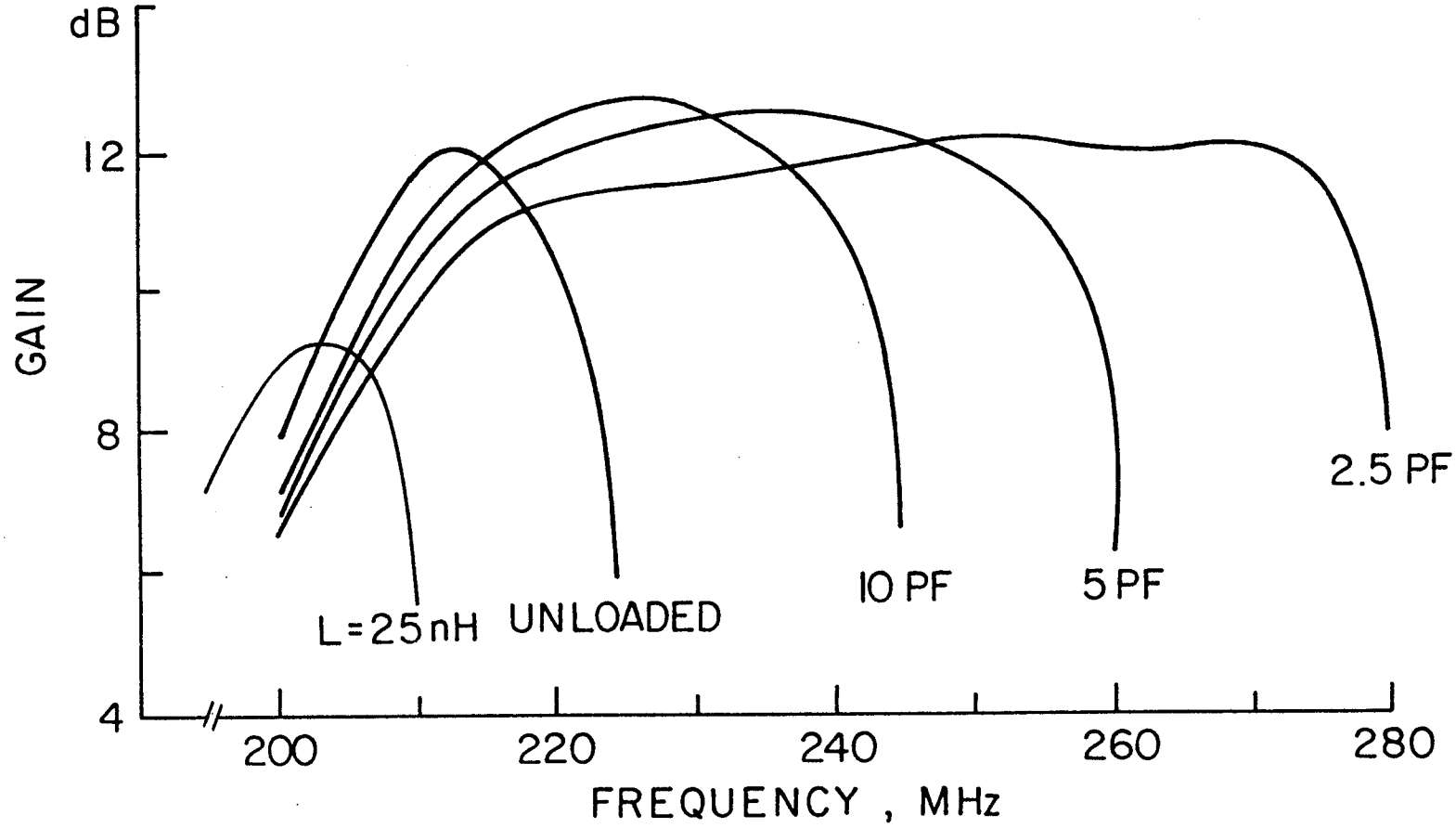

Fig. 3-2: Directive gain of an 8-element array loaded at $\phi = 0$ and π. $b_1 = 22.75$ cm, $b_2 = 23.8$ cm, $b_i = 21.45$ cm ($i = 3, 4, \ldots, 8$), element spacing = 21.45 cm, and $\Omega_2 = 2 \ln(2\pi b_2/a) = 12$. Only the directors are loaded.

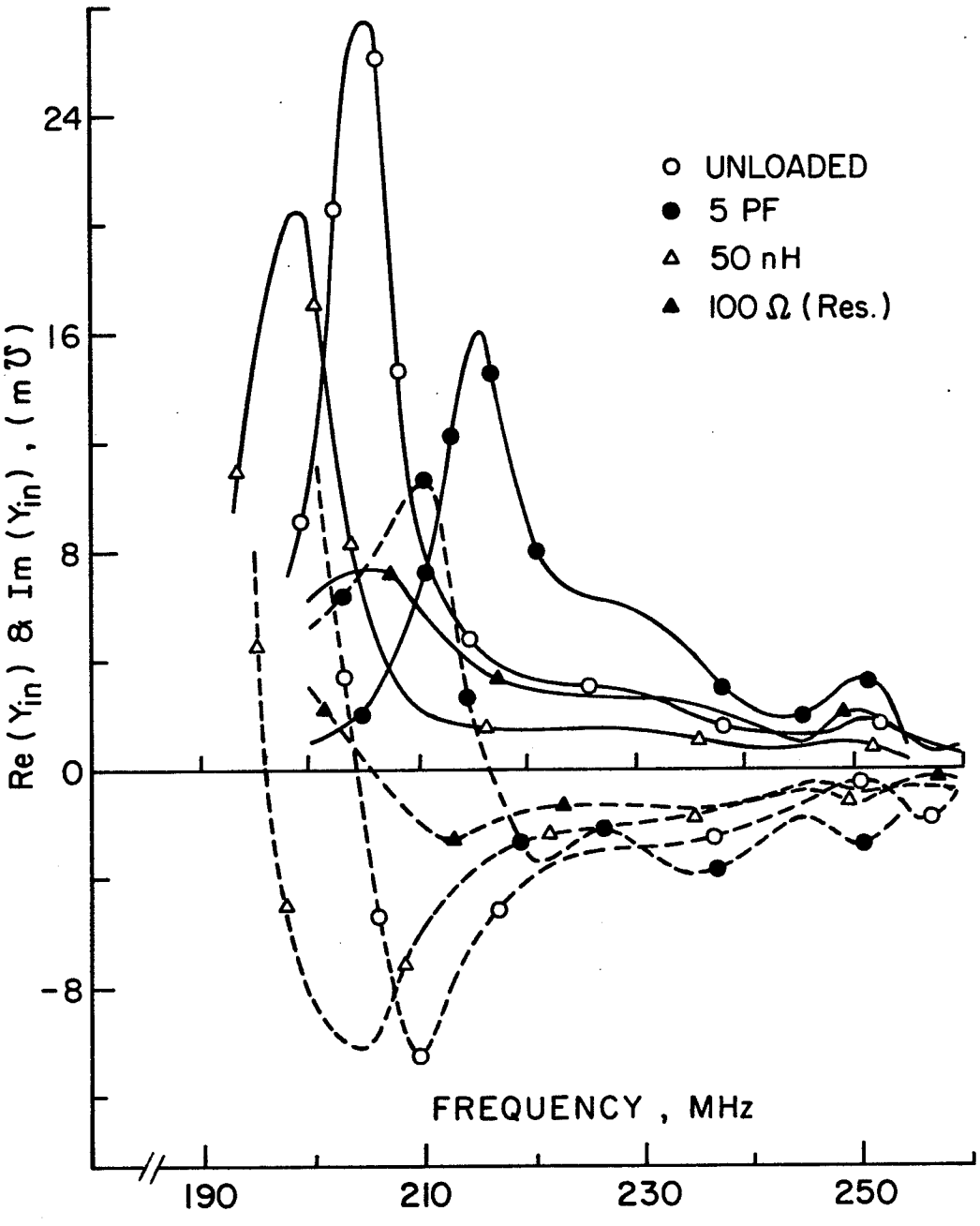

Fig. 3-3: Input impedance of an 8-element array as a function of frequency. The directors are loaded with C = 5 PF at ϕ = 0 and π and the exciter loading at $\phi = \pi$ is the parameter. The geometry is the same as in figure (3-2). ——— real part, ------ imaginary part.

The directors are loaded by $C = 5$ PF capacitors and the exciter loading at $\phi = \pi$ is the parameter. It is interesting to see that resistive loading of the exciter gives relatively smooth behaviour for the input admittance through the entire 3dB bandwidth of the array. Although an inductive loading of the exciter also gives constant input admittance, its real part is always smaller than the imaginary part within the 3dB bandwidth. Notice that for a capacitively (or inductively) loaded exciter, the first maxima of $Re(Y_{in})$ shifts to the right (or left) of the unloaded case. A resistive loading does not result in any shift, but does lead to a damping effect. Beyond the maximum peak, the real part remains at the level of the unloaded case. It was found that the damping effect increases with increasing resistive loading. It was also noticed that with a resistive loading of the exciter, the gain of the array remains relatively unchanged. This is due to the fact that for long arrays the radiation results predominantly from the currents on the directors and the exciter current has only small effects. Figure (3-4) compares the magnitude of the current distribution on a loaded exciter ($R = 100\Omega$) with that of an unloaded one. It is clear that the variation of the current on the loaded exciter is much smoother than that of the unloaded exciter. This indicates a travelling type current distribution and consequently, the array input admittance is less sensitive to the frequency variation.

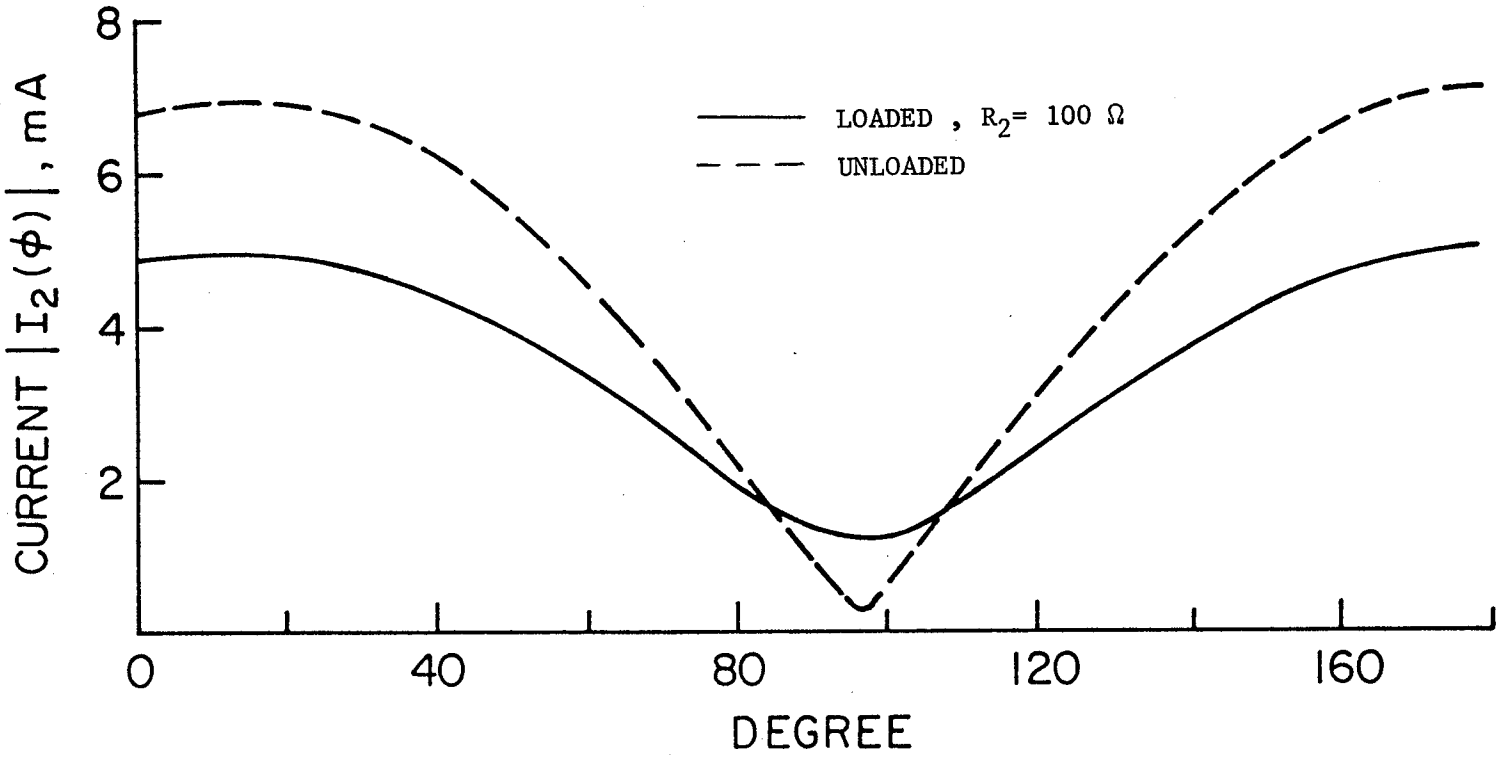

Fig. 3-4: The distribution of current on exciter of an 8-element array with and without lumped resistive loading. The directors are loaded with C = 5 PF at $\phi = 0$ and π. The geometry is the same as in figure (3-2)

3.7 Conclusion

In this chapter the effects of double loading on the performance of circular loop arrays were investigated. The analysis of the results revealed that to increase the gain bandwidth product of a Yagi loop array, the directors must be loaded capacitively. It was shown in the previous chapter that the loading of the reflector inductively reduces the low frequency cutoff and consequently further increases the array's bandwidth. For multi-loadings of the reflector a similar effect is also expected.

If a relatively smooth variation of the input admittance is required, the exciter may then be loaded resistively. This does not deteriorate the efficiency of the antenna significantly, as long as the resistive loading is not too large. This is due to the fact that the radiation of the array is mostly due to the currents on the directors.

The results also showed that the loading of the array at $\phi = 0$ and $\phi = \pi$, have equivalent effects. Because of this equivalence of the loads, it may seem unnecessary to load the array at two separate locations. However, in view of the limitation on the available active loads (varactors) and their price range, it may become advantageous to use two separate loads to simulate a single one.

CHAPTER IV

CONTINUOUS IMPEDANCE LOADING OF LOOP ARRAYS

4.1 Introduction

The properties of circular loop antennas with lumped impedances were investigated in the last two chapters. This chapter is devoted to loop antennas with continuous impedance loading along their circumferences.

It has already been demonstrated for the cylindrical linear antennas that continuous impedance loading can be used to broaden the frequency response of the input impedance and far field pattern [40]-[43]. A single loop antenna with a continuous impedance loading has been studied by Lin [25] and Smith [26]. Lin examined the input impedance of the imperfectly conducting loop antennas by the numerical and the differential equation methods and showed that a uniform resistive loading could be used to achieve a broadband characteristic of the input impedance [25]. Smith analyzed a single loop antenna with a uniform resistive loading by the Fourier series method [26]. He also examined the effects of the resistive loading on the radiating efficiency and the far-zone field patterns of the antenna. In this chapter, the work is extended to arrays of coaxial circular loop antennas with distributed but arbitrary impedance loading. The numerical results are given for the distributed uniform resistive and tapered reactive loadings which are of practical interest.

Also, the validity of the assumption of inifinite conductivity for materials such as Aluminum and Copper is examined.

4.2 Formulation of the Problem

Consider the array of Figure (1-1) where the elements are made of an imperfectly conducting wire of radius a_i. The effect of the finite conductivity can be assumed to be equivalent to a continuous loading of the loop wire with a per unit length impedance of $Z_{Li}(\phi_i)$ on the i^{th} element. If the thin wire approximations $a_i << b_i$ and $a_i << \lambda$ are made, then the applied tangential field on the surface of the i^{th} loop may be shown to satisfy the following equation

$$E^a_{\phi_i} = -\frac{V_i}{b_i} U_i(\phi_i) + Z_{Li}(\phi_i)\, I_i(\phi_i)\, [1 - U_i(\phi_i)] \qquad (4.1)$$

$$(i = 1, 2, \ldots, N)$$

where V_i, b_i and $U_i(\phi_i)$ are the same as defined in Chapter I. The induced electric field E^i_ϕ on the antenna surface, maintained by the current and charges on the i^{th} element, may be expressed as

$$E^i_\phi = -\sum_{j=1}^{N} \frac{1}{b_i} \frac{\partial \Phi_{ij}}{\partial \phi_{ij}} + j\omega A_{\phi ij} \quad , \quad i = 1, 2, \ldots, N \qquad (4.2)$$

where Φ_{ij} and A_{ij} are the scalar and the vector potentials, respectively. Using equations (4.1) and (4.2) an integral equation for the current $I_i(\phi_i)$ can be obtained which, following the previous approach for the perfectly conducting loops, may be shown to be

$$\frac{V_i\, U_i(\phi_i)}{b_i\, \delta\phi_i} - Z_{Li}(\phi_i)\, I_i(\phi_i)\, [1 - U_i(\phi_i)] = \frac{jn_o}{4\pi b_i} \sum_{j=1}^{N} \int_0^{2\pi}$$

$$[kb_j \cos(\phi_i - \phi_j') + \frac{1}{kb_i} \frac{\partial^2}{\partial^2 \phi_i}]\, W_{ij}(\phi_i - \phi_j')\, I_j(\phi_j') d\phi_j'$$

$$i = 1, 2, \ldots, N \qquad (4.3)$$

Again, by an expansion of the current $I_i(\phi_i)$ and the kernel W_{ij} in Fourier series of the azimuthal coordinate and after some manipulation one finds

$$\int_0^{2\pi} \left[\frac{V_i U_i(\phi_i)}{\delta\phi_i} - Z_{Li}(\phi_i)\, b_i\, [1 - U_i(\phi_i)] \sum_{n=0}^{\infty} I_i^n \cos n\phi_i \right] e^{jm\phi_i} d\phi_i$$

$$= \sum_{j=1}^{N} Z_{ij}^m I_j^m \qquad i = 1, 2, \ldots, N \qquad (4.4)$$

Equation (4.4) can be solved to yield the current modes I_i^n for any desired load distribution. The number of required modes M for an accurate evaluation of the input admittance depends on the geometry of the array and is approximately given by $M \simeq \frac{b_i}{a_i}$ [12]. After these current modes are obtained, other antenna characteristics can easily be found from the previously developed equations. Equation (4.4) is for any arbitrary load distribution $Z_{Li}(\phi_i)$. In general, it may not have an exact solution for arbitrary forms of $Z_{Li}(\phi_i)$. In such cases a numerical method must be utilized to solve (4.4) for the current modes I_i^n. The simplest form of the load distribution is the uniform impedance loading which is considered in the next sections.

4.3 Uniform Load Distribution $Z_{Li}(\phi_i)$

This type of impedance distribution is the simplest case of antenna loadings and all practical antennas made of conductive metals fall into this category. Substituting $Z_{Li}(\phi) = Z_{Li}$ in (4.4) and following the necessary steps, while neglecting the integral of $U_i(\phi_i)\, I_i(\phi_i)$, (Appendix IV-A), one finds

$$V_i \frac{\sin n\, \delta\phi_i/2}{n\, \delta\phi_i/2} - Z_{Li} b_i \pi I_i^n \cdot \varepsilon_n = \sum_{j=1}^{N} Z_{ij}^n I_j^n \tag{4.5}$$

where

$$\varepsilon_n = \begin{cases} 2 & \text{for } n = 0 \\ 1 & \text{for } n > 0 \end{cases} \tag{4.6}$$

Equation (4.5) can be written in the matrix form for all n

$$[Z_{ij}^{'n}][I_j^n] = [\beta_i^n] \qquad n \geq 0 \tag{4.7}$$

where β_i^n is as defined in (1.9) and

$$Z_{ij}^{'n} = Z_{ij}^n + \varepsilon_n \pi b_i Z_{Li} \delta_{ij} \tag{4.8}$$

in which δ_{ij} is the Kronecker delta function. The impedance matrix $[Z_{ij}^{'n}]$ is different from the previous impedance matrix $[Z_{ij}^n]$ only in the principal diagonal elements. Therefore, the same discussion about $[Z_{ij}^n]$ is applicable to $[Z_{ij}^{'n}]$. That is, for $n > m_o$ where m_o is an integer determined by the geometry of the array, the matrix $[Z_{ij}^{'n}]$ degenerates into a diagonal one. Thus, a relation for $I_i(\phi)$ similar to equation (1.16) can be obtained in which Z_{ii}^n and y_{ij}^n are replaced by $Z_{ii}^{'n}$ and $y_{ij}^{'n}$, respectively and $[y_{ij}^{'n}]$ is the inverse of the impedance matrix $[Z_{ij}^{'n}]$. If the uniform

load distribution is resistive, then the efficiency of the antenna will be reduced. This deterioration of the efficiency is certainly an important effect and is discussed in the next section.

4.4 Efficiency of the Antenna with a Uniform Resistive Loading

To calculate the antenna efficiency we need the radiated and the dissipated powers of the antenna. The radiated power P_r can be obtained from the integration of the Poynting vector over a large spherical surface at the far field zone, or from the following equation

$$P_r = \frac{1}{2\eta_o} \int_0^{\pi} r^2 \sin\theta d\theta \int_0^{2\pi} |E(\theta,\phi)|^2 \, d\phi \qquad (4.9)$$

The expressions for the radiation fields of an N-element antenna was given in (1.25) which can be reduced to the form

$$E(\theta,\phi) = E_\theta \hat{\theta} + E_\phi \hat{\phi}$$

with

$$|E(\theta,\phi)|^2 = |E_\theta|^2 + |E_\phi|^2 \qquad (4.10)$$

To calculate the radiated power we, therefore, need to integrate $|E_\phi|^2$ and $|E_\theta|^2$ separately. To simplify the work we can modify the expression for E_ϕ to the form

$$|E_\phi|^2 = \frac{\eta_o^2}{16r^2} \left[\sum_{i=1}^{N} A_i \cdot \sum_{n=0} \gamma_i \cos n\phi_i\right] \cdot \left[\sum_{i=1}^{N} A_i^* \cdot \sum_n \gamma_i^{n*} \cos n\phi_i\right] \qquad (4.11)$$

where * indicates the complex conjugate and

$$A_i = kb_i \exp(jkd_{il} \cos\theta) \qquad (4.12)$$

$$\gamma_i^n = j^n I_i^n [J_{n-1}(x_i) - J_{n+1}(x_i)] \qquad (4.13)$$

with

$$x_i = kb_i \sin\theta$$

For loop arrays the number of significant modes in the array, in particular for a Yagi array, is usually very limited [16]. Therefore, for accurate evaluation of the radiated power the summation in equation (4.11) may be evaluated only over the first few modes. A term by term integration of equation (4.11) over ϕ gives

$$\int_0^{2\pi} \left(\sum_{n=0} \gamma_i^n \cos n\phi_i \cdot \sum_{n=0} \gamma_j^{n*} \cos n\phi_i \right) d\phi_i = \pi \sum_{n=0} \varepsilon_n \gamma_i^n \gamma_j^{n*} \qquad (4.14)$$

where

$$\varepsilon_n = \begin{cases} 2 & \text{for } n = 0 \\ 1 & \text{for } n > 0 \end{cases} \qquad (4.15)$$

and using $(Z + Z^*) = 2\mathrm{Re}(Z)$, therefore

$$\int_0^{\pi} \int_0^{2\pi} |E_\phi|^2 \sin\theta r^2 d\theta d\phi = \frac{\eta_o^2}{16} \pi \left[\int_0^{\pi} \sum_{i=1}^{N} \left(|A_i|^2 \sum_{n=0} \varepsilon_n |\gamma_i^n|^2 \sin\theta d\theta \right. \right.$$

$$\left. \left. + 2\,\mathrm{Re} \int_0^{\pi} \sum_{i=1}^{N-1} A_i \left(\sum_{j=i+1}^{N} A_j^* \sum_{n=0} \varepsilon_n \gamma_i^n \gamma_j^{n*} \right) \sin\theta d\theta \right] \qquad (4.16)$$

which requires a final integration over θ. This integration is carried out numerically.

In a similar manner, the integration of $|E_\theta|^2$ gives the following results

$$\int_0^{\pi} \int_0^{2\pi} |E_\theta|^2 r^2 \sin\theta d\theta d\phi = \frac{\eta_0^2 \pi}{16} \int_0^{\pi} \left(\sum_{i=1}^{N} |A_i|^2 \sum_{n=1} |\gamma_i'^n|^2 \right) \sin\theta\cos\theta d\theta$$

$$+ 2\,\mathrm{Re} \int_0^{\pi} \sum_{i=1}^{N-1} A_i \left(\sum_{j=i+1}^{N} A_j^* \gamma_i'^n \gamma_j'^{n*} \right) \cos\theta\sin\theta d\theta \qquad (4.17)$$

where

$$\gamma_i'^n = j^n I_i^n [J_{n-1}(x_i) + J_{n+1}(x_i)] \qquad (4.18)$$

Now, summation of (4.16) and (4.17) gives the radiated power P_r in the form

$$P_r = \frac{\pi\eta_o}{32}\left[\int_0^{\pi} \sum_{i=1}^{N} |A_i|^2 \left(\sum_{n=0} \varepsilon_n |\gamma_i^n|^2 + \sum_{n=1} \gamma_i'^n \cos\theta \right) \sin\theta d\theta + \right.$$

$$\left. 2\, R_e \int_0^{\pi} \sum_{i=1}^{N-1} A_i \left[\sum_{j=i+1}^{N} A_j^* \left(\sum_{n=0} \varepsilon_n \gamma_i^n \gamma_j^{n*} + \cos\theta \sum_{n=1} \gamma_i'^n \gamma_j'^{n*} \right) \right] \sin\theta d\theta \right] \qquad (4.19)$$

The dissipated power can be calculated from

$$P_D = \frac{1}{2} \sum_{i=1}^{N} \int_0^{2\pi} Re[Z_{Li}(\phi)] |I_i(\phi)|^2 \, b_i \, d\phi \qquad (4.20)$$

which for constant $Z_{Li}(\phi)$ becomes

$$P_D = \frac{1}{2} \sum_{i=1}^{N} b_i \, Re[Z_{Li}] \int_0^{2\pi} |I_i(\phi)|^2 \, d\phi$$

Substituting $I_i(\phi) = \sum_{n=0} I_i^n \cos n\phi$ in the above equation gives

$$P_D = \frac{1}{2} \sum_{i=1}^{N} [b_i \, R_{Li} \, \pi \sum_{n=0} \varepsilon_n I_i^n] \qquad (4.21)$$

where

$R_{Li} = Re\,(Z_{Li})$.

Again, by selecting only the first few terms from the summation over n, the driving point power can be calculated with a reasonable accuracy. Finally, from the radiated and the dissipated powers the antenna efficiency can be defined in the form

$$\text{efficiency} = \frac{P_r}{P_D + P_r} \tag{4.22}$$

which can be calculated readily by using equations (4.19), (4.21) and (4.22). The above approach utilizes the integration of the radiation field and, therefore, needs only a few current modes to give sufficiently accurate results[16]. An alternative method for determining the efficiency exists which uses the input admittance and this is explained in Appendix (IV-B). However, the input admittance is a local characteristic and its calculation usually requires a significant number of modes.

4.5 Results and Discussion for Distributed Uniform Resistive Loading

For a solid conductor of circular cross-section with radius a, the definition of the per unit length impedance and an expression for its calculation are given in [44]. For highly conducting materials of conductivity σ, the per unit length impedance may be computed from

$$Z_i = \frac{1 + j}{2\pi a \sigma d_s} \tag{4.23}$$

where $d_s = \sqrt{\frac{2}{\omega\mu\sigma}}$ is the skin depth and μ is the permeability of the conductor. Antennas with fairly high internal impedance per unit length are likely to be made by coating a dielectric loop with a layer of conducting material [25]. If in the frequency range of concern the thickness of the conducting layer d is less than its skin depth, then the impedance per unit length is essentially the dc resistance

which is given by

$$Z_i = \frac{1}{2\pi a d \sigma} \tag{4.24}$$

The above formula together with equations given in the previous section are utilized to study the effects of the constant and continuous resistive loading on the characteristics of Yagi loop arrays. The investigation is restricted to arrays where only the exciter is loaded. This type of loading is selected because a resistive loading of the parasitic elements increases the antenna loss and deteriorates the antenna's overall efficiency significantly. The resistive loading of the exciter should decrease the efficiency as well, but it is also expected to improve the broadband characteristics of the antenna. As a result, only the effects of the uniform resistive loading of the exciter on the Yagi loop arrays' characteristics will be investigated.

Figure (4-1) shows the real and imaginary parts of Z_{in} of a 14-element array for different exciter loadings. It is seen that the real part of the input impedance increases with increasing resistive loading, but the relative variation of $Re(Z_{in})$ decreases. For example, for $Z_{L2} = 250\ \Omega/m$ the maximum variation of $Re(Z_{in})$ from 190 to 215 MHz is less than 54% of the initial value, while for the unloaded case and within the same frequency range, this variation is over 400%. The variation of the directive gain of the array with frequency for different exciter loadings is shown in Fig. (4-2). There is only a negligible change in the directive gain with the exciter loading, since G_d is mainly

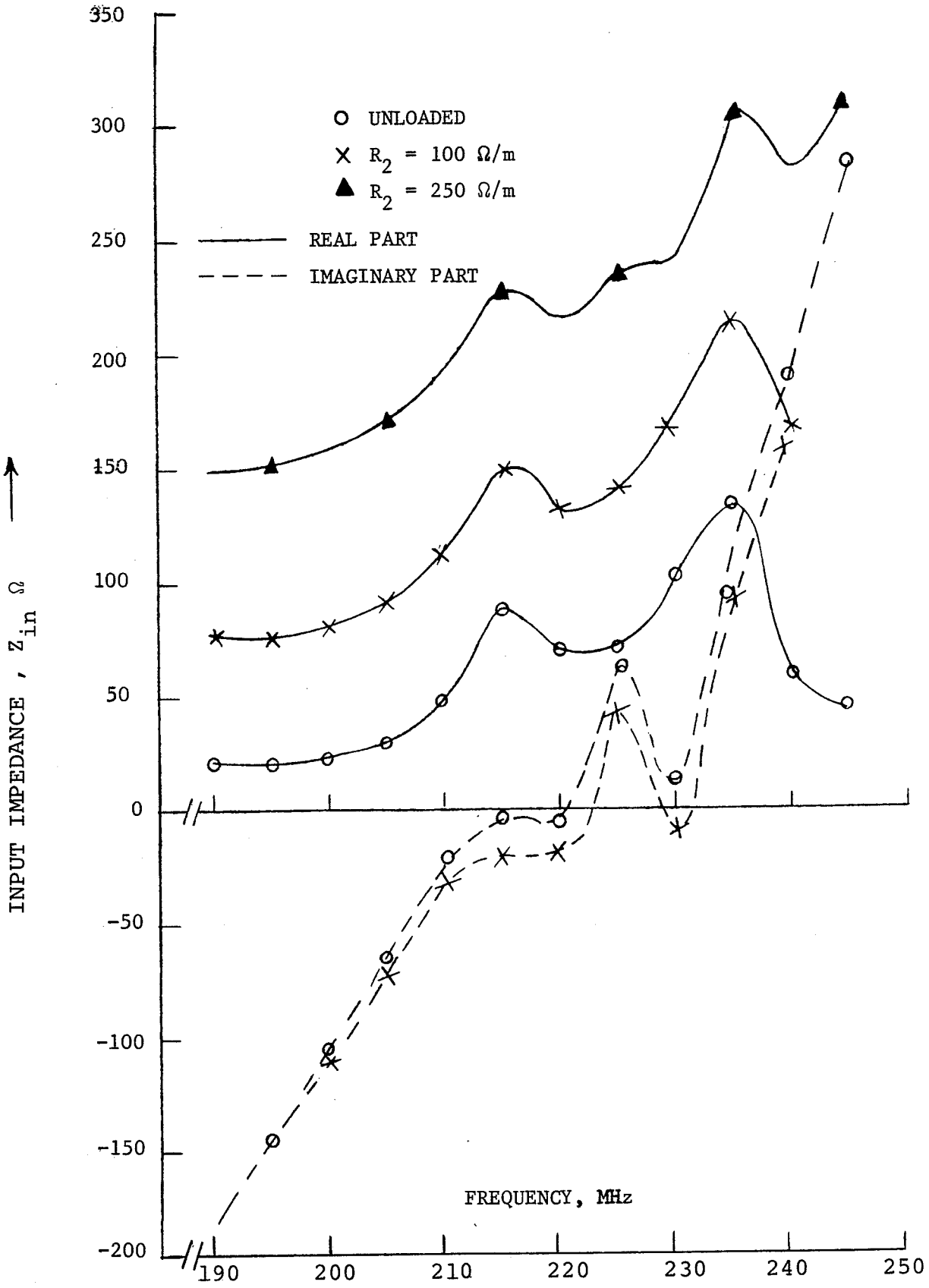

Fig. 4-1: The input impedance of a 14- element array for several continuous loading of exciter. $b_1 = 1.2\ b_3$, $b_2 = 1.1\ b_3$, $b_i = 20$ cm ($i = 3, 4, \ldots, 14$), element spacing = 20 cm, $b_2/a = 38.94$.

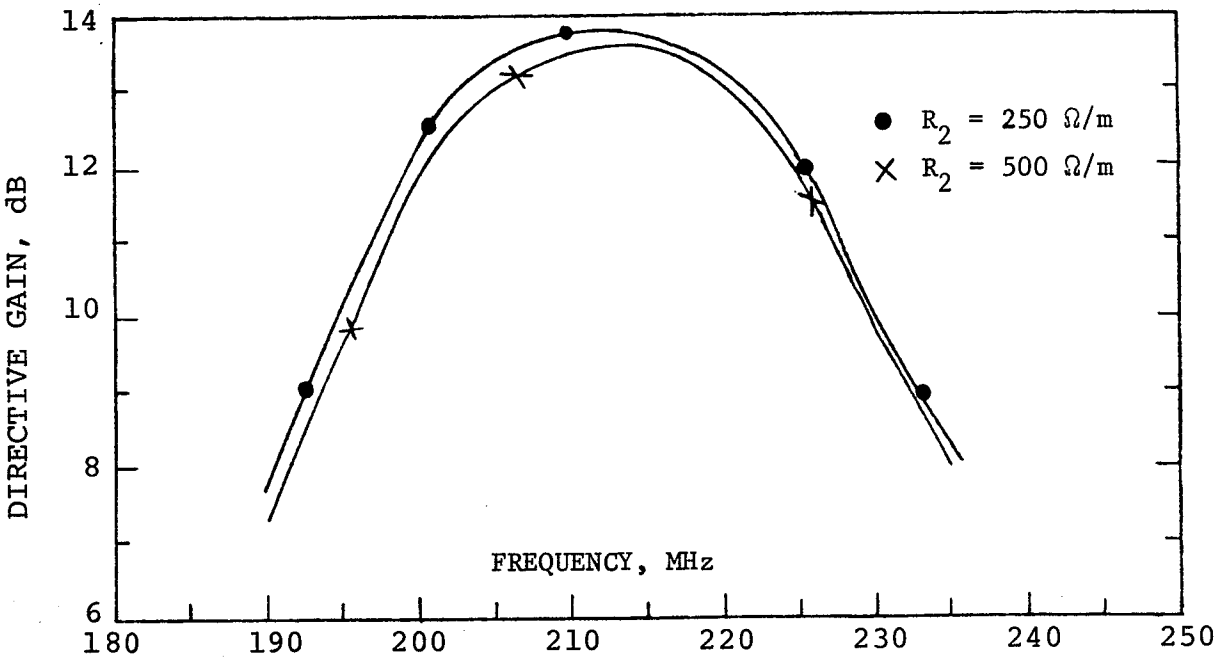

Fig. 4-2: Effect of continuous loading of exciter on the directive gain of the 14-element array in figure (4-1) as a function of frequency

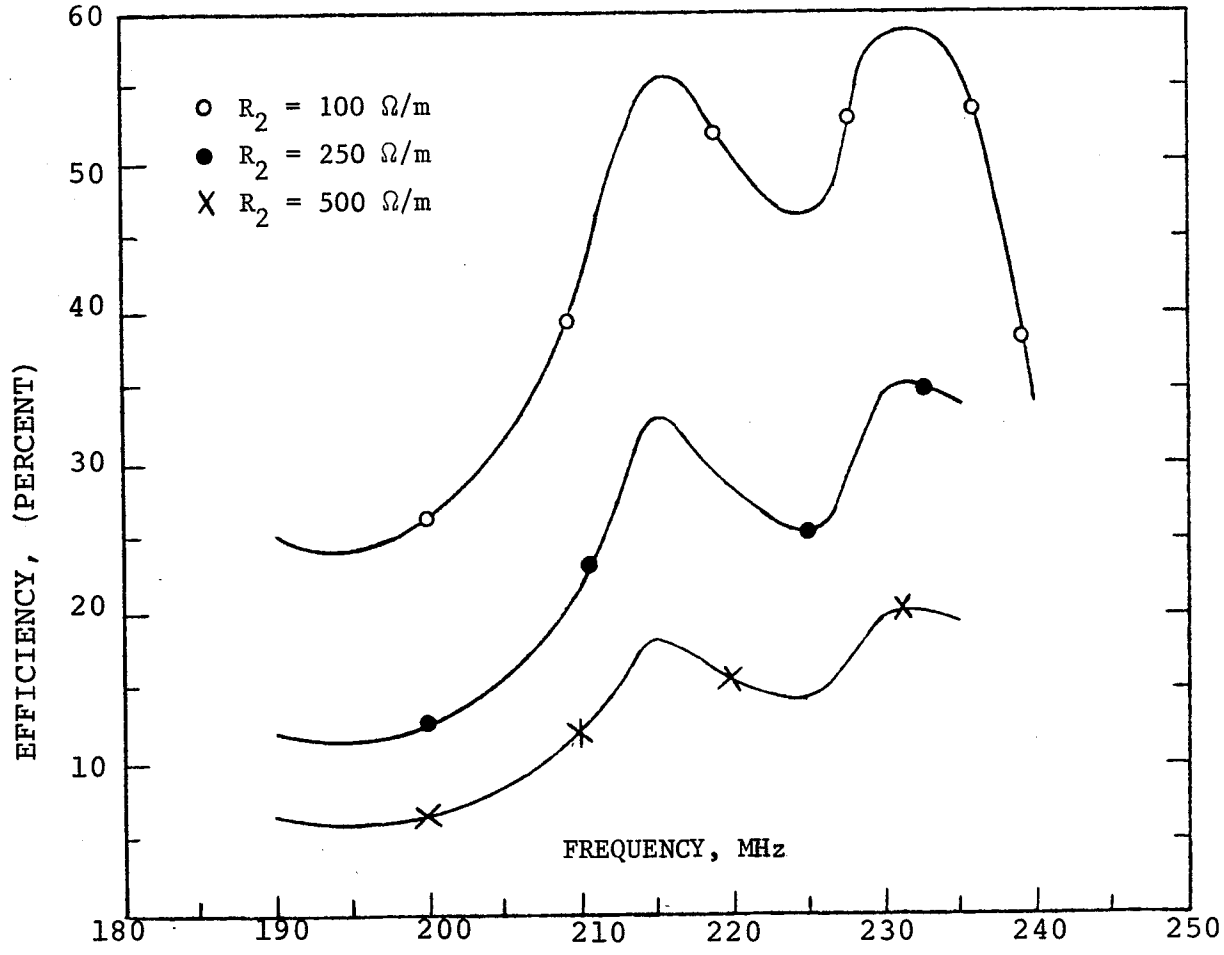

Fig. 4-3: Variation of the efficiency of the array in figure (4-1) with frequency for different exciter loading distribution

controlled by the size and spacing of the parasitic elements. Figure (4-3) depicts the variation of the efficiency of the above array with frequency for different exciter loadings. It is interesting to see that the highest efficiency within 3dB bandwidth is for $kb \simeq 0.9$. Directors of this size was also found previously to give a better directivity for Yagi arrays [45]. The distribution of the phase and the relative magnitude of the current on the exciter of the above array at $f = 210$ MHz are plotted in Figs. (4-4) and (4-5). It is seen that the phase of the current for larger load distribution has a more gradual change near $\phi = 90°$. The relative magnitude of the current has also a smoother variation than that of the perfect conductor. These facts indicate that the current distribution on the loaded exciter has a larger percentage of travelling wave type currents. Therefore, the input impedance should be less sensitive to frequency variation.

In summary, resistive loading of the exciter in a Yagi loop array improves the broadband characteristics of the antenna. However, resistive loading of the antenna decreases its efficiency. For this reason the remaining part of this chapter is devoted to a study of the possibility of broadening the array by utilizing a purely distributed reactive loading.

4.6 Tapered Capacitive Loading

An interesting form of the reactive loading is an exponentially increasing capacitive loading which was first used by Rao et al. [46] for dipole antennas. This type of

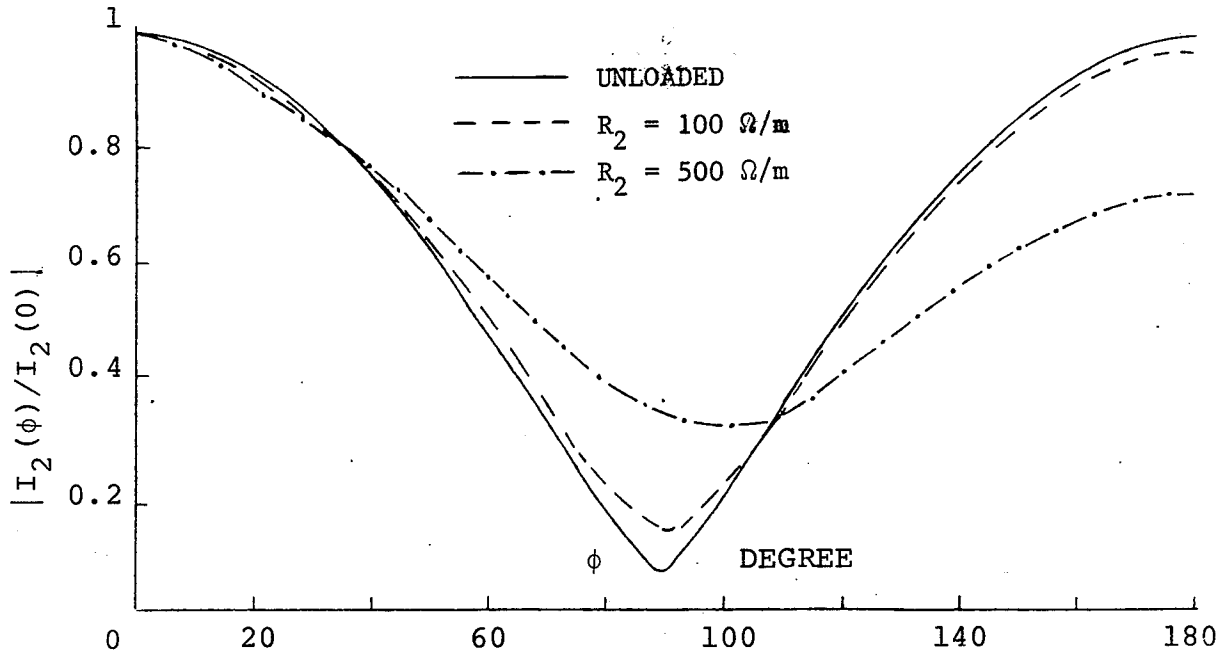

Fig. 4-4: Relative magnitude of the current distribution on the continuously loaded exciter of the array in figure (4-1) for various exciter loadings and at f = 210 MHz.

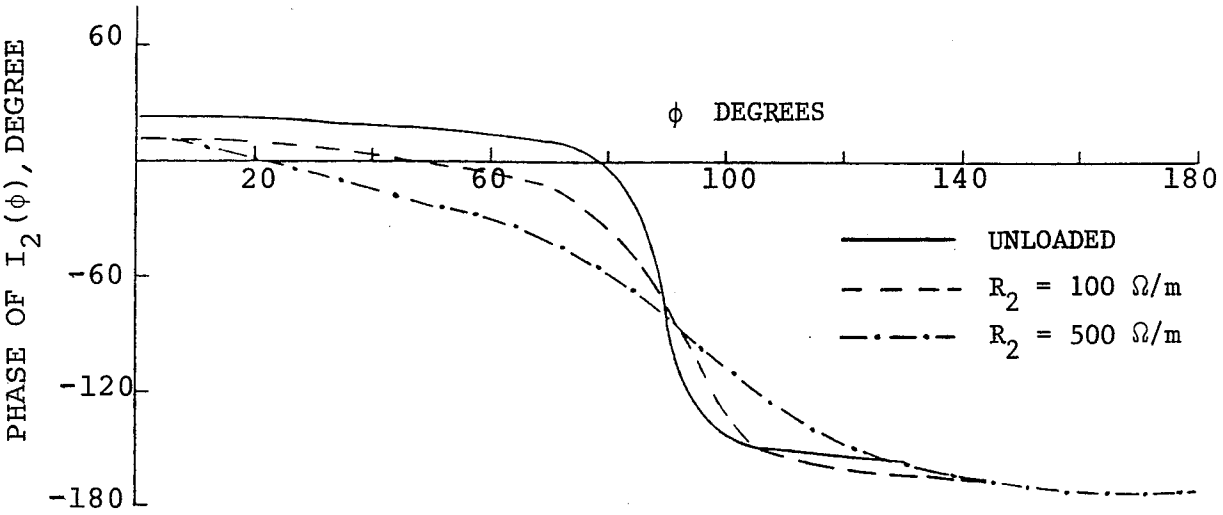

Fig. 4-5: The phase of the current distribution on the continuously loaded exciter of the array in figure (4-1) for various exciter loading and at f = 210 MHz.

load distribution has also been studied by Lin [25] for a single loop antenna using the numerical method. His method, however, is lengthy and time consuming. Furthermore, the results in [25] for unloaded loops show large disagreements with the results of the Fourier series method which in turn agrees very well with Kennedy's experimental data [47]. This discrepancy is indicated in figure (4-6) in which the input impedances of an unloaded loop computed by Lin (Ref. [25] figures 7 and 8) is shown along with the results from the Fourier series method. For $kb > 0.8$ the results show different behaviour and indicate large differences. One can, therefore, safely assume that this discrepancy of Lin's results with the experimental data for the unloaded loop should also exist for the loaded antennas. Thus, a further and an accurate investigation of the loop antennas with tapered capacitive loading is needed and will be carried out here by using the Fourier series method. This type of load distribution is given by [25].

$$Z_{Li}(\phi) = -j\, B_i \left[\exp(\alpha_i b_i |\phi_i|) - 1\right] \tag{4.25}$$

where B_i and α_i are arbitrary constants. Substituting (4.25) in (4.4) yields

$$V_i \frac{\sin m\, \delta\phi_i/2}{m\, \delta\phi_i/2} + j\, B_i\, b_i \sum_{n=0}^{M-1} I_i^n \int_{-\pi}^{\pi} (e^{\alpha_i b_i |\phi_i|} - 1) \cos n\phi_i \; e^{jm\phi_i}\, d\phi_i = \sum_{j=1}^{N} Z_{ij}^m\, I_j^m$$

$$i = 1, 2, \ldots, N \tag{4.26}$$

where (M-1) is the number of the significant modes. Equation

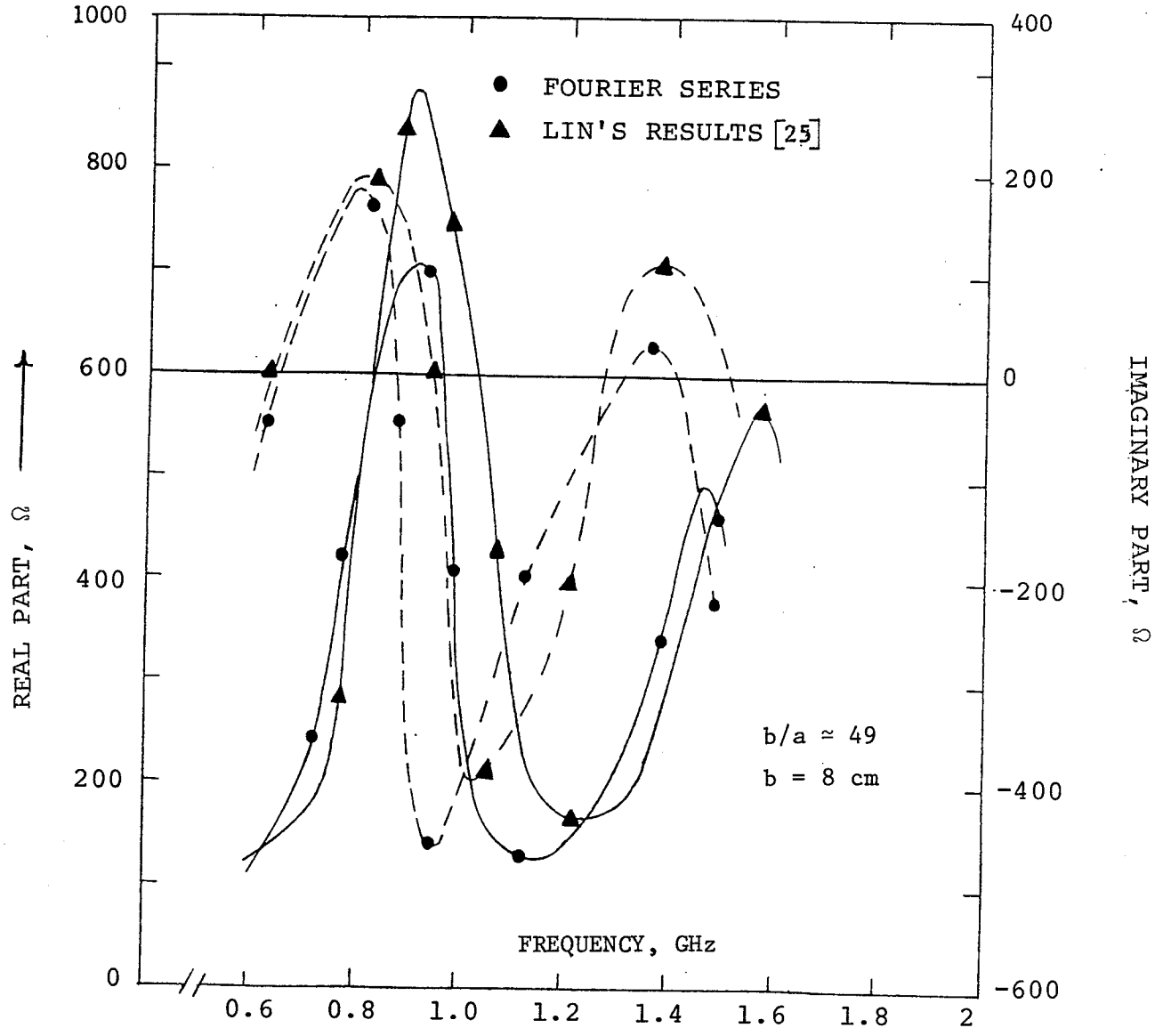

Fig. 4-6: Comparison between the input impedances of an unloaded loop computed by numerical technique [25] and Fourier series method. ——— real part, ------- imaginary part

(4.26) may be written in the form

$$V_i \frac{\sin m\,\delta\phi_i/2}{m\,\delta\phi_i/2} + \frac{j\,B_i\,b_i}{2} \sum_{n=0}^{M} I_i^n \int_{-\pi}^{\pi} \left[e^{j(m+n)\phi_i} + e^{+j(m-n)\phi_i} \right] e^{\alpha_i b_i |\phi_i|}\, d\phi_i - j\,B_i \varepsilon_m\, b_i \pi\, I_i^m = \sum_{j=1}^{N} Z_{ij}^m\, I_j^m ,$$

$$i = 1, 2, \ldots, N \qquad (4.27)$$

the integral in (4.27) can be simplified to

$$\int_{-\pi}^{\pi} e^{j(m\pm n)\phi_i}\, e^{\alpha_i b_i |\phi_i|}\, d\phi_i = \int_0^{\pi} e^{[\alpha_i b_i - j(m\pm n)]\phi_i}\, d\phi_i + \int_0^{\pi} e^{[\alpha_i b_i + j(m\pm n)]\phi_i}\, d\phi_i = \frac{1}{\alpha_i b_i - j(m\pm n)} \cdot \left[e^{[\alpha_i b_i - j(m\pm n)]\pi} - 1 \right] + \frac{1}{\alpha_i b_i + j(m\pm n)} \left[e^{[\alpha_i b_i + j(m\pm n)]\pi} - 1 \right] \qquad (4.28)$$

Substituting (4.28) in (4.27) gives

$$V_i \frac{\sin m\,\delta\phi_i/2}{m\,\delta\phi_i/2} + \frac{j\,B_i\,b_i}{2} \sum_{n=0}^{M} I_i^n \left(Q_i^{n,m} + R_i^{n,m}\right) - j\,B_i b_i \varepsilon_m \pi\, I_i^m = \sum_{j=1}^{N} Z_{ij}^m\, I_j^m \quad , \; i = 1,2,\ldots,N \text{ and } m = 0,1,2,\ldots,M \qquad (4.29)$$

where $Q_i^{n,m}$ and $R_i^{n,m}$ are given in (4.28) and involve only terms with (m-n) and (m+n) modes, respectively. For all modes m, $0 \leq m \leq (M-1)$ equation (4.29) can be written in the following matrix form

$$\begin{bmatrix} [\phi_{11}^{n,m}], & [Z_{12}^{m}], & [Z_{13}^{m}], & \ldots, & [Z_{1N}^{m}] \\ [Z_{21}^{m}], & [\phi_{22}^{n,m}], & [Z_{23}^{m}], & \ldots, & [Z_{2N}^{m}] \\ \cdot & \cdot & \cdot & \cdot & \cdot \\ \cdot & \cdot & \cdot & \cdot & \cdot \\ \cdot & \cdot & \cdot & \cdot & \cdot \\ [Z_{N1}^{m}], & [Z_{N2}^{m}], & [Z_{N3}^{m}], & \ldots, & [\phi_{NN}^{n,m}] \end{bmatrix} \begin{bmatrix} [I_1^m] \\ [I_2^m] \\ \cdot \\ \cdot \\ \cdot \\ [I_N^m] \end{bmatrix} = \begin{bmatrix} [V_1] \\ [V_2] \\ \cdot \\ \cdot \\ \cdot \\ [V_N] \end{bmatrix} \tag{4.30}$$

where $[\phi_{ii}^{n,m}]$ is an M x M matrix with (n,m = 0,1,2,..., M-1)

$$\phi_{ii}^{n,m} = (Z_{ii}^{m} + j\, B_i b_i \varepsilon_m \pi)\, \delta_{n,m} - \frac{jB_i b_i}{2} (Q_i^{n,m} + R_i^{n,m}) \tag{4.31}$$

and $[Z_{k\ell}^{m}]$ is an M x M diagonal matrix given by

$$[Z_{k\ell}^{m}] = \begin{bmatrix} Z_{k\ell}^{1} & 0 & 0 & \ldots & 0 \\ 0 & Z_{k\ell}^{2} & 0 & \ldots & 0 \\ 0 & 0 & 0 & \ldots & Z_{k\ell}^{M} \end{bmatrix}$$

Here, $[I_i^m]$ and $[V_i]$ are M x 1 matrices with their elements respectively given by I_i^m and V_i for m = 0,1,2, ...,M-1. It is obvious that the coefficient matrix in (4.30) is an (N x M) square matrix. Therefore, it may appear inconvenient to use (4.30) for large Yagi arrays. On the other hand, it was recently reported [16] that, generally, it is adequate to use only the dominant mode for determining the radiation field of a loop Yagi array. Other modes, which are necessary for the calculation of the input admittance, can be obtained by considering only a few directors (usually two)

adjacent to the exciter. Therefore, the apparant large size of the coefficient matrix in (4.30) does not introduce any difficulties for obtaining the current distribution of the array elements. Once these currents are known, other array characteristics can be obtained readily.

We are now in a position to investigate the effect of the tapered reactive loading on various characteristics of the coaxial loop arrays. For brevity, only the results for a loaded single loop are presented here.

4.7 Results and Discussion for a Loaded Antenna

Based on the theory presented in the last section, a computer program was developed to study the characteristics of a single loop antenna with tapered capacitive loading. Figure (4-7) demonstrates the effects of such loadings on the driving point admittance of a loop antenna. It is seen that the maxima and the minima of the conductance and the susceptance are shifted to the right as α_1 is increased from zero to 15. This variation with frequency also decreases as α_1 increases. Therefore, with a suitable choice of B_1 and α_1, the input admittance can be made less sensitive to the frequency variation. Figure (4-8) shows the variation of the directive gain of the antenna with frequency for different values of α_1. For low frequencies ($kb < 1$) the gain of a loaded loop is smaller than that of the unloaded one and the difference between the gains increases with increasing the constant α_1. On the other hand, it decreases with increasing the frequency ($kb > 1$). In fact, the directive

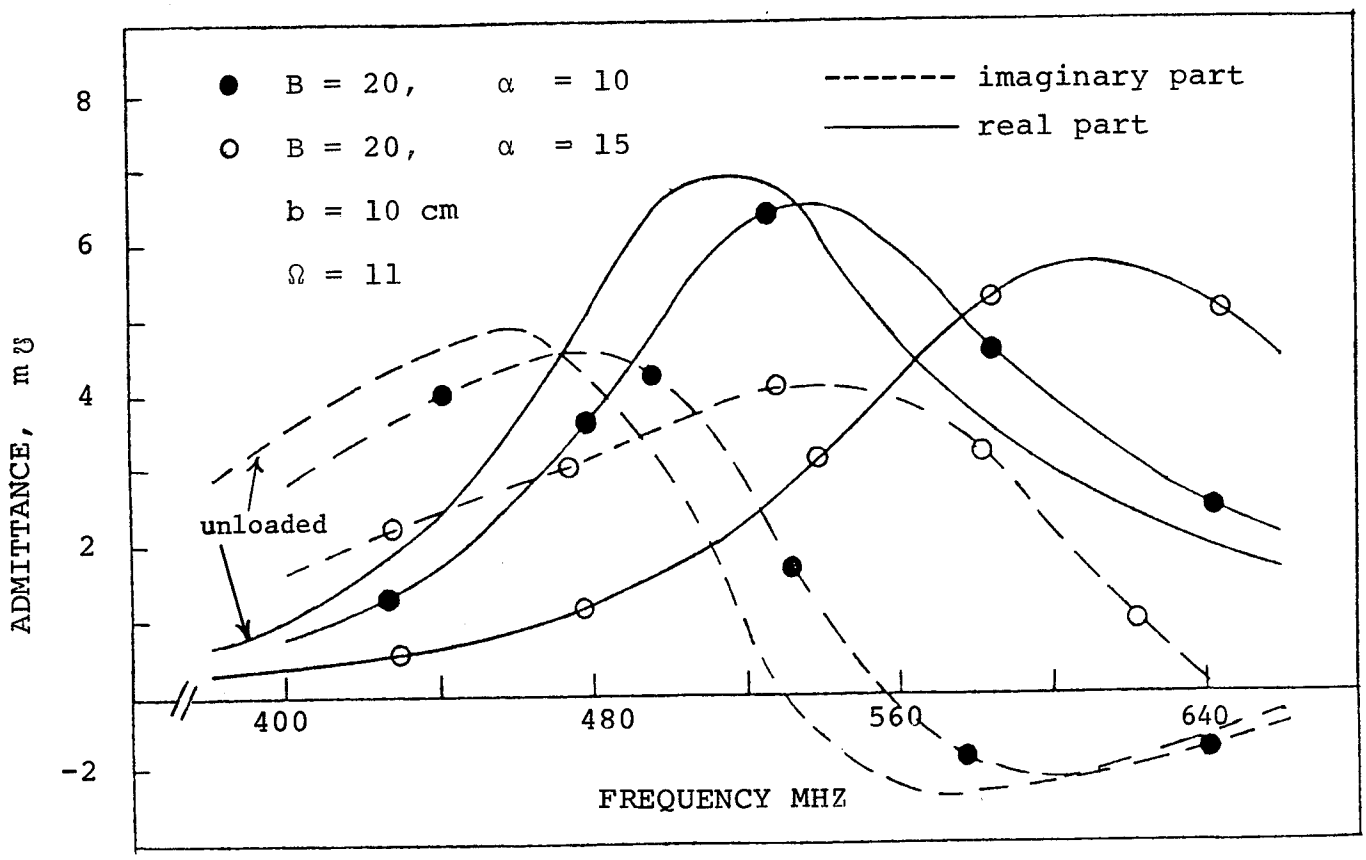

Fig. 4-7: Effect of tapered capacitive loading on the input admittance of a loop antenna as a function of frequency. ——— real part, ------ imaginary part

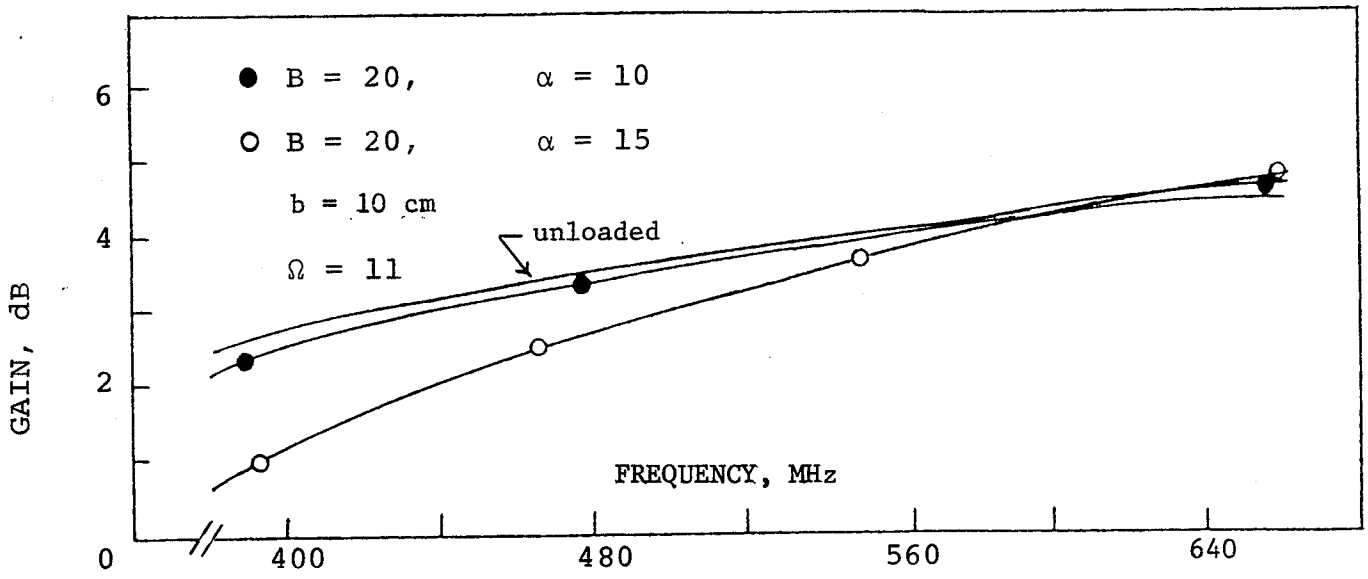

Fig. 4-8: Variation of the directive gain of a loop antenna with frequency for various tapered capacitive loadings.

gain of a loaded loop antenna becomes slightly larger than that of the unloaded antenna, at certain frequencies which depend on the value of α_1. This means that the center frequency of operation has shifted to higher frequencies.

4.8 Conclusion

Coaxial circular loop arrays with distributed impedance loading have been studied in this chapter by a simple extension of the Fourier series solution for the perfectly conducting loops. It was shown that, in general, a broadband characteristic can be obtained by distributed impedance loading. The constant resistive loading was studied in more detail since it can be fabricated readily. The travelling wave portion of the current distribution was increased by introducing the distributed resistive loading into the antenna system. The introduction of a dissipative load resulted in a decrease of the efficiency, but it improved the broadband characteristics of the antenna. The loss of the overall efficiency in a transmitting system is often the price to be paid in order to achieve the broadband and the directional properties. If the lossy element is not added to the antenna itself, it may be added to the feeding network in order to make the system broadband. However, the system will then become more complicated. On the other hand, the efficiency should not be of major concern in a receiving antenna for which the requirements of a broadband, directivity and a simplicity of the structure are usually the most important factors. It has already been reported that resistive antennas are being designed for use in satellite communications [43].

CHAPTER V

PLANAR LOOP ARRAYS AND THEIR APPLICATION TO BACKFIRE ANTENNAS

5.1 Introduction

In an investigation of circular loop arrays it was found that, when the separation distance between adjacent elements decreases, the series representing the Fourier coefficients of the kernel, equation (1.12), converge very slowly and their accurate computation becomes a tedious task [12] and [17]. On the other hand, it has also been found that the gain of an end-fire array increases as the spacing between its adjacent elements decreases and the gain reaches a maximum when the total spacing approaches zero [48]. In this chapter a method is described which enables one to study compact coaxial loop arrays with considerable ease. The approach is general and, therefore, applicable to the limiting case when the separation distance between the adjacent elements becomes zero. This limiting case generates a new antenna which, due to its planar structure, we will call here a "planar coaxial loop antenna". The method is also utilized to investigate backfire antennas constructed entirely with circular loop elements. The performance of such antennas are then compared with those of backfire antennas with a solid reflector. A good portion of this chapter is devoted to the investigation of backfire antennas with a solid reflector

utilizing a loop antenna as the exciter.

5.2 The New Technique

The coefficient K_{ij}^{n} in the Fourier expansion of the kernel in the starting integral equation was presented in (1.8) and is given again here for the continuity of the discussion

$$K_{ij}^{n} = \frac{1}{2\pi} \int_{0}^{2\pi} \frac{e^{-jkb_i R_{ij}(\phi)}}{R_{ij}(\phi)} \cdot e^{jn\phi}\, d\phi \qquad (5.1)$$

in a closed form this equation is given by [12]

$$K_{ij}^{n} = -jkb_i \sum_{n=0}^{\infty} \frac{(y/2Z)^{2m+n}}{m!\,(n+m)!}\, h_{n+2m}^{2}(Z) \qquad (5.2)$$

$$(i, j = 1, 2, \ldots N; \quad n = 0, 1, \ldots.)$$

where all parameters in (5.1) and (5.2) are the same as those defined in Chapter I. When m in equation (5.2) increases, the real part of the spherical Hankel function decreases, but its imaginary part increases. Therefore, the imaginary part of the series in (5.2) remains as the dominant part. It can be shown that for fixed kb_i and kb_j the convergence of (5.2) becomes slower as the spacing d_{ij} decreases, [12] and [17]. In the limit when d_{ij} approaches zero, on the order of thousands of terms in the summation becomes necessary to yield an accurate value for the function K_{ij}^{n}.

Numerical integration of equation (5.1) is also costly since the real part of the integrand around $\phi \simeq 0$ becomes very large and thus it requires a large amount of computer

time for an accurate computation of the integral. Consequently, a modification of equation (5.1) is necessary to simplify its numerical evaluation. To overcome this difficulty the large variation of the integrand is extracted by adding and subtracting $1/R_{ij}(\phi)$ to the integrand. Therefore, equation (5.1) is modified to

$$K_{ij}^{n} = \frac{1}{\pi}\int_0^{\pi}\left[\frac{e^{-jkb_iR_{ij}(\phi)}}{R_{ij}(\phi)}\cos n\phi - 1\right]d\phi + \frac{1}{\pi}\int_0^{\pi}\frac{d\phi}{R_{ij}(\phi)} \qquad (5.3)$$

where

$$R_{ij}(\phi) = [1/b_i^2\ (b_j^2 + b_i^2 + d_{ij}^2 - 2b_ib_j\cos\phi)]^{\frac{1}{2}}$$

changing ϕ to $2\theta + \pi$ in the second integral of equation (5.3) gives

$$I = \int_0^{\pi}\frac{d\phi}{R_{ij}(\phi)} = \int_{-\pi/2}^{0}\frac{2b_i\,d\theta}{(b_i^2 + b_j^2 + d_{ij}^2 + 2b_jb_i\cos2\theta)^{\frac{1}{2}}} \qquad (5.4)$$

Using the identity $\cos2\theta = 1 - 2\sin^2\theta$ and changing the variable θ to $-\phi$ yields

$$I = A\cdot\int_0^{\pi/2}\frac{d\phi}{(1 - C^2\sin^2\phi)^{\frac{1}{2}}} \qquad (5.5)$$

where

$$A = \frac{2b_i}{[(b_i + b_j)^2 + d_{ij}]^{\frac{1}{2}}}$$
$$C^2 = b_j\,A^2/b_i \qquad (5.6)$$

Since $b_j^2 + b_i^2 \geq 2b_ib_j$ (equal when $b_j = b_i$), and $(b_i + b_j)^2 \geq 4b_ib_j$, even in the limit when $d_{ij} = 0$, the coefficient C^2 is always less than unity. Hence, the integral in equation (5.5) is a complete Elliptic integral of the first kind [49] defined by

$$F(\pi/2,\ C) \quad = \quad \int_0^{\pi/2} \frac{d\phi}{\sqrt{1 - C^2\sin^2\phi}} \qquad (5.7)$$

Substituting (5 7) and (5 5) in (5 3) gives

$$K_{ij}^{n} \quad = \quad \frac{1}{\pi} A\ F(\pi/2,\ C) + \frac{1}{\pi} \int_0^{\pi} \left(\frac{e^{jkb_i R_{ij}(\phi)}}{R_{ij}(\phi)} \cos n\phi - 1\right) d\phi \qquad (5.8)$$

The Elliptic integral (5.7) is tabulated in the literature and can also be evaluated readily by a polynomial approximation [49]. Thus, it only remains to evaluate the remaining integral of equation (5.8). Its integrand, however, is a relatively smooth function and can be computed numerically. To investigate the behaviour of this integrand, its real part is compared with that of equation (5.1) in figure (5-1) (for $n = 0$, $n = 1$ only). It is evident that the latter has much smoother variations and its numerical integration is trivial. The imaginary part of the integrands are smooth functions of ϕ and are not included in the figure.

In the following sections, the application of this method to co-planar coaxial loop antennas is discussed.

5.3 Planar Circular Loop Arrays

Planar loop array is a new type of antenna and a literature survey indicates that it has not, so far, been investigated. In this array the axial separation of the loops, d_{ij}, is zero (figure 5-2a) and the convergence of the series in equation (5.1) is very slow. The above method, however, gives the results with considerable ease. Figure (5-2b) shows the computed currents of a 14-element array for different

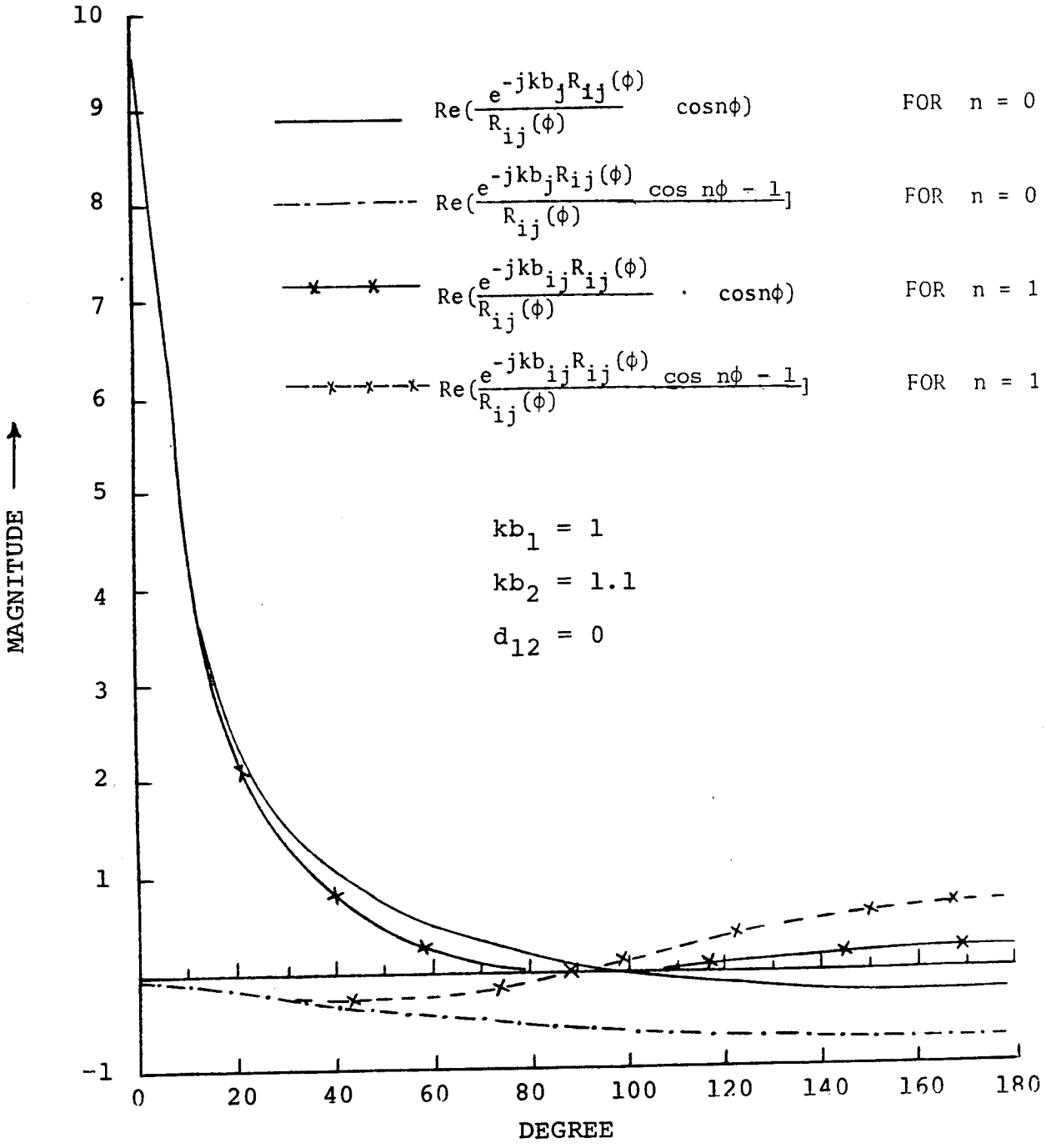

Fig. 5-1: Variation of the integrands of equations (5-8) and (5-1), (real parts only)

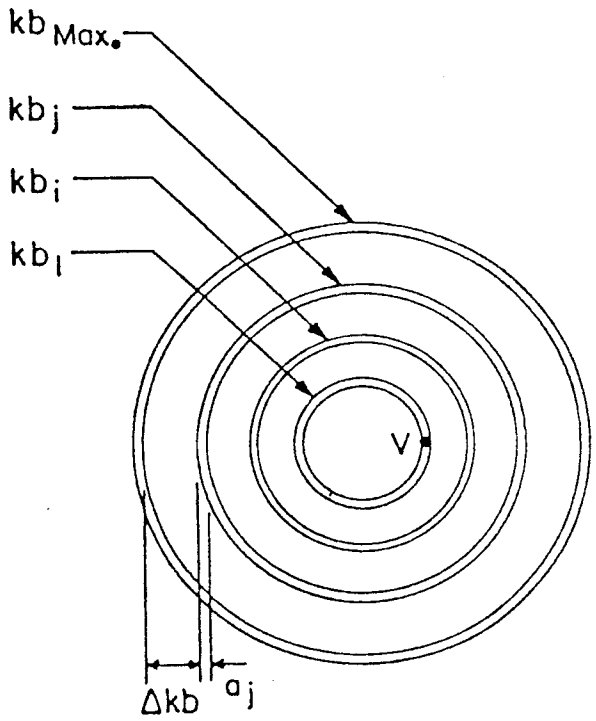

Fig. 5-2a: Geometry of a coaxial planar loop array

Fig. 5-2b: Magnitude of loop currents on a 14-element coaxial planar array at $\phi = 0$

loop separations. Only the smallest loop is excited and for the selected dimensions the loop currents decrease rapidly within the first three loops, but remain relatively constant in the remaining elements. This indicates the existence of a weak surface wave along the array [50]. The coaxial gain of such an array is also investigated and is shown in figure (5-3). It indicates a maximum gain of about 6dB regardless of the array parameters. In addition, this maximum gain is obtained when the largest element has a radius of about 0.75λ. This interesting fact was also verified for arrays with different number of loops and separations.

After an intensive investigation of the planar circular loop arrays, the following properties were identified:

a) When only the smallest loop is excited, the dominant mode on the other elements is the same as the dominant mode of the excited loop, no matter how large the parasitic elements are. A similar situation was also established, previously, for loop Yagi arrays with unequal elements [17].

b) If the largest element in the array is excited, then each loop will have its respective dominant mode, again similar to loop Yagi arrays [17]. When only the largest element is excited, the array does not radiate significantly and the real part of its input admittance, $Re(Y_{in})$, is normally small. Even for large values of $Re(Y_{in})$ the directive gain along the axis of the array will not be large, since for this case

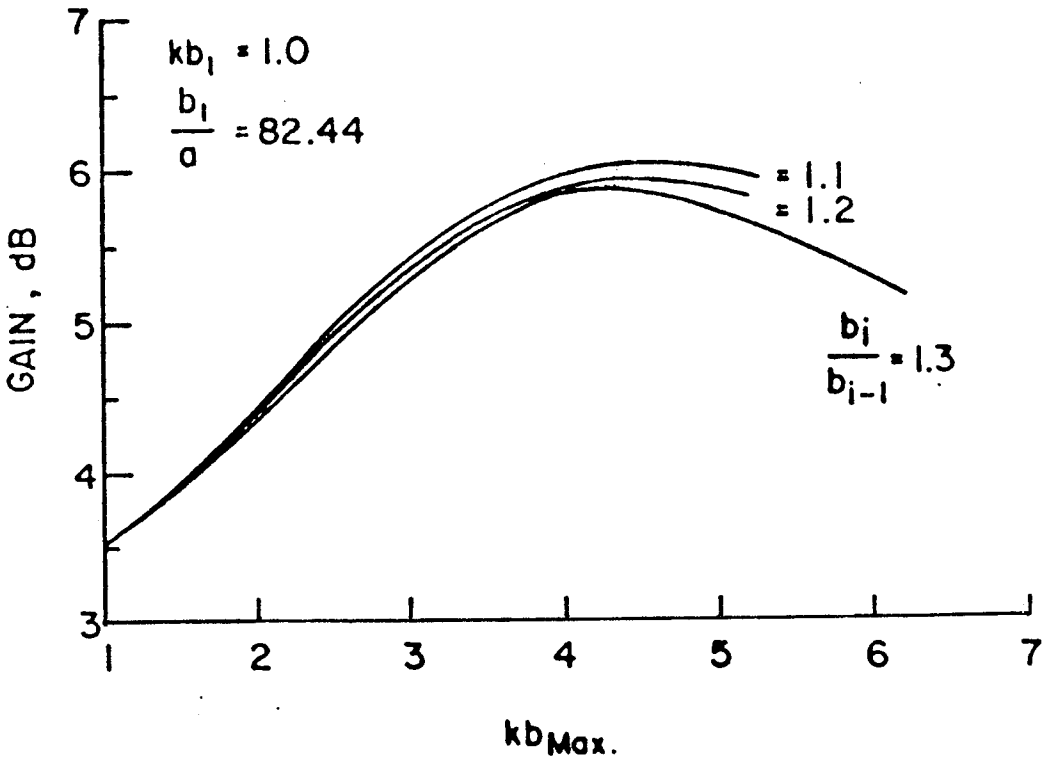

Fig. 5-3: Variation of the gain with array radius

the exciter is a large loop which is known to have a small axial gain.

c) Since the parasitic elements not in the neighbourhood of the exciter have small currents relative to that of the exciter, the input admittance of the array [$Re(Y_{in})$] is not significantly altered by adding or subtracting a parasitic element to the array. The sensitivity of the $Re(Y_{in})$ to the number of array elements was found to depend on the ratio of the elements radii. For $b_i/b_{i-1} = 1.1$ it was the most sensitive to the number of elements. Whereas, for $b_i/b_{i-1} > 1.1$ it had noticeable variation, but its variation was found to be less than 10% when the array elements were increased from 3 to 6.

5.4 Backfire Antennas

A backfire antenna radiates in opposite direction to that of endfire. Antennas employing the backfire principle conceived by Ehrenspeck [51]-[52] have been the subject of extensive experimental studies [53]-[55]. This technique provides a means for increasing significantly the directivity of an endfire antenna without increasing its length. Typical experimental gain increases of 6 to 8dB over a conventional endfire Yagi of equal length are obtained by an application of the backfire principle [56]. Later, Ehrenspeck [57] developed a "short backfire" antenna for which the backfire principle was applied to a single dipole "exciter" antenna rather than to an endfire array. A gain of 13dB was

achieved with this configuration. A short backfire antenna has the structure of a simple, open ended circular cavity with a dipole exciter placed at an appropriate location inside the cavity and a small reflecting plate placed in the open end to reduce the direct radiation from the exciter.

Although backfire antennas have been studied extensively by experimental methods, due to their complicated structure, very little is known about their behaviour. Chen et al. [56] gave an approximate calculation of the radiation fields of a short backfire antenna based on the measured aperture fields. Zuker [58] has studied a long backfire antenna theoretically and provided some approximate data for design. The same problem was studied in [59] - [61] by applying the image theory. In [59] Nielsen and Pontoppidan assumed that the reflector could be treated as an infinite planar reflector, so that a complete image of the array could be introduced. The mutual impedances between all dipoles, real as well as imaginary, were determined by the EMF method and sinusoidally distributed currents were assumed in all elements. The surface currents induced on the infinite reflecting plane by the currents of the exciting dipoles were then determined. The field of the array with a finite reflecting plane was eventually calculated by superposition of the fields due to the exciting dipoles and the surface currents on the part of the infinite plane that corresponds to the actual finite plane. The analysis is direct and gives readily useful results for backfire antennas with dipole

elements and with a plane surface reflector. This approach, however, may introduce some difficulties in computing the characteristics of a long Yagi backfire antenna due to the required large surface reflector. Since the application of the image theory, for determining the mutual impedances gives results to a reasonable approximation only if the dimension of the reflecting plane are very large compared to the distance of the plane from the farthest element, the longer the Yagi array, the larger the reflecting plane will be and, therefore, extensive computer time and storage are required to determine the surface current distribution.

Recently, Ehrenspeck [62] introduced a new backfire antenna. The new design consists of a reflecting surface, a peripheral rim of adjustable width, and a feed system in the reflector center. The antenna was then optimized by varying the frequency and rim width to find its highest directive gain which was reported to be about 18dB.

The characteristic of the one-element loop antenna with a finite reflector were recently analyzed by Rojarayanont and Sekiguchi [63]. The current distribution on the loop antenna with a finite reflector was assumed to be the same as the loop current with an infinite reflector. Then, the current induced on the finite reflector by the exciting current of the loop was calculated. Assuming this current distribution on the finite reflector, the characteristics of one-element loop antenna with a finite reflector were obtained.

The advantage of the short backfire antenna is clear by noticing the structural advantage of a plane reflector over a parabolic dish, especially when the gain is less than 20dB. In the remaining part of this chapter, we will study the backfire antennas using a circular loop as the exciter. We expect to obtain a higher backfire gain since a one wavelength loop antenna has a higher gain than a half wavelength dipole.

Four different kinds of reflectors for the backfire antenna are discussed: i) an infinite reflector, ii) a finite solid reflector (a disk), iii) a disk reflector with a solid peripheral rim, and iv) concentric planar loops with and without peripheral rim, where the rim is also made of circular loops. Aside from the structural advantages of the backfire antenna constructed only with an array of coaxial circular loops, it also lends itself to exact analytical investigation. A circular loop antenna in front of an infinite reflector is discussed first and is given in the next section.

5.4.1 A Single Loop Antenna in Front of an Infinite Reflector

The exact current distribution of a loop antenna near an infinite reflector, its input impedance and the radiation characteristics are analyzed by the theory given in Chapter I. Using the image theory the problem reduces to that of an array with two identical elements and with $V_2 = -V_1$. Since the physical antenna radiates only above the ground plane, we therefore, use one half of the radiation field which falls

above the reflector. Figure (5-4) shows the directive gain of such an antenna along the axis of the loop antenna as a function of the loop spacing from the conducting plane and for several sizes of the loop. The directive gain of a half wavelength dipole antenna above the ground plane (due to Kraus [64]) is also given in figure (5-4) for comparison. It is seen that the gain approaches a constant value as the spacing decreases. This is in good agreement with the results of Kraus [64] for a lossless and a half wavelength dipole antenna. For practical antennas which have some finite loss, the gain will, however , decrease as spacing decreases. This is due to large current discussed below. It is also seen that the gain decreases with increasing the spacing. The system also has a higher gain and a wider bandwidth for a large exciter size. The maximum directive gain of a single loop antenna is about 4.6dB for $kb \simeq 1.45$. The maximum directive gain of a loop antenna with $kb = 1.4$ over a ground plane is 10dB which, therefore, is 5.4dB higher than an isolated loop antenna. This gain is also 1dB higher than the gain of 2-element loop antenna with $kb_1 = kb_2 = 1.3$ under an optimum excitation [65]. It should be mentioned here that the 10 dB is the optimum gain of a 2-element array which radiates into virtual half space.

Figures (5.5) and (5.6) show the input impedance of a loop antenna over a ground plane as a function of spacing and for several sizes of the exciter. Owing to the presence of the ground plane, the driving-point impedance of the antenna is, in general, different from that of its free space value. As shown in figure (5-5), the real part of the input

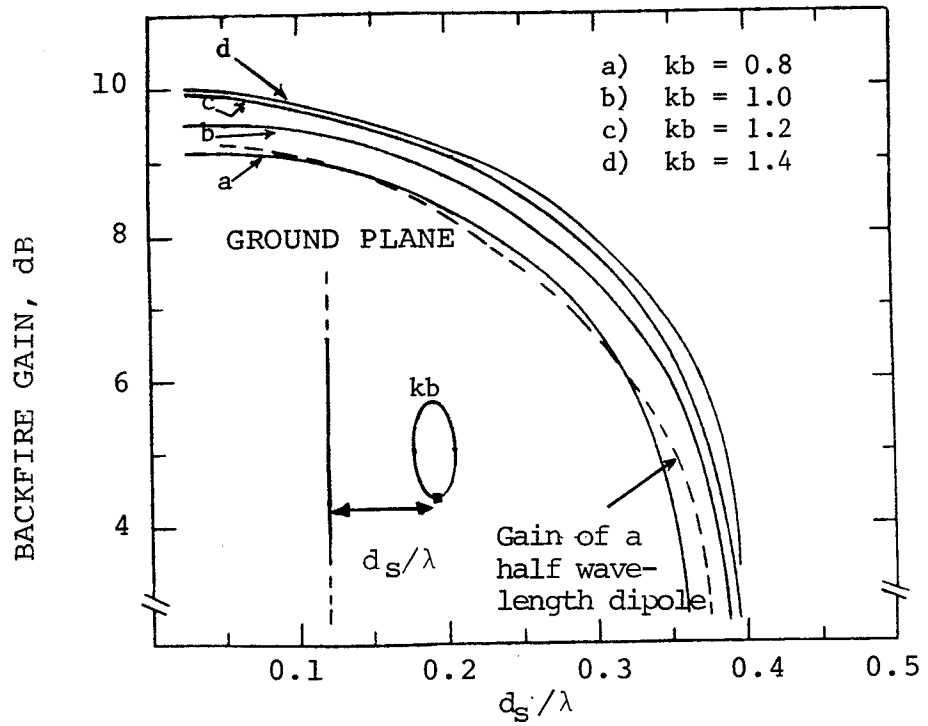

Fig. 5-4: Backfire gain of a loop antenna as a function of d_s/λ for various size of loops

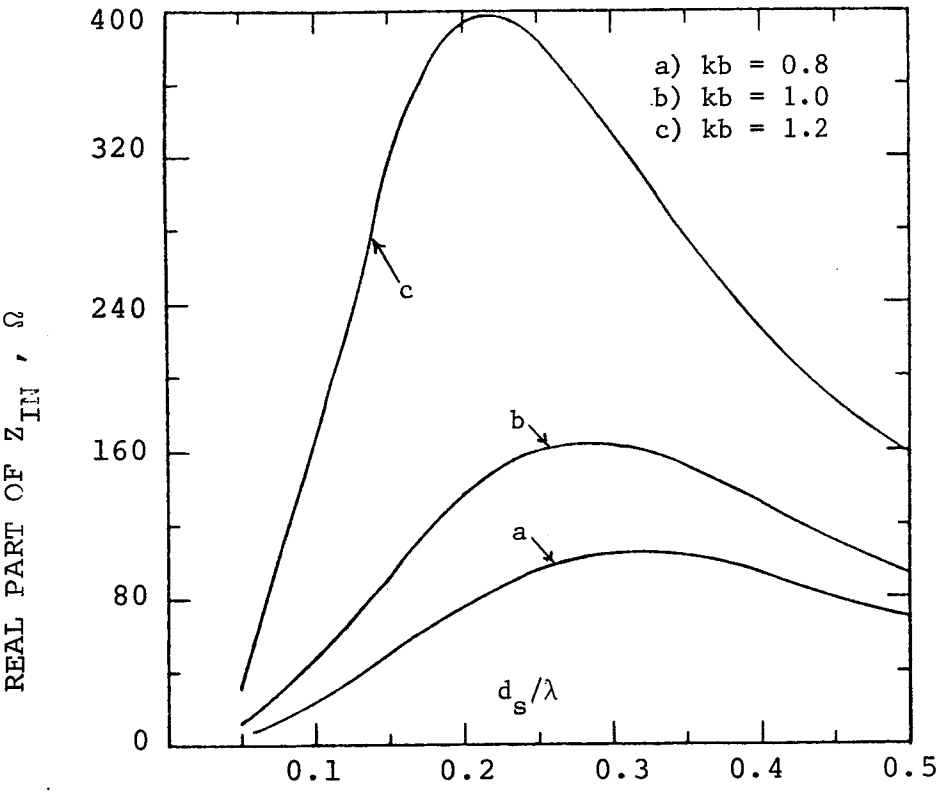

Fig. 5-5: Real part of input impedance of a loop antenna as a function of its spacing from perfectly conducting ground for various size of loops

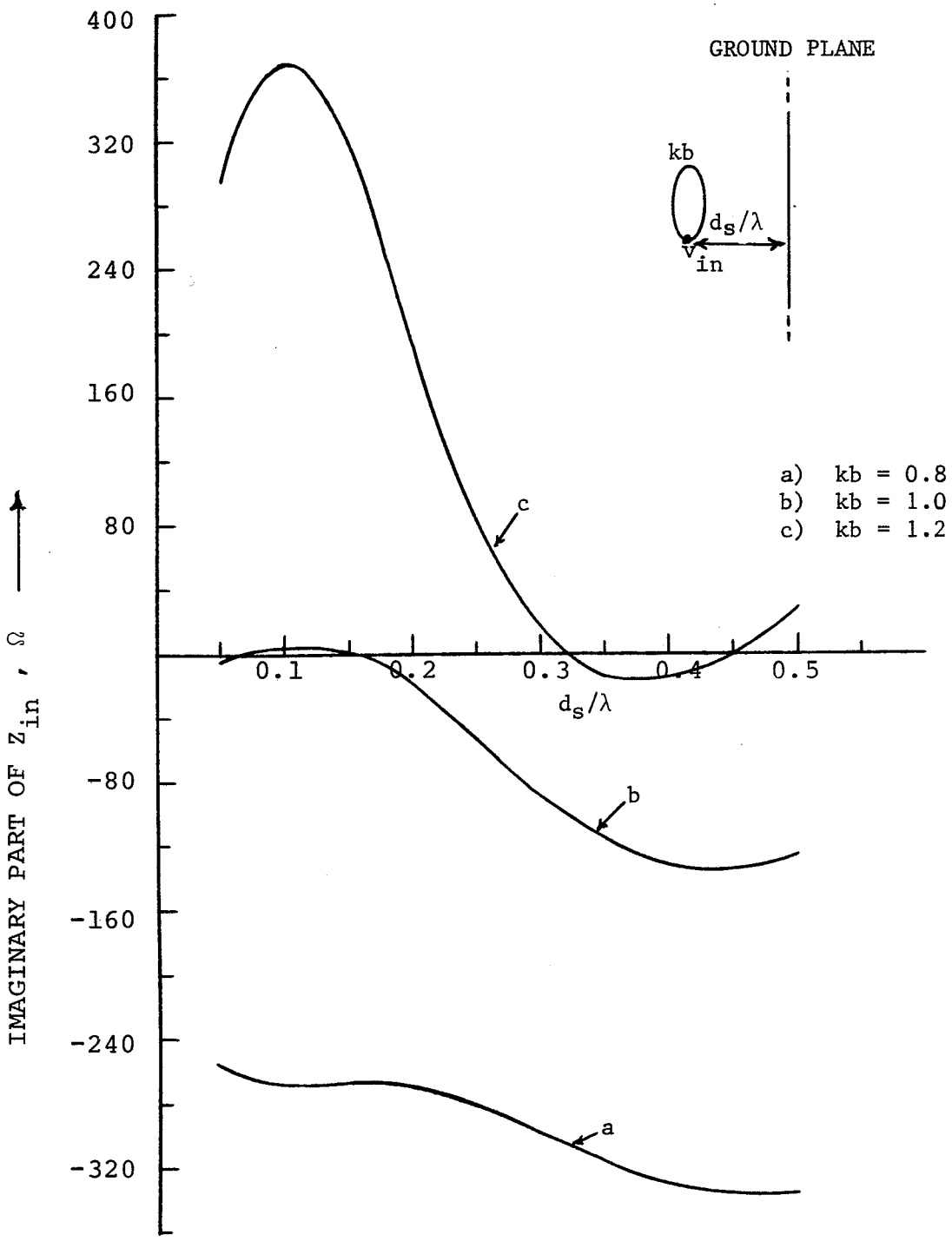

Fig. 5-6: Imaginary part of input impedance of a loop antenna as a function of its spacing from perfectly conducting ground for various size of loops.

impedance increases with increasing spacing and after reaching a maximum, it decreases with a further increase of the spacing. It is expected that both the real and the imaginary parts of the input impedance approach their free space values as the spacing becomes very large. It is interesting to note that the $Im(Z_{in})$ is very small for $d_s/\lambda \leq 0.2$ and $kb = 1$. Therefore, it is easier to match the antenna to the feeding system. Figure (5-7) illustrates the input current of the exciter loop as a function of the height of the antenna from the ground plane. It is interesting to note that the current on a closely spaced loop is very large and decreases as the height increases. However, the radiation resistance, figure (5-5), is relatively small for small spacing. Hence, a considerable reduction in the radiation efficiency may result if the structure were made of lossy material.

In summary, a single loop antenna above a ground plane is the simplest backfire antenna. With this simple geometry a gain as high as 10dB is achievable. A closer spacing gives a higher directive gain but may result in a deterioration of the efficiency, if the antenna has loss resistances. Referring to figures (5-4)-(5-6), it is recommended to use $kb = 1$ as the exciter element since it gives a better input impedance performance.

Since the antenna and its image have currents of equal magnitude, but opposite phase, there is a zero radiation in the direction of the ground plane, that is, in the direction normal to the loop antenna axis ($\theta = \pi/2$). In practice, the reflector size is finite and, therefore, the above results

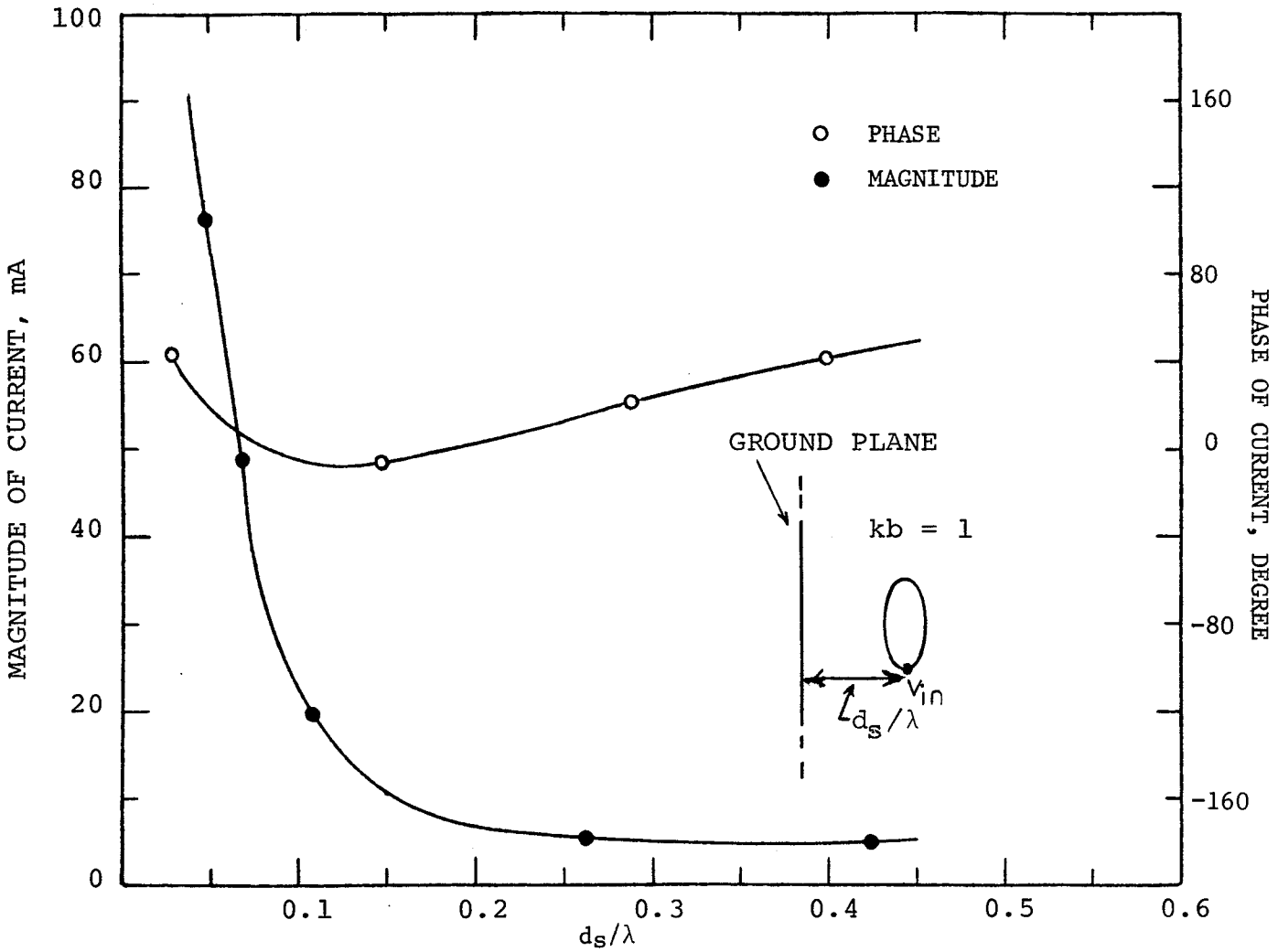

Fig. 5-7: The input current of a single loop antenna as a function of its spacing from perfectly conducting ground plane

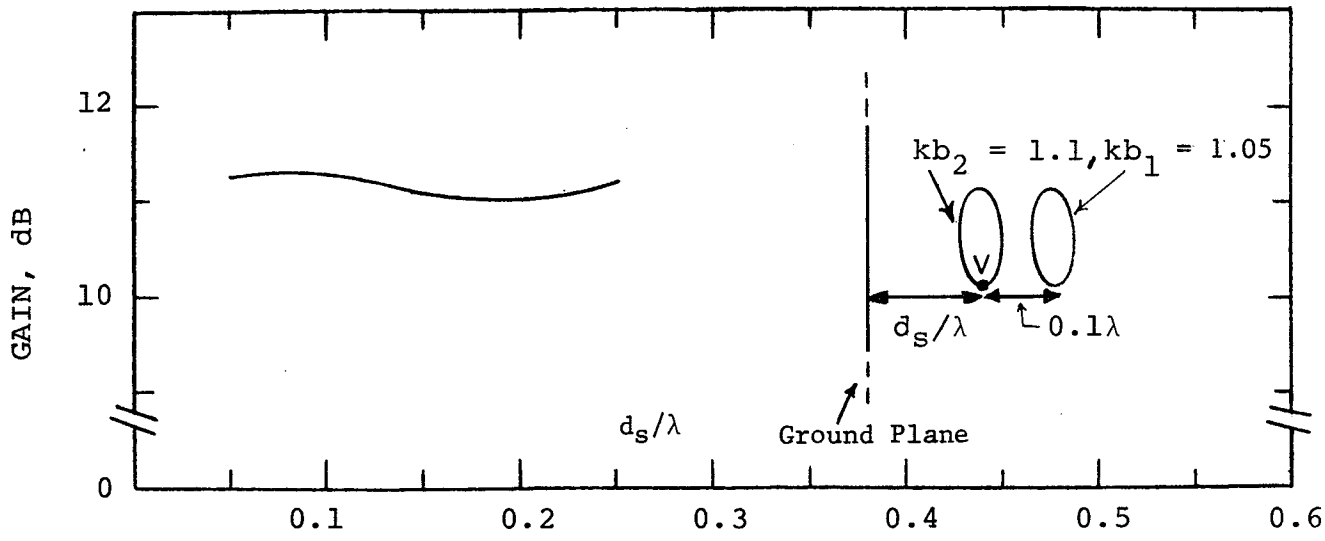

Fig. 5-8: Backfire gain of a 2-element loop array as a function of the array spacing from perfectly conducting ground plane

may not seem to be useful. However, if the reflector is several times larger than the loop diameter and the antenna is not too far from the reflector, the results given here will be applicable to the first order of approximation. The directive gain of this simple geometry still can be improved with placing an array of circular loops in front of the flat sheet reflector. Figure (5-8) shows the directive gain of a 2-element array above the ground plane as a function of its distance from reflector. One of the loops in the array acts as the secondary reflector which enhances the radiation towards the flat sheet reflector. The geometry of this two element array is selected for maximum radiation toward the reflector and is found to be for $kb_2 = 1.1$, $kb_1 = 1.05$ (the reflector) at a spacing of $d_{12}/\lambda = 0.1$ [45]. It is interesting to see that the addition of a reflector loop increases the backfire gain by more than 1dB over that of the structure without the reflector loop. On the other hand, the gain becomes relatively independent of the exciter to the main reflector spacing. Therefore, this spacing can be used as a mean to control the input impedance of the antenna. If the antenna above the ground plane is a long Yagi array, with its exciter as the second farthest element from the flat sheet reflector, the backfire gain will be 6dB over the isolated array. This is due to the fact that the maximum obtainable gain from endfire antennas is directly proportional to their lengths, provided the phase velocity is progressively adjusted to its optimum value as the antenna length is lengthened. The gain of an ordinary endfire antenna under

this optimum condition is about $10\ell/2$ above the isotropic value, where ℓ is the length of the structure [51]. Because the electromagnetic wave travels the physical length of the array twice in the case of a backfire antenna, this antenna acts like an ordinary endfire antenna with twice the length, and the phase velocity must be adjusted accordingly. We then expect to have a gain 3dB higher than that of the isolated Yagi array. The other 3dB increase in the gain is due to the Yagi and its image, which carries one half of the total power and radiates into virtual half space.

So far, the characteristics of a circular loop or an array of circular loops in front of an infinite reflector were investigated. The next section is devoted to study the radiation characteristics of a single loop in front of a finite reflector.

5.4.2 Backfire Antenna with a Finite Reflector

In a practical antenna the reflector has a finite size, which complicates the analytical solution. The problem of a finite circular reflector can be solved as the limiting case of an oblate spheroid [66]. However, due to the difficulties in computation of the spheroidal function, the solutions are usually hard to utilize practically. The introduction of a rim around the reflector further complicates the problem and an analytical solution becomes impossible to obtain. In the present work, we have therefore, decided to use a numerical method to study the problem of backfire antennas with a finite reflector. For a circular reflector, with and without a rim, the geometry has rotational symmetry and as such, can be stu-

died by computer programs available for these geometries. We have used a program which is based on the moment method and was prepared by Ole Rydahl [67] and [68]. Since the program does not use circular loop antenna as a source, it was decided to use a number of infinitesimal dipoles, located on a circle with the radius of the exciter, in order to simulate the desired exciter. The current for each dipole is selected in such a way that they represent the current distribution of the loop antenna. Figure (5-9) compares the radiation fields in the H and E-planes of a one wavelength loop antenna with those of eight infinitesimal dipoles located uniformly on a circle with $kb = 1$. Due to the symmetry only one half of the radiation patterns are shown. A good agreement between the results can be seen. The ring of dipoles then is used as a feed for finite backfire antennas. The finite reflector is chosen to be a disk. Figure (5-10) depicts the variation of the backfire gain with the diameter of the disk, when the ring of dipoles is located 0.15λ from the reflector. It is seen that the backfire gain increases with increasing diameter of the reflector and after reaching a relative maximum decreases with a further increase of the disk diameter. The maximum backfire gain is about 10.25dB which occurs for a disk diameter of about 1.45 wavelengths. This is about 1dB greater than the gain of a one wavelength loop antenna placed 0.15λ above the ground plane (figure 5-4). The decrease of the backfire gain with a further increase of the reflector diameter beyond 1.45λ may be due to the phase and the amplitude of the current on the reflector.

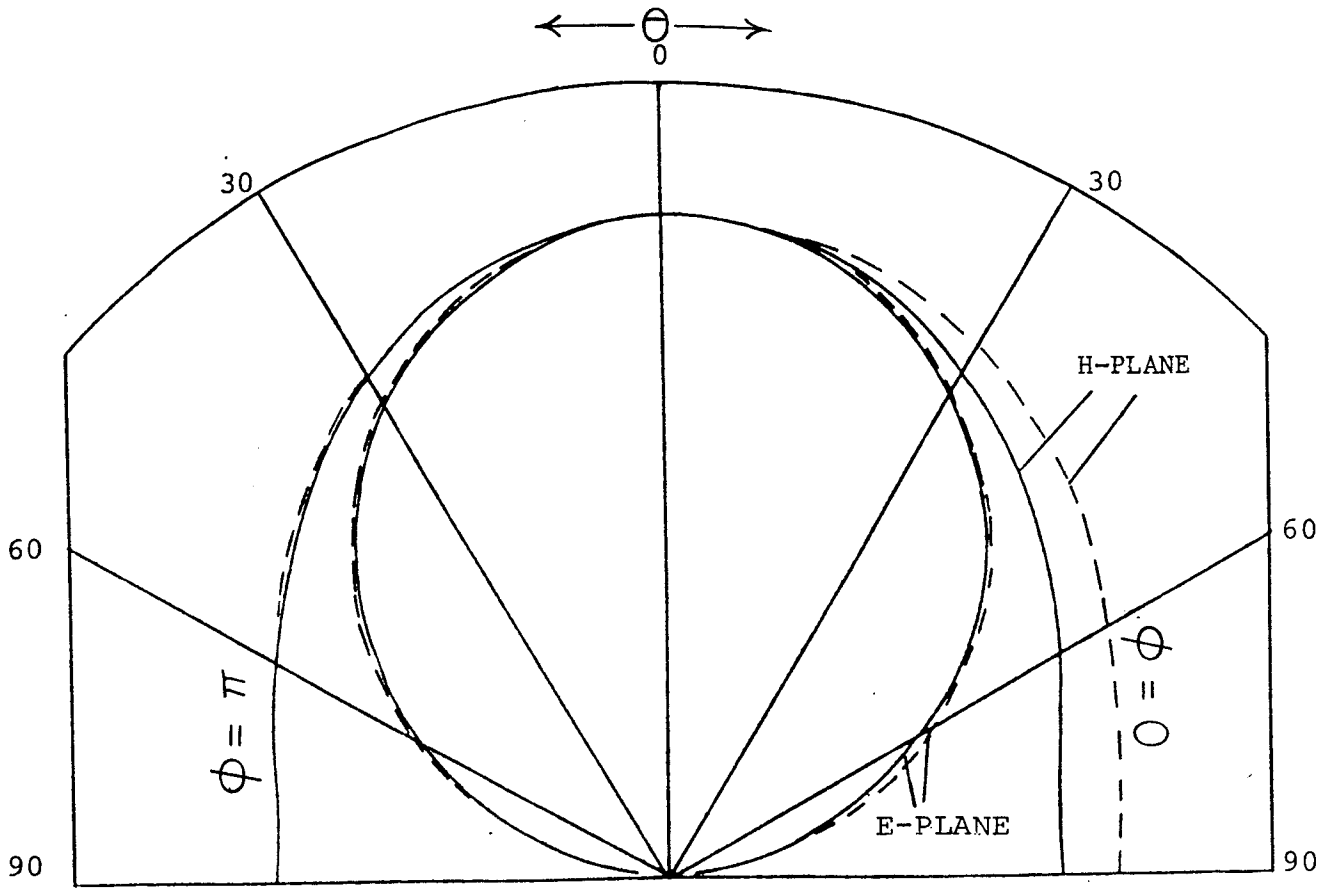

Fig. 5-9: Comparison of the radiation field of a one wavelength loop antenna against that of eight infinitesimal dipoles located uniformly on a circle with kb = 1. ———— field of dipoles, ------- field of loops

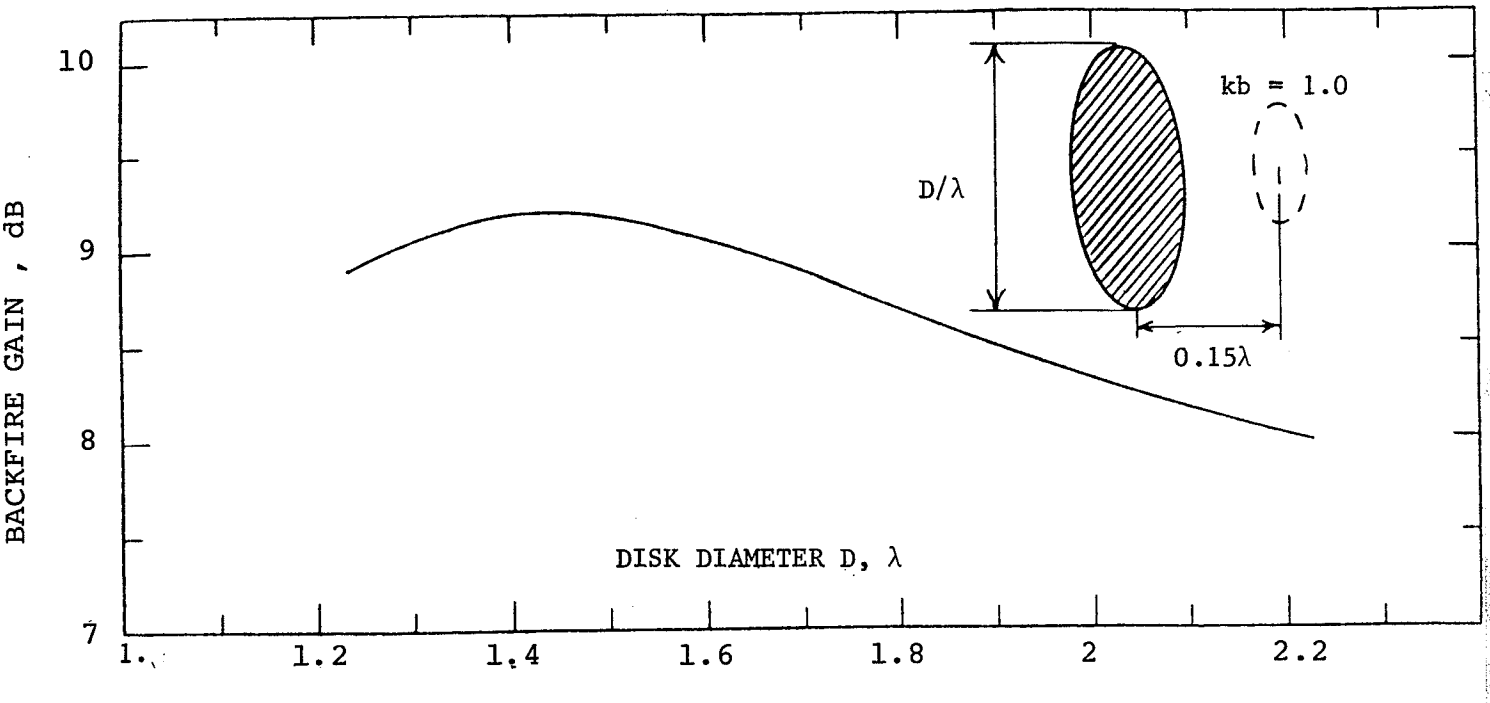

Fig. 5-10: Variation of the backfire gain with diameter of solid disk reflector

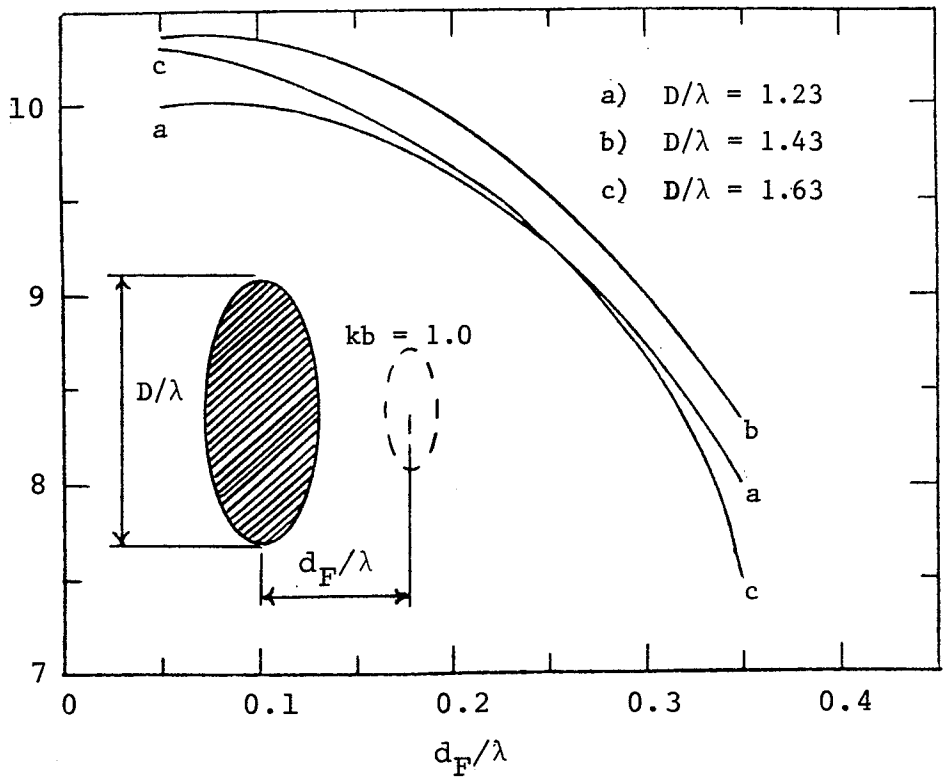

Fig. 5-11: Variation of the backfire gain as a function of the exciter spacing for various size of solid disk reflectors.

For a reflector diameter larger than 1.45λ fields produced by the currents on the reflector should be subtracted from each other, since the maximum gain of the antenna is obtained only if the field of all the currents on the disk add in phase.

Figure (5-11) shows the variation of the backfire gain of the above antenna as a function of the feed spacing and for various disk diameters. It is interesting to note that for a finite reflector, the behaviour of the backfire gain with the feed spacing is similar to that of an infinite reflector (figure 5-4). For both cases the backfire gain increases with decreasing distance of the loop antenna from the reflector.

Finally, figure (5-12) shows the current distribution on a disk reflector of radius 0.716λ with the exciter located 0.15λ away from the disk. Both the radial and the circumferential currents on the reflector are mostly concentrated in a region with circumference of about one wavelength ($D \simeq 0.36$). For $D > 0.36$ the components of the current begin decreasing rapidly with increasing R and the radial current I_R approaches zero near the edge of the disk. There is, however, a sudden increase in the ϕ component of the current I_ϕ near the disk's edge, which indicates the singularity of I_ϕ at the edge. It is also interesting to note that the phase of I_R and I_ϕ are almost constant in the region $D \leq 0.36$ where most of the current is concentrated.

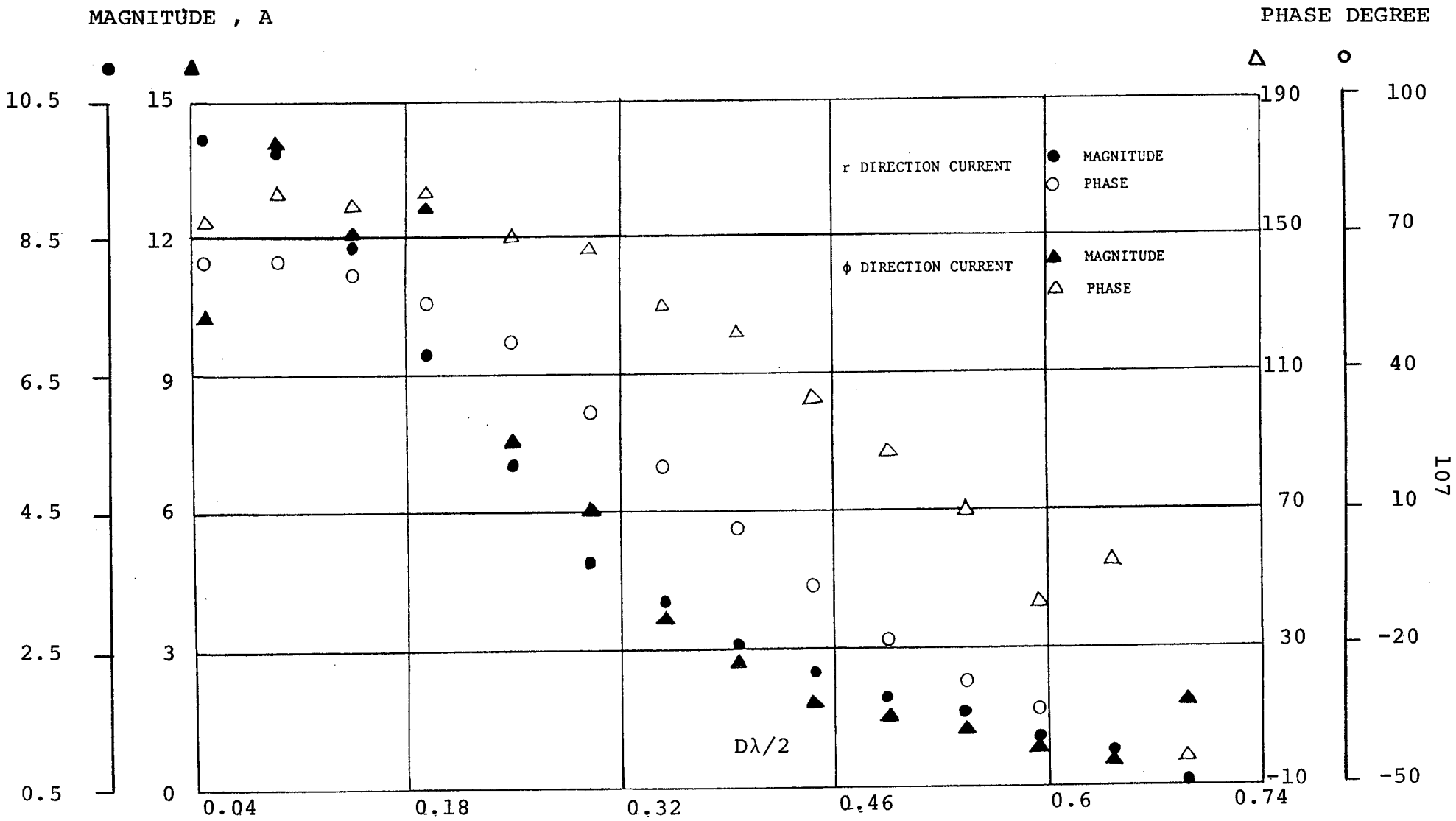

Fig. 5-12: Current distribution on a solid disk reflector of radius 0.716λ. The exciter is located 0.15λ from the disk.

Thus, the maximum gain of a loop in front of a disk reflector is about 10.25dB. It was mentioned earlier that for dipole fed backfire antennas, the addition of a peripheral rim to the disk reflector improves the backfire gain over that of a flat reflector. The following section is concerned with the investigation of such an antenna.

5.4.3 Backfire Antenna with a Rim

In this section, the numerical investigations are carried out for a disk reflector antenna with a rim around the disk. Figure (5-13) shows the variation of the backfire gain of such an antenna with the length of the peripheral rim and for various sizes of the disk diameter. As seen in the figure, the maximum gain is about 13.3dB and occurs for a reflector diameter and a rim length of about 1.75λ and 0.65λ, respectively. This indicates that the addition of the peripheral rim to the reflector surface increases the optimum size of the disk, since for a rimless antenna the optimum size of the diameter was obtained to be 1.45λ (figure 5-10). This increase in the optimum size of the reflector, and consequently an increase in the gain of the antenna, may be attributed to the improvement of the aperture field distribution due to the peripheral rim. Figure (5-14) shows the magnitude of the aperture fields, in both E and H-planes, at a distance of 0.25λ from the rim edge. It is seen that the radiating aperture of the antenna extends outside of the physical dimension of the structure, as was reported for the dipole feed case [62]. The magnitude of the field in the

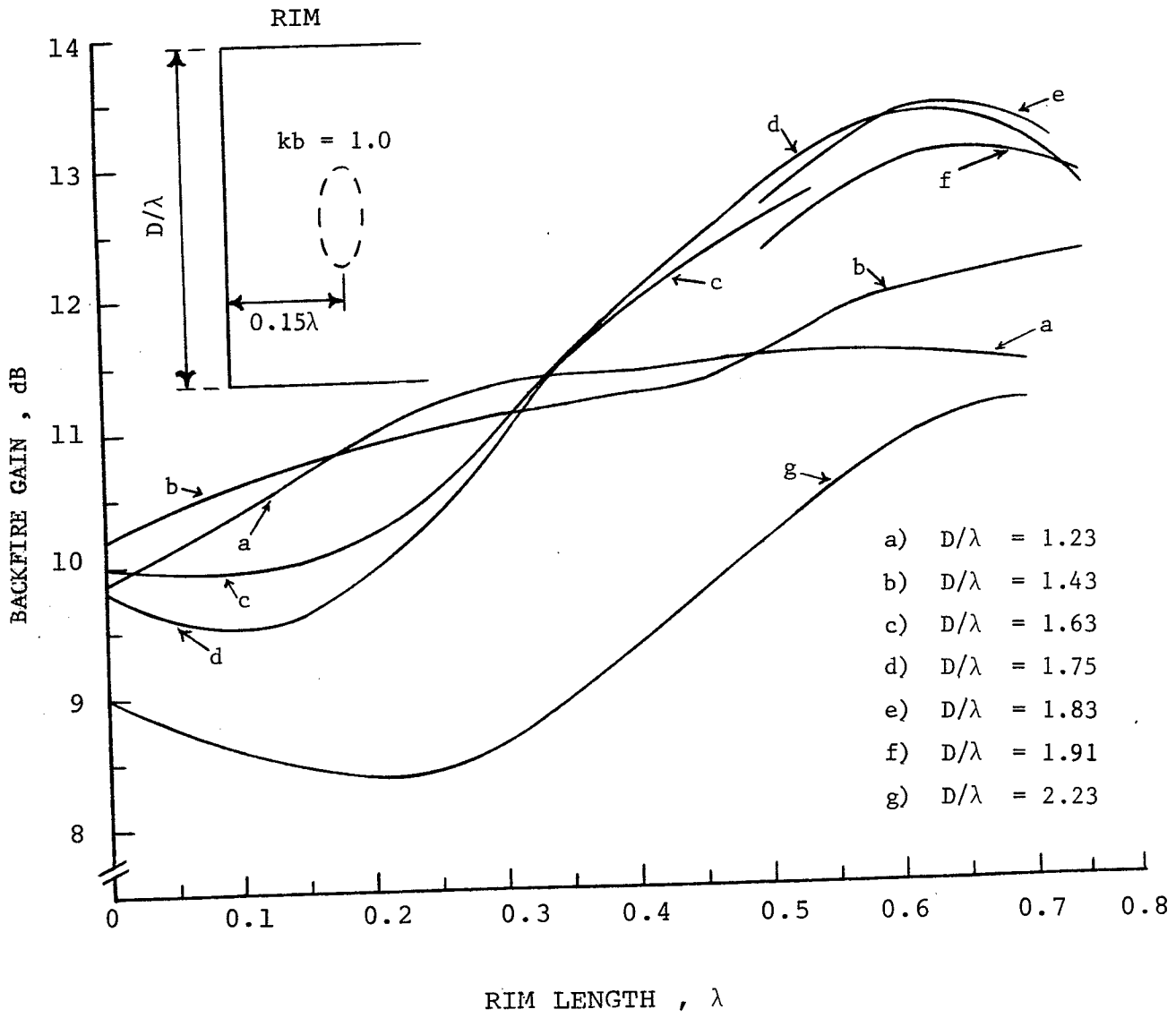

Fig. 5-13: Variation of the backfire gain with the length of the rim for various sizes of disk diameter

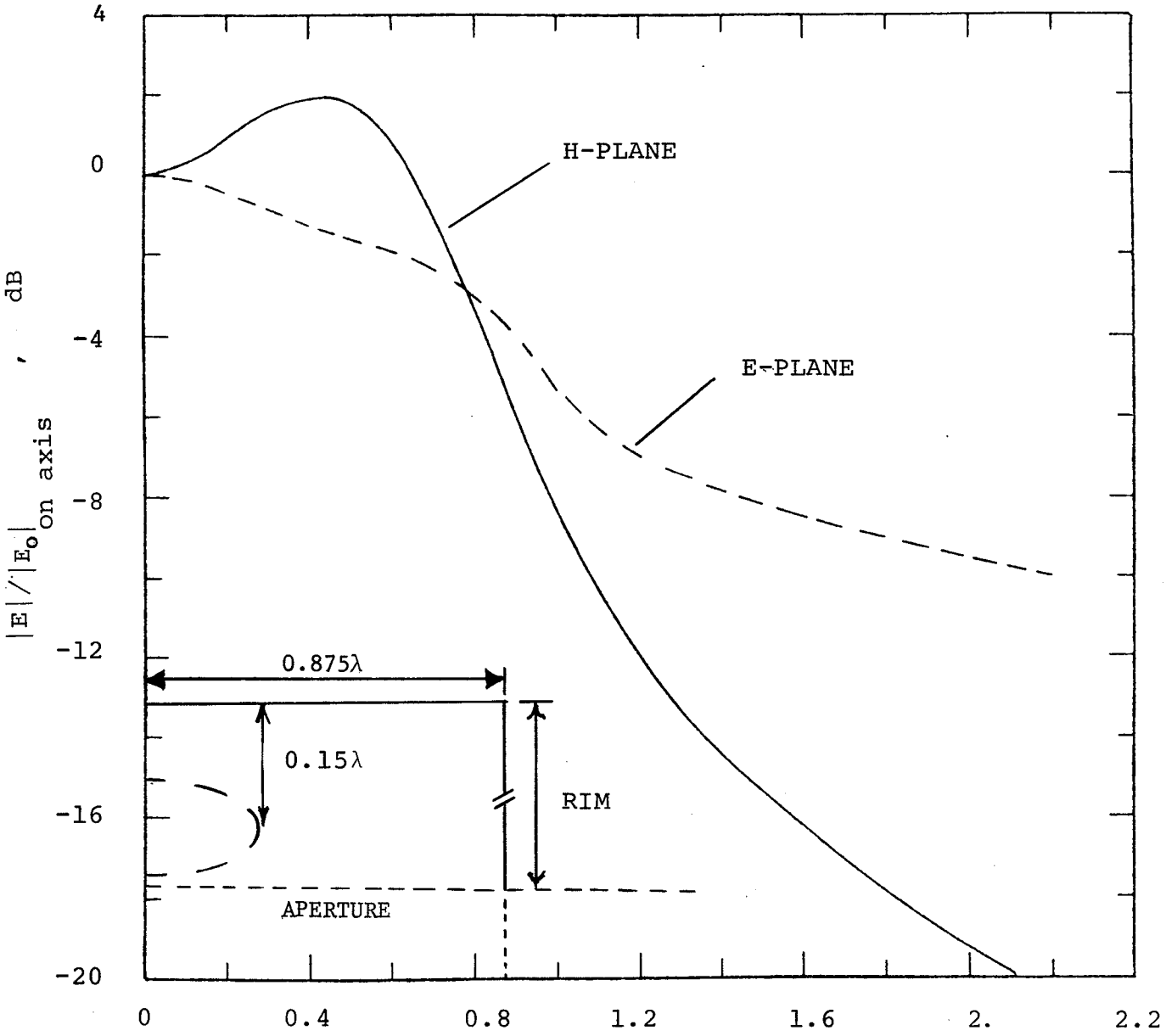

Fig. 5-14: Amplitude distribution in aperture of a solid backfire antenna with disk reflector of radius 0.875λ, rim length = 0.65λ and exciter spacing 0.15λ

H-plane increases initially, but tend to decrease rapidly in the vicinity of the aperture edge. It reaches 10dB below the aperture center value at a distance of about 0.2λ beyond the edge of the rim. In the E-plane, however, the field decreases continuously from the aperture center, but the rate of decrease is slower. It reaches the 10dB value at approximately 1.3λ from the aperture edge. This increase in the radiating aperture of the antenna explains the higher directivity obtained for this structure. It should be mentioned here that Ehrenspeck has reported a gain of 14.2dB for a reflector of diameter 1.75λ and a rim length of about 0.6λ [62]. However, he used a short backfire feed (SBF), a dipole feed with a reflector disk in front of it, or an array of SBF, since a single dipole can only illuminate reflector areas of approximately $2\lambda^2$ [62]. Ehrenspeck, unfortunately, does not provide any information about the SBF.

Since the gain of a one wavelength circular loop antenna is greater than that of a half-wave dipole, its effective area should also be greater. The relation between the effective area of an antenna and its power gain is given by [69]

$$A = \frac{G\lambda^2}{4\pi} .$$

For a one wavelength loop $A_\ell = 2.21\lambda^2/4\pi$ and for a half wave dipole $A_d = 1.64\lambda^2/4\pi$. The difference between A_ℓ and A_d may indicates that reflector areas greater than $2\lambda^2$ can be used for a single circular loop. In fact curves d ,

e and f given in figure (5-13) show that for the reflector areas greater than approximately $2.7\lambda^2$ the gain decreases. That is, for larger reflectors a single loop can not illuminate properly the active reflector areas and an SBF (a single loop with a disk reflector in front of it), whose effective radiating aperture is larger than that of a single circular loop, must be used. It should be noted that the approximate area which can be illuminated properly by a single loop antenna may also be found from the knowledge of A_ℓ, A_d and the approximate maximum area illuminated properly by a single half-wave dipole, which is given by $2\lambda^2$. That is

$$\frac{A_\ell}{A_d} \cdot (2\lambda^2) \simeq 2.7\lambda^2$$

which is the same as that obtained numerically in the above investigation.

5.4.4 Backfire Antenna with Planar Concentric Loops as a Reflector

It is often necessary to reduce the weight, windage (wind loading parameter), or obstruction of view which accompanies the solid reflectors studied in this chapter. In the remaining part of this chapter, we will investigate the possibility of employing planar concentric loops to construct reflectors in a backfire antenna.

Figure (5-15) shows the backfire gain of a single loop antenna in front of planar concentric loops as a function of the exciter spacing from the reflector. The size of

the exciter and the smallest loop on the reflector are selected to be 1.1 and 1.05, respectively [45]. In addition, the ratio of the radii (the ratio parameter) of two consecutive loops on the reflector is assumed as a parameter in figure (5-15). It is seen that the backfire gain decreases as spacing increases. This behaviour is similar to that of a single loop antenna in front of a reflector disk (figure 5-11). Notice that the backfire gain is almost independent of the ratio parameter. However, the best results are obtained when the ratio parameter and the circumference of the largest loop on the reflector are about 1.2 and 4.5λ, respectively. It is interesting to note that the optimum size of the reflector loop is about the same as the reflector disk. Figure (5-16) shows the variation of the gain with the exciter spacing where the number of loops which construct the reflector is the parameter. In all cases the size of the largest loop on the reflector is about 4.5λ. It is seen that 5 or 6 loops are enough to construct the reflector. An extensive investigation was carried out in order to obtain the best possible choice for the size of the smallest loop (kb_2) on the reflector loop. It was found that the size of kb_2 depends on the size of the exciter, kb_1. The best performance was obtained when $kb_1 = 1.0$ and $kb_2 = 1.1$, or $kb_1 = 1.1$ and $kb_2 = 1.05$, or finally $kb_1 = 1.2$ and $kb_2 = 1.1$. The last two sets of kb_1 and kb_2 give slightly larger backfire gain, than the first set, since the antenna composed of only these two loops have a strong back radiation

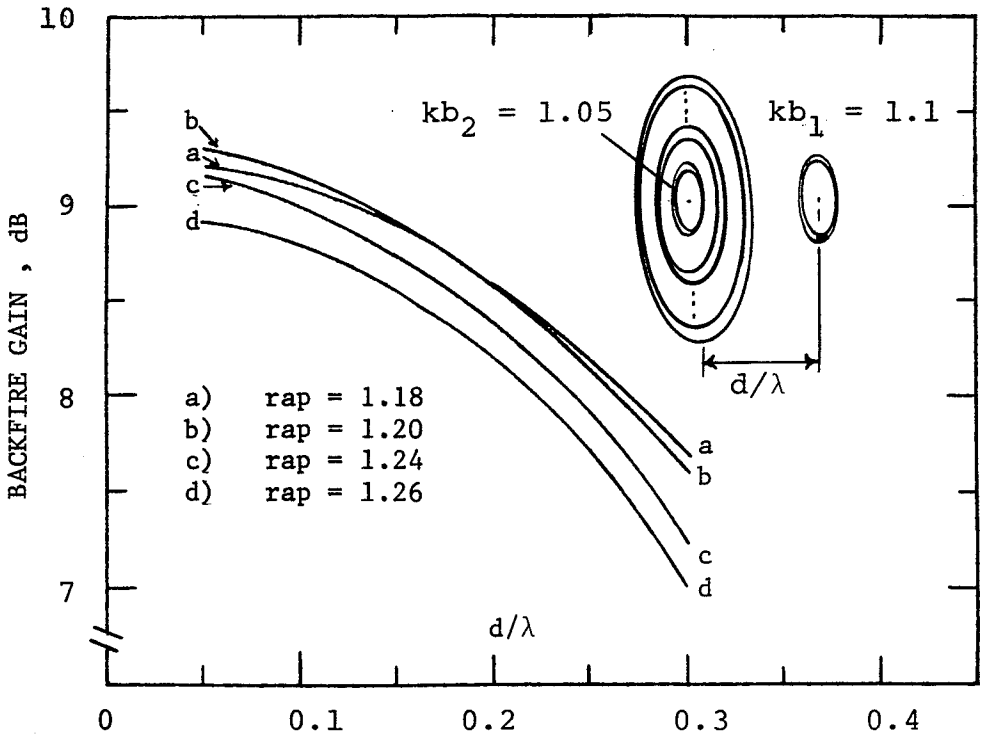

Fig. 5-15: Backfire gain of a loop antenna in front of coaxial planar loops as a function of exciter spacing and for various ratio parameter, rap

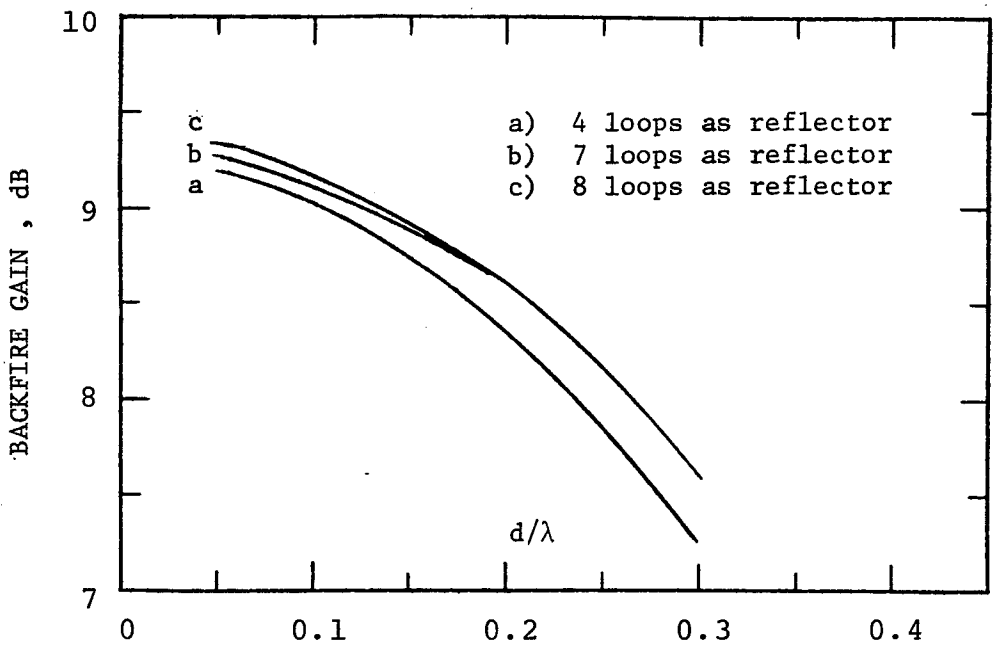

Fig. 5-16: Variation of the backfire gain with exciter spacing. The number of loops on the reflector is the parameter and $kb_{Max.} \tilde{} 4.5$ for all cases

[12] and [45].

Figure (5-17) gives the backfire gain of an antenna similar to that of figure (5-15) as a function of the reflector to exciter spacing. In this figure the size of the exciter, kb_1, is the parameter and the size of the smallest loop on the reflector, kb_2, always satisfies the relation $kb_2 = kb_1 + 0.1$. In addition, the ratio parameter is kept constant and equal to 1.2. It is seen that for $kb_1 = 0.9$, the backfire gain is very poor and for $kb_1 \geq 1$ the gain initially increases with increasing spacing and after reaching a maximum it decreases with a further increase of the spacing. An important conclusion from this behaviour is that, when the exciter is smaller than the smallest loop on the reflector, the backfire behaviour departs from that of a single loop above an infinite ground plane for the exciter spacing less than 0.15λ. Figure (5-18) compares the H-plane far field radiation of the disk reflector with that of loop reflector for exciter spacing of 0.15λ. The agreement between the two radiation patterns is very good in the backfire direction. As expected, the front radiation for the loop reflector is larger than that of the solid reflector.

5.4.5 Backfire Antenna with Peripheral Rim Constructed With Loops

In this case, the loop reflector has a peripheral rim which is also constructed with circular loops. Figure (5-19) shows the variation of the backfire gain as a function of

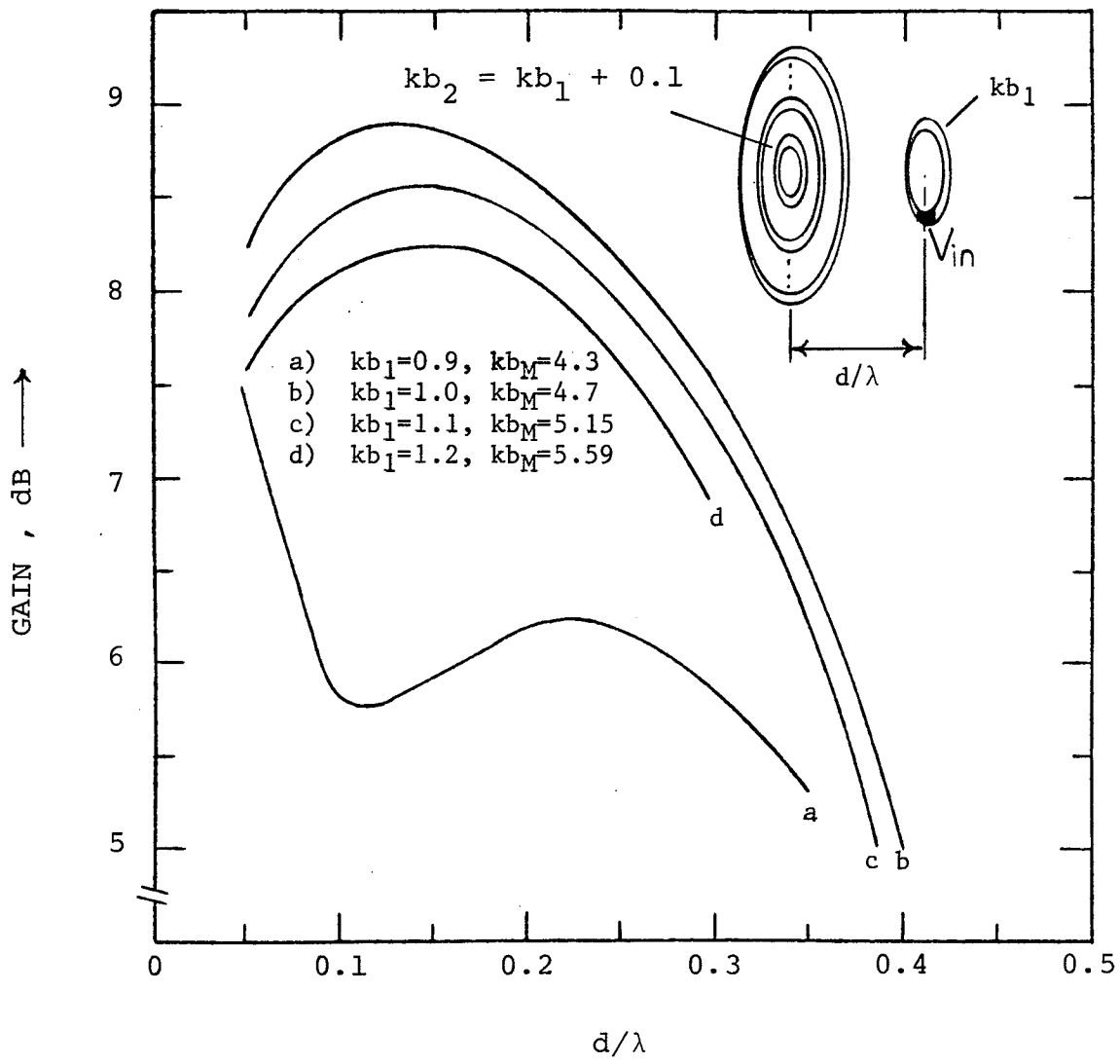

Fig. 5-17: Variation of the backfire gain with exciter spacing. The size of the exciter, kb_1, is the parameter and the size of the smallest loop on the reflector, kb_2, always satisfies the relation $kb_2 = kb_1 + 0.1$

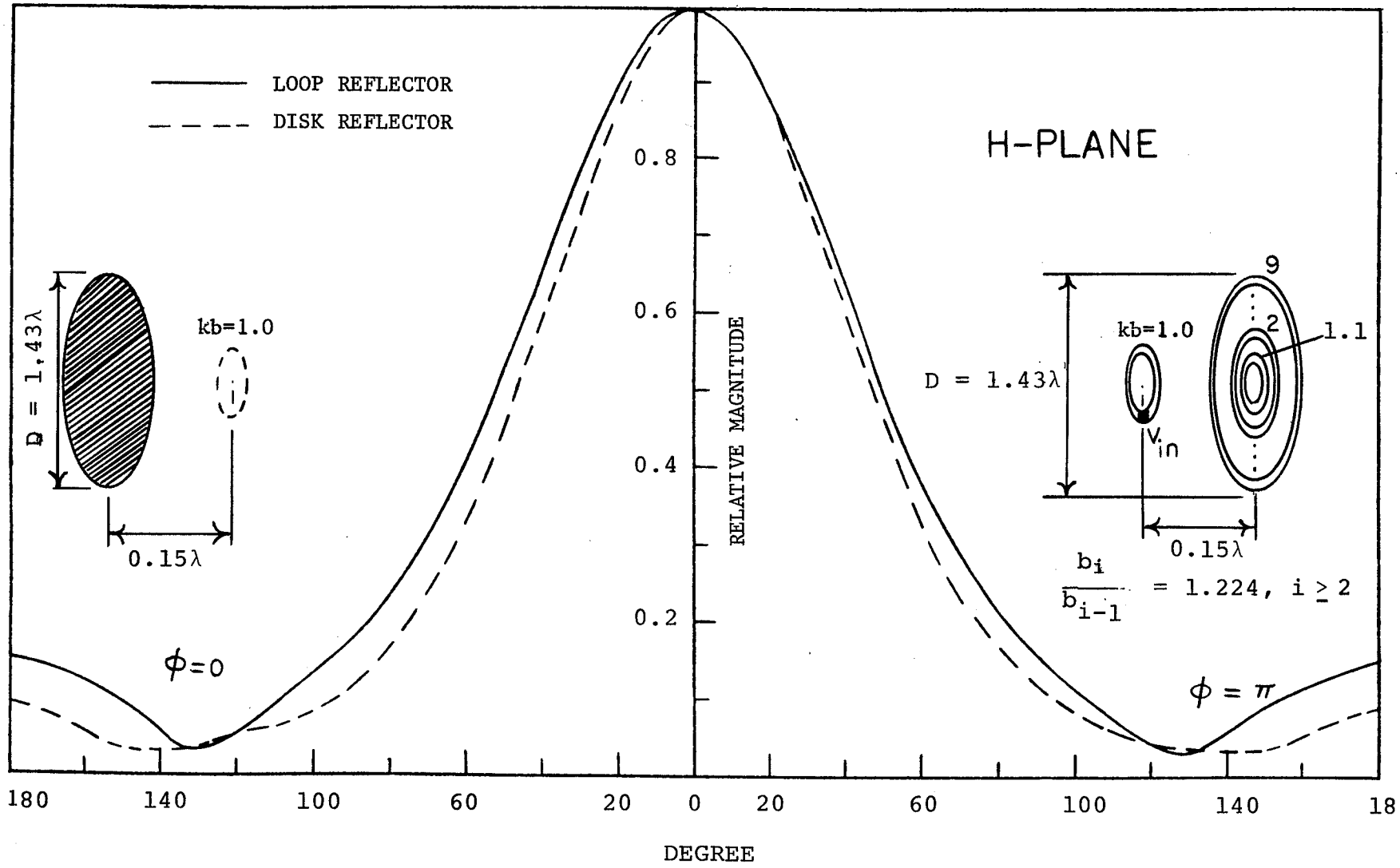

Fig. 5-18: Comparison of the H-plane for field radiation of a backfire antenna with disk reflector against that of a backfire antenna with loop reflector. The exciter is located 0.15λ from the reflector and its size, $kb_1 = 1$. The reflector diameter $D \simeq 1.43\lambda$

the rim length and for various diameters of the loop reflector. The size of the exciter (kb_F) and consequently the size of the smallest loop in the reflector (kb_S) are chosen to be 1.0 and 1.1, respectively, in order to compare the results of this antenna with those of the solid reflector. As mentioned earlier, a better gain performance can be achieved with $kb_F = 1.1$ ($kb_S = 1.05$) or $kb_F = 1.2$ ($kb_S = 1.1$). The maximum gain in figure (5-19) is about 12.3dB which is obtained from curve f which corresponds to a reflector diameter and a rim length of $D \simeq 1.93\lambda$ and 1.1λ, respectively. It is seen that for $D \geq 1.75\lambda$ the maxima of the curves are within 0.2dB of that of curve d, for which the maximum occurs for a rim length of about 0.65λ. It also gives a superior gain performance over the other curves in figure (5-19) for rims smaller than 0.65λ. In addition, the geometry related to curve d has the structural advantage of a smaller size and lower cost over e and f, with about the same optimum gain. It is also interesting to observe that, at the maximum of curve d, the size of the rim and the diameter of the loop reflector are about the same as those of the solid reflector given in curve d of figure (5-13). Their optimum gain differ only by approximately 1.2dB. Figure (5-20) compares the far field radiation pattern of the solid reflector with that of loop reflector in both the E and H-planes. Their agreement in backfire direction is good. However, there is approximately a 6.4dB difference between the level of the first side lobes in the H-plane.

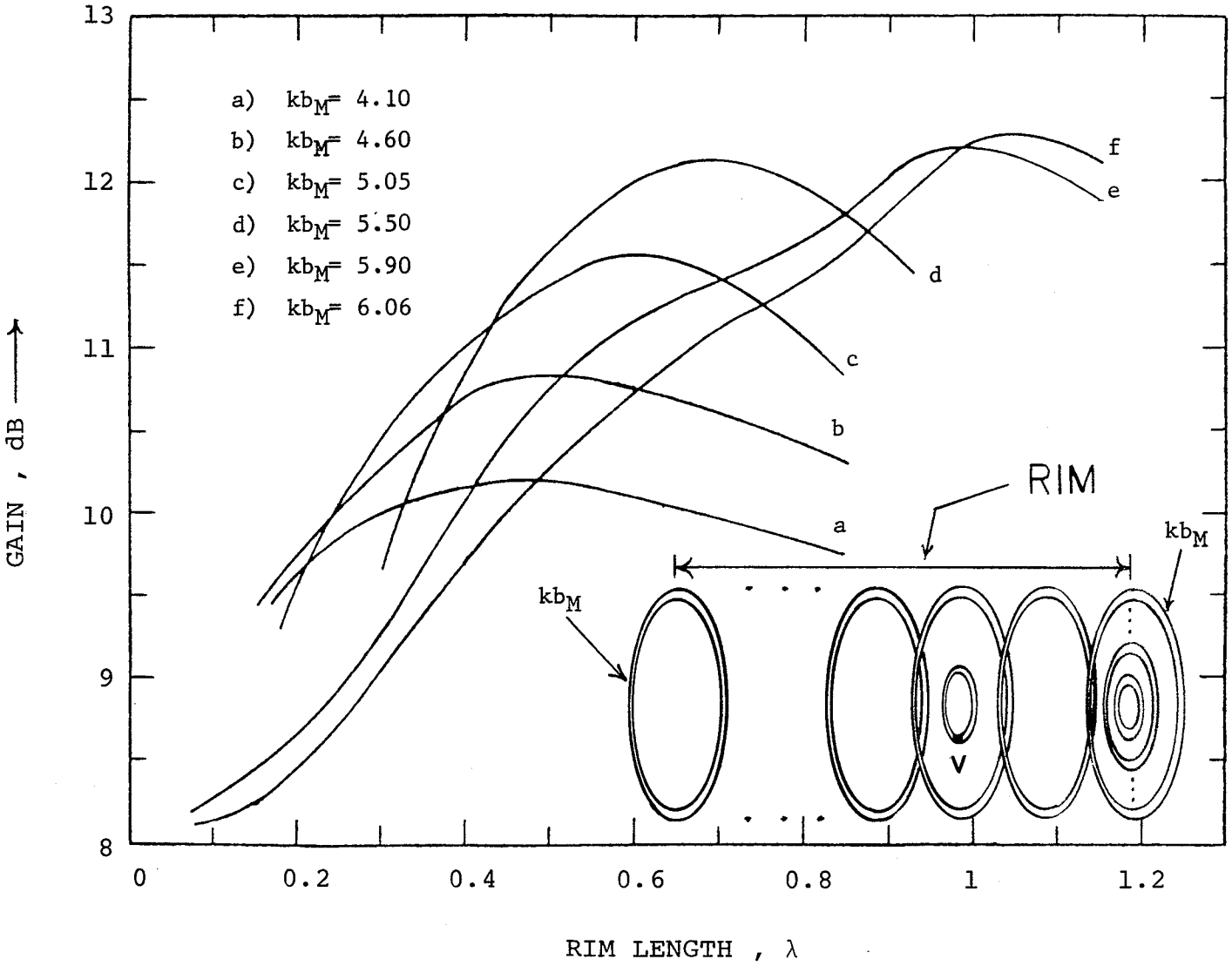

Fig. 5-19: Variation of backfire gain as a function of the rim length and for various diameters of the loop reflector

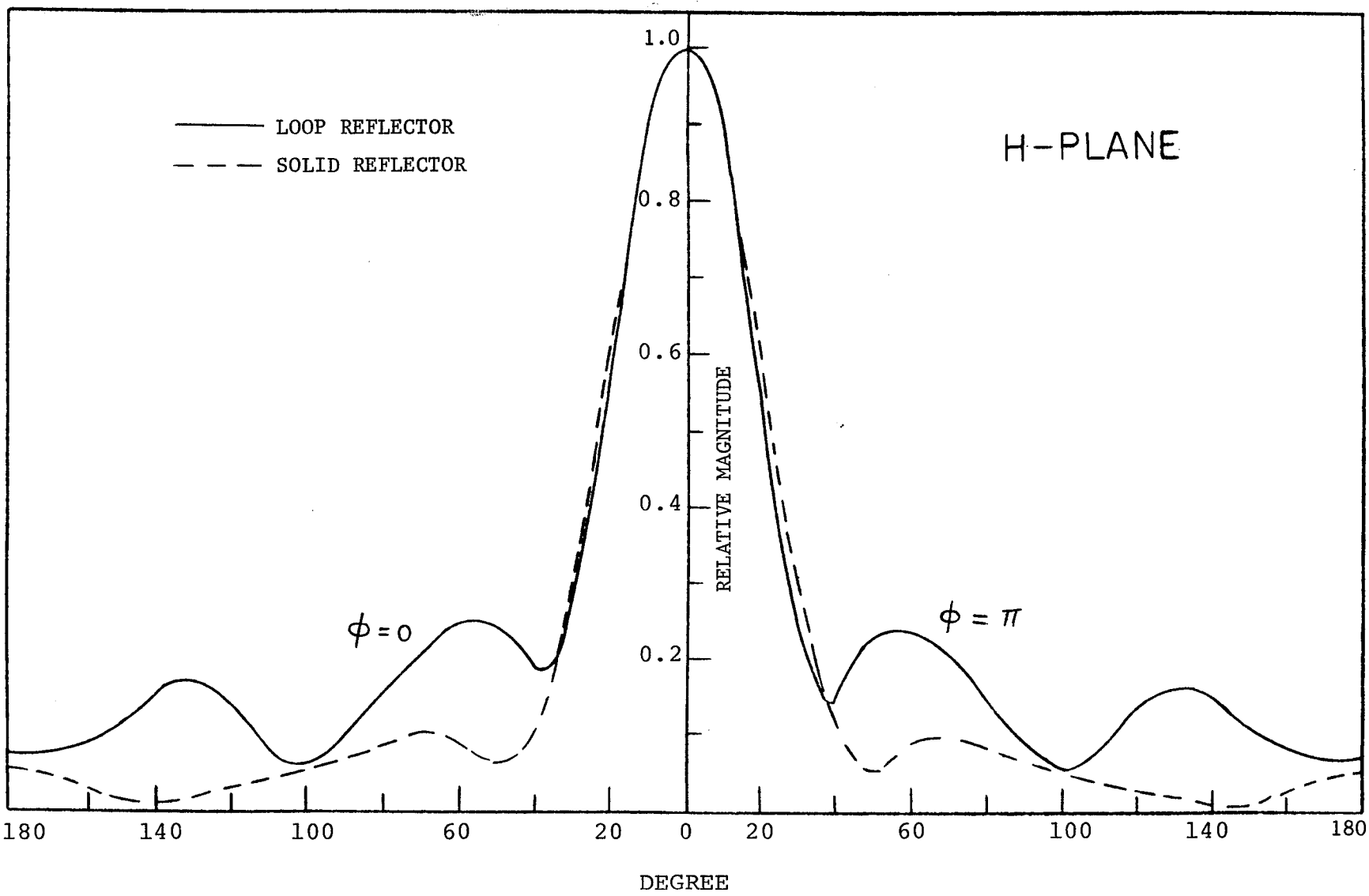

Fig. 5-20a: Comparison of the H-plane far field radiation of a backfire antenna with solid disk reflector and rim against that of a backfire antenna with loop reflector and rim (total of 13 loops). The exciter size $kb_1 = 1$ and located 0.15λ from the reflector, rim length = 0.65λ, reflector diameter D = 1.75λ

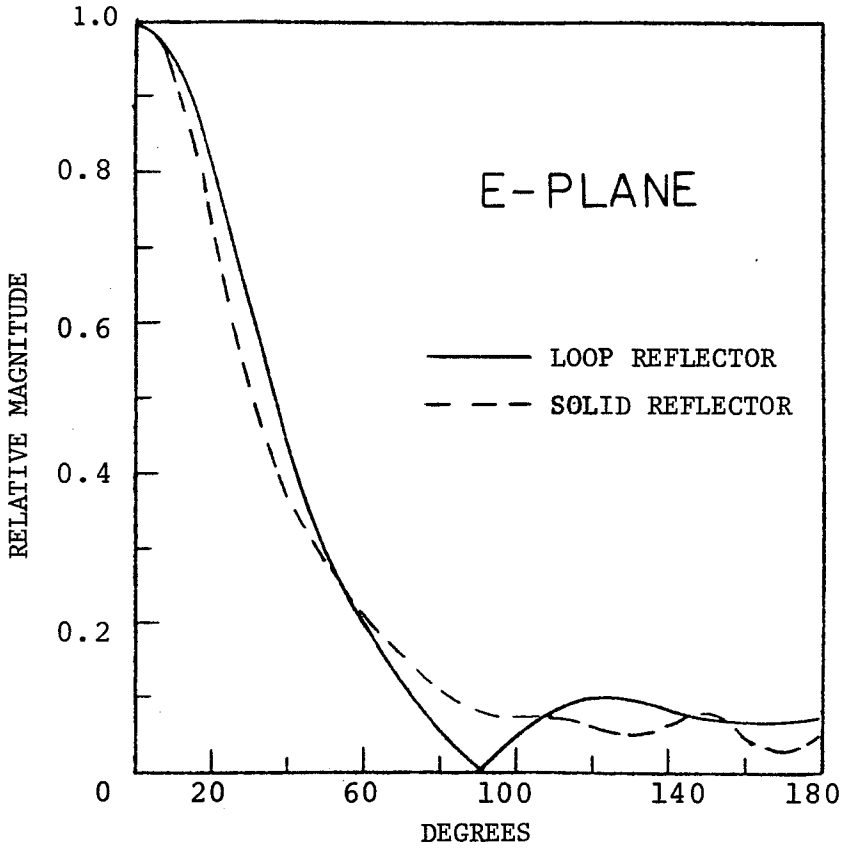

Fig. 5-20b: Comparison of the E-plane far field radiation of a backfire antenna with solid disk reflector and rim against that of a backfire antenna with loop reflector and rim (total of 13 loops). The exciter size $kb_1 = 1$ and located 0.15λ from the reflector, rim length = 0.65λ, reflector diameter $D = 1.75\lambda$

5.5 Summary

The radiation properties of planar loop arrays and backfire antennas were investigated in this chapter. In the beginning, a general method was developed which enables one to study compact coaxial loop arrays. The method was used to study the characteristics of a new type of antenna, i.e., a planar loop array. It was shown that the array supports a very weak surface wave along itself and radiates mainly in the broadside direction.

The technique was then used to investigate the radiation characteristics of backfire antennas constructed entirely with loops. That is, arrays of coaxial loops were employed to construct the peripheral rim and the reflector. The comparison was made between this new type of backfire antenna and the conventional one with a solid reflector. It was found that the optimum size of the reflector is approximately the same for both kinds of reflectors. For antennas with or without a rim, the diameters of the reflectors were found to be 1.75λ and 1.43λ, respectively. The length of the rim at optimum gain was also found to be about the same for both kinds of reflectors, and was about 0.65λ. Moreover, the optimum gain of the solid reflector was found to be only about 1dB larger than that of the loop reflector. It was found that as few as 6 loops are sufficient to construct the optimum size of the reflectors and almost the same number of loops are required to form the optimum peripheral rim. Furthermore, aside from the structural advantages that the

new backfire antenna has over the solid reflector, i.e., reduction of weight, windage, or obstruction of view, it also lends itself to exact analytical investigation.

CHAPTER VI

CHARACTERISTICS OF TWO INFINITE AND FINITE CONCENTRIC LOOP ARRAYS WITH LOADED ELEMENTS

6.1 Introduction

The analysis presented in the preceding chapters has been restricted to single circular loop arrays. This chapter deals with the analysis of wave propagation on two infinitely long and concentric loop arrays. This kind of structure was recently investigated by the so called "antenna theory" method which consists basically of calculating the electric field due to all elements when a surface wave is propagating along the structure [70]. The phase velocity of the propagating wave along the array has revealed that the array possesses two distinct passbands, corresponding respectively to the resonance of the outer and the inner sub-arrays and are separated by a stopband. The width of the stopband normally depends on the ratio of the loop radii for the outer and the inner arrays. It increases as the ratio of the radii increases and this increase tends to shift the bandwidth of the first passband to lower frequencies. In addition, the bandwidth of the second passband is found to be generally much smaller than that of the first passband. From a practical point of view one, therefore, should design an antenna which has relatively wide operating bands in both passbands. It is also desirable to investigate the method of excitation of this dual array.

This chapter considers both of the above problems. The "circuit theory" method developed in Chapter II is combined with the technique given in Chapter V in order to investigate the radiation properties of finite and infinite arrays of two concentric loops. To improve the bandwidth characteristics, the loading of the array elements with a reactive impedance element is considered. Although the analysis is general, only the numerical results for loading of the inner array are studied. The first passband, corresponding to the outer array, is designed to have a relatively wide characteristic.

The excitation of finite Yagi arrays with concentric loops are also studied in this chapter. Three different methods of excitation are considered; only the outer sub-array is excited, both sub-arrays are excited or, only the inner one is excited. It is shown that, from a practical point of view, the excitation of only the outer sub-array seems to give the most superior gain and input impedance characteristics.

6.2 A Relation for the Phase Velocity

The geometry of the array is shown in figure (6-1), where all its parameters are defined. The array is extended to infinity in both directions and it is assumed that the first mode is propagating along the array. Therefore, the currents on the elements of the reference cell, consisting of the inner and the outer loop located on the xy plane, can be presented as

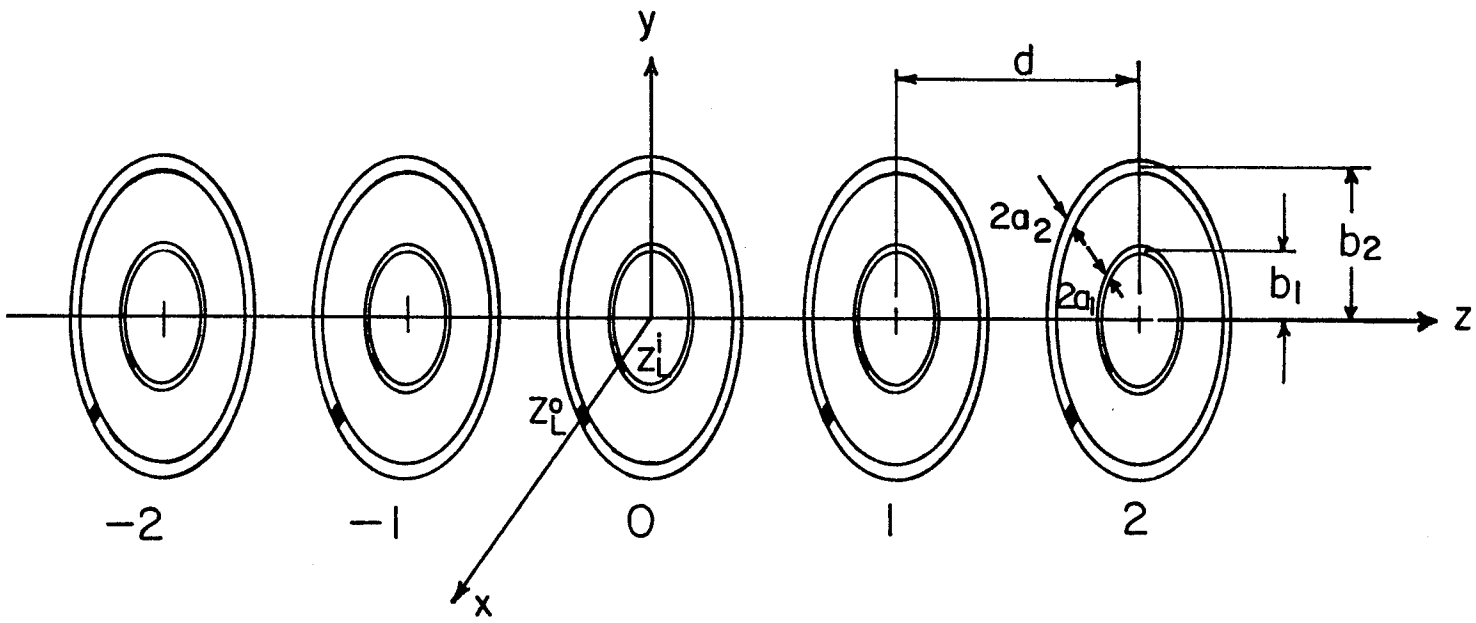

Fig. 6-1: An infinite array of concentric loops

$$I_0^i(\phi) = I_0^i \cos\phi$$
$$I_0^o(\phi) = I_0^o \cos\phi \qquad (6.1)$$

where the superscripts i and o are related to the inner and the outer loops, respectively. For propagation along the z direction with no attenuation, the current distribution on equal size loops of adjacent cells differ only by a phase factor $e^{-j\beta d}$ (with a time factor $e^{j\omega t}$), where β is the propagation constant of the travelling wave along the array. In order to apply the boundary conditions on the element surface, the loads Z_L^i and Z_L^o are replaced by a constant voltage generators V^i and V^o, respectively. Now the application of the boundary conditions can be carried out in a manner similar to that explained in Chapter II. The final result gives

$$I_0^i \sum_{m=-\infty}^{\infty} Z_{0m}^1 e^{-j\beta md} + I_0^o \sum_{m=-\infty}^{\infty} \hat{Z}_{0m}^1 e^{-j\beta md} = -Z_L^i I_0^i$$
$$I_o^i \sum_{m=-\infty}^{\infty} \hat{Z}_{0m}^1 e^{-j\beta md} + I_0^o \sum_{m=-\infty}^{\infty} Z_{0m}^{11} e^{-j\beta md} = -Z_L^o I_0^o \qquad (6.2)$$

which in a matrix form becomes

$$\begin{bmatrix} \sum_{m=-\infty}^{\infty} Z_{0m}^1 e^{-j\beta md} + Z_L^i & \sum_{m=-\infty}^{\infty} \hat{Z}_{0m}^1 e^{-j\beta md} \\ \sum_{m=-\infty}^{\infty} \hat{Z}_{0m}^1 e^{-j\beta md} & \sum_{m=-\infty}^{\infty} Z_{0m}^{11} e^{-j\beta md} + Z_L^o \end{bmatrix} \begin{bmatrix} I_0^i \\ I_0^o \end{bmatrix} = 0 \qquad (6.3)$$

This set of homogeneous algebraic equations has a solution if its determinant vanishes. That is,

$$\left(\sum_{m=-\infty}^{\infty} Z^1_{0m}\, e^{-j\beta md} + Z^i_L\right)\left(\sum_{m=-\infty}^{\infty} Z'^1_{0m}\, e^{-j\beta md} + Z^o_L\right) - \left(\sum_{m=-\infty}^{\infty} \hat{Z}^1_{0m}\, e^{-j\beta md}\right)^2$$

$$= 0 \tag{6.4}$$

If this condition is fulfilled, the resulting ratio of the outer to the inner current is given by

$$\frac{I^o_0}{I^i_0} = -\frac{\sum_{m=-\infty}^{\infty} \hat{Z}^1_{0m}\, e^{-j\beta md}}{\left(\sum_{m=-\infty}^{\infty} Z'^1_{0m}\, e^{-j\beta md} + Z^o_L\right)} \tag{6.5}$$

In the above equations Z^1_{0m}, Z'^1_{0m} and $\hat{Z}^1_{0m}$ are defined as

$$Z^1_{0m} = j\frac{\pi\eta_0}{2}\left(kb_1\frac{K^2_{0m} + K^0_{0m}}{2} - \frac{1}{kb_1}K^1_{0m}\right) \tag{6.6}$$

$$Z'^1_{0m} = j\frac{\pi\eta_0}{2}\left(kb_2\frac{K'^2_{0m} + K'^0_{0m}}{2} - \frac{1}{kb_2}K'^1_{0m}\right) \tag{6.7}$$

$$\hat{Z}^1_{0m} = j\frac{\pi\eta_0}{2}\left(kb_1\frac{\hat{K}^2_{0m} + \hat{K}^0_{0m}}{2} - \frac{1}{kb_2}\hat{K}^1_{0m}\right) \tag{6.8}$$

where

$$K^n_{0m} = \frac{1}{2\pi}\int_0^{2\pi} \frac{\exp[-jkb_1 R_{0m}(\phi) + jn\phi]}{R_{0m}(\phi)}\, d\phi \quad , \quad m > 0$$

with

$$R_{0m}(\phi) = \frac{|m|d}{b_1}\left[1 + \left(\frac{2b_1}{md}\right)^2 \sin^2\phi/2\right]^{\frac{1}{2}} \tag{6.9}$$

$$\hat{K}^n_{0m} = \frac{1}{2\pi}\int_0^{2\pi} \frac{\exp[-jkb_2 \hat{R}_{0m}(\phi) + jn\phi]}{\hat{R}_{0m}(\phi)}\, d\phi \tag{6.10}$$

$$\hat{R}_{0m}(\phi) = \frac{|m|d}{b_2}\left[1 + \left(\frac{b_1 - b_2}{md}\right)^2 + \frac{4b_1b_2}{(md)^2}\sin^2\phi/2\right]^{\frac{1}{2}} \tag{6.11}$$

$m > 0$

and K'^n_{0m} is the same as K^n_{0m} with b_1 and R_{0m} replaced

by b_2 and R'_{0m} where

$$R'_{0m}(\phi) = \frac{|m|d}{b_2}\left[1 + \left(\frac{2b_2}{md}\right)^2 \sin^2 \phi/2\right]^{\frac{1}{2}}, \quad m > 0 \qquad (6.12)$$

R_{00}, K^n_{00} and K'^n_{00} are as defined in (1.7) and (1.8).

Equation (6.4) is a transcendental equation. In order to solve this equation, we will try to find a solution for the three infinite summations in (6.4). This is done in the next section.

6.3 Evaluation of the Infinite Series in Equation (6.4)

A close look at the infinite series involving Z^1_{0m} and Z'^1_{0m} reveals that they are similar to the infinite series given in equation (2.4) of Chapter II. Therefore, their solution can be found using an identical procedure to that presented in Chapter II. The remaining infinite series involves $\hat{Z}^1_{0m}$ and will be stated here. The infinite summation can be subdivided into three summations in the following way

$$\sum_{m=-\infty}^{\infty} \hat{Z}^1_{0m} e^{-j\beta md} = \left[\sum_{-\infty}^{-(M'+1)} + \sum_{-M'}^{M'} + \sum_{M'+1}^{\infty}\right] \hat{Z}^1_{0m} e^{-j\beta md} \qquad (6.13)$$

since $b_1 b_2 > b_1^2$

and $(b_1 - b_2)^2 < b_1^2$ for $b_2/b_1 < 2$

Therefore, $4b_1b_2 >> (b_1 - b_2)^2$ and for sufficiently large m one can neglect the term $\left(\frac{b_1 - b_2}{md}\right)^2$ in equation (6.11). Thus, the new form of $\hat{K}^n_{0m}$ becomes

$$\hat{K}^n_{0m} \simeq \frac{b_2}{d} e^{-jk|m|d}/|m| \frac{1}{\pi} \int_0^{\pi} e^{jx\cos\phi} \cos n\phi \, d\phi ,$$

$$\text{for } |m|d/b_2 >> 1 \qquad (6.14)$$

where $x = kb_1b_2/|m|d$. The above integral is again related to the Sommerfeld representation of the Bessel function. Thus,

$$\hat{K}^n_{0m} = j^n \frac{b_2}{d} e^{-jk|m|d}/|m| \; J_n(x) \tag{6.15}$$

Therefore, equation (6.8) modifies to the form

$$\hat{Z}^1_{0m} = \frac{j\pi\eta_o}{2} \frac{b_2}{d} \left[kb_1 \frac{J_0(X) - J_2(X)}{2} - \frac{j}{kb_2} J_1(X)\right] e^{-jk|m|d}/|m| \tag{6.16}$$

substituting (6.16) in (6.13) gives relations similar to those obtained for equation (2.4) in Chapter II. Therefore, in general, the solution of (6.4) is closely related to the solution of an isolated array. The numerical solution of (6.4) gives the propagation constant β from which the phase velocity of the launched wave can be obtained. This is done in the following section.

6.4 The Numerical Results for the Phase Velocity

A computer program was developed to calculate the phase constant β from the transcendental equation (6.4). The method which is used to calculate the phase constant β is the central point method which was explained in Chapter II. Again, the range of variation of β is limited by

$$kd \leq \beta d \leq \pi$$

as was discussed previously. Figure (6-2) compares the numerical results of equation (6.4) for an unloaded array with those obtained experimentally [70]. A good agreement between these results can be observed in both passbands. The second

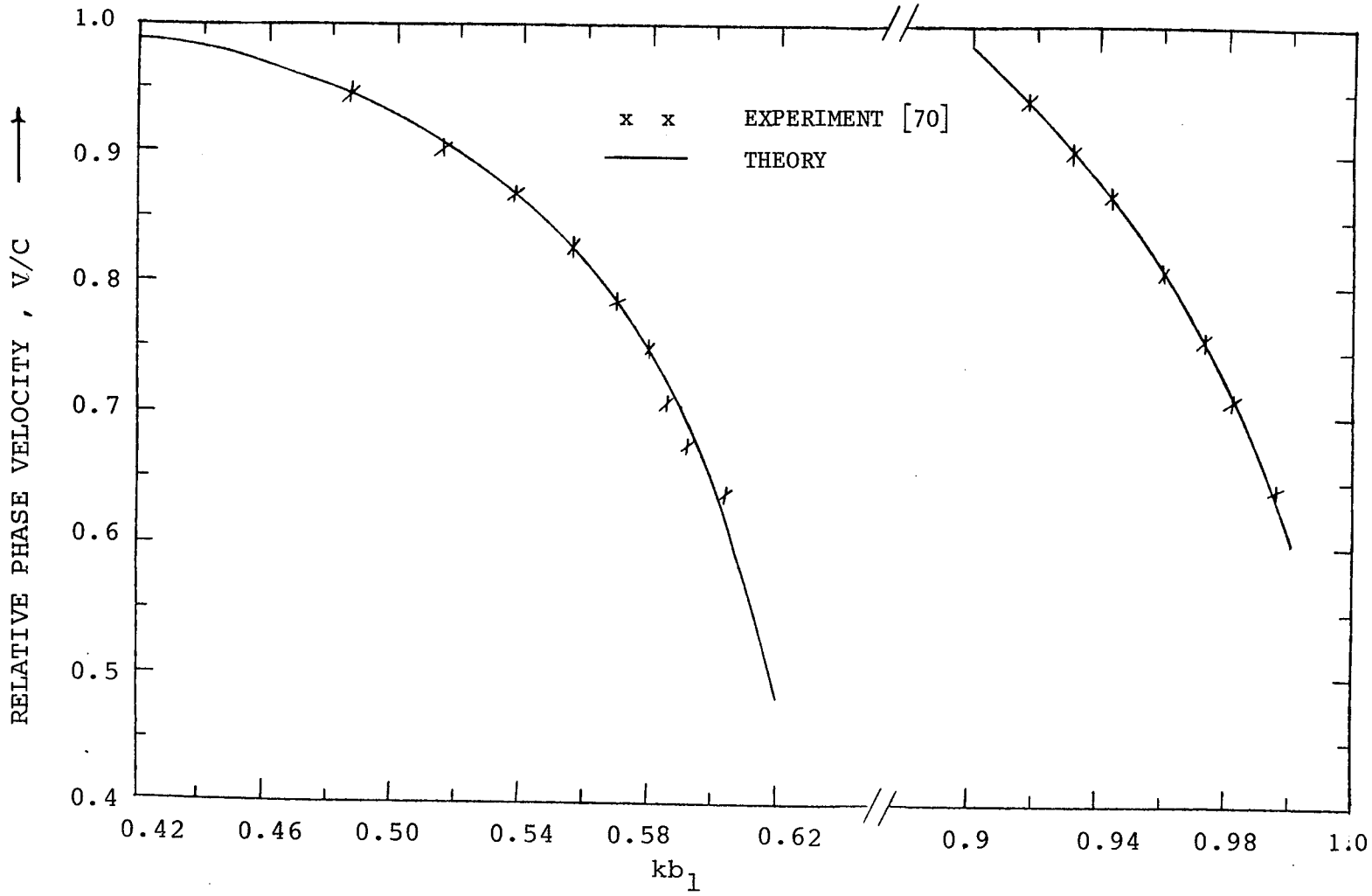

Fig. 6-2: Comparison of the numerical results against that of experiment. $b_2/b_1 = 1.62$, $d/b_1 = 0.92$, $a/b_1 = 0.38$

passband, however, is much smaller than the first one. To improve this passband we assume that the inner loops are loaded reactively and the outer sub-array is unloaded. Figure (6.3) shows the results for such a loaded array. It is interesting to see that loading the inner loops has a negligible effect on the phase velocity within the first passband, but it has a large effect on the second passband. A capacitive loading of the inner elements shifts the center frequency of the second passband upward which results in an improved isolation between the two passbands. An inductive loading of the small sub-array shifts the center frequency of the second passband to lower frequencies and therefore, reduces the separation between the passbands. A capacitive loading of the inner elements also increases the phase velocity and for a given phase velocity extends the range of the operating frequency. Thus, from the previous discussion given in Chapter II we can conclude that the gain of the finite array must also behave in a similar manner. We will not, therefore, attempt to discuss further the effect of the loading on finite arrays. Instead, however, we will consider the excitation problem of concentric loop Yagi arrays.

6.5 The Excitation Problem

When a finite Yagi array of concentric loops is used as an aerial, a major question which arises is the method of excitation can be used to launch efficiently, the travelling waves, on both sub-arrays in their respective passbands. This section studies the excitation problem and an attempt is

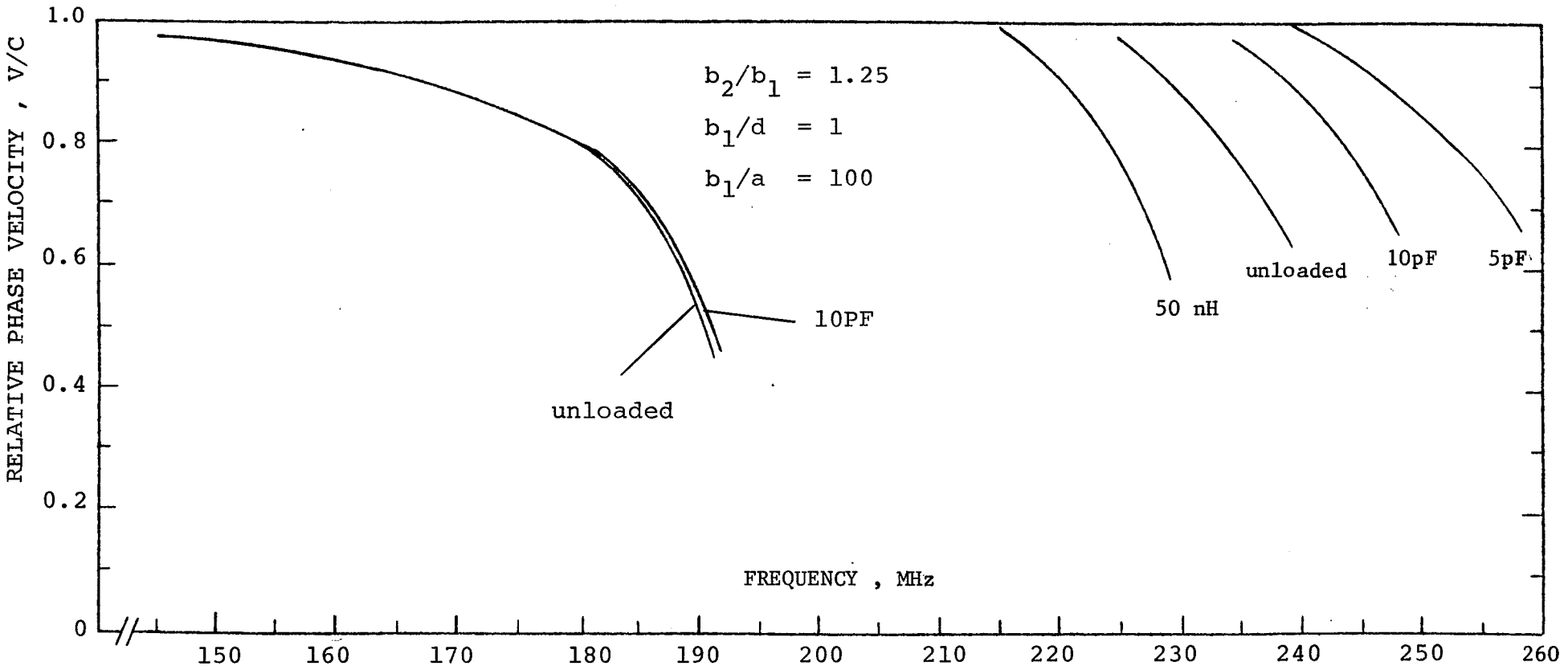

Fig. 6-3: Variation of the relative phase velocity of an infinite concentric loop array with frequency for various loading of inner array. $b_2/b_1 = 1.25$, $d/b_1 = 1$, $b_1/a = 100$, $b_1 = 20$ cm

made to find the best possible answer. A computer program was developed to investigate the characteristics of finite concentric loop arrays. The program is general and can be used for any number of loops in the array with any loop size and loop spacing or outer to inner loop ratio. In the program, the odd and even numbers are related to the inner and the outer loops, respectively. Initially, an 18-element array consisting of nine uniform inner and outer loops is considered. It is called uniform since there is no change in size of the inner or the outer loops along the array. Furthermore, they are positioned uniformly along the z-axis. Three different methods of excitation are considered; only the outer sub-array is excited, both sub-arrays are excited, or only the inner one is excited. As in conventional Yagi arrays, the first cell (loop No. 1 and 2) is considered as the reflector for the array. The real parts of the input admittances resulting from these three different methods of excitation are shown in figures (6-4) and (6-5). Figure (6-4) shows the real parts of the input admittances of the arrays when both inner (kb_3) and outer (kb_4) loops are excited. $Re(Y_4)$, the real part of the input admittance looking into the port connected to the outer loop kb_4, has a maximum in the first passband and becomes negative at $f = 200$ MHz and remains negative within the second passband. On the other hand, $Re(Y_3)$ is very small [relative to $Re(Y_4)$] and positive at the lower edge of the first passband and becomes negative within the rest of the first passband and the stopband. It

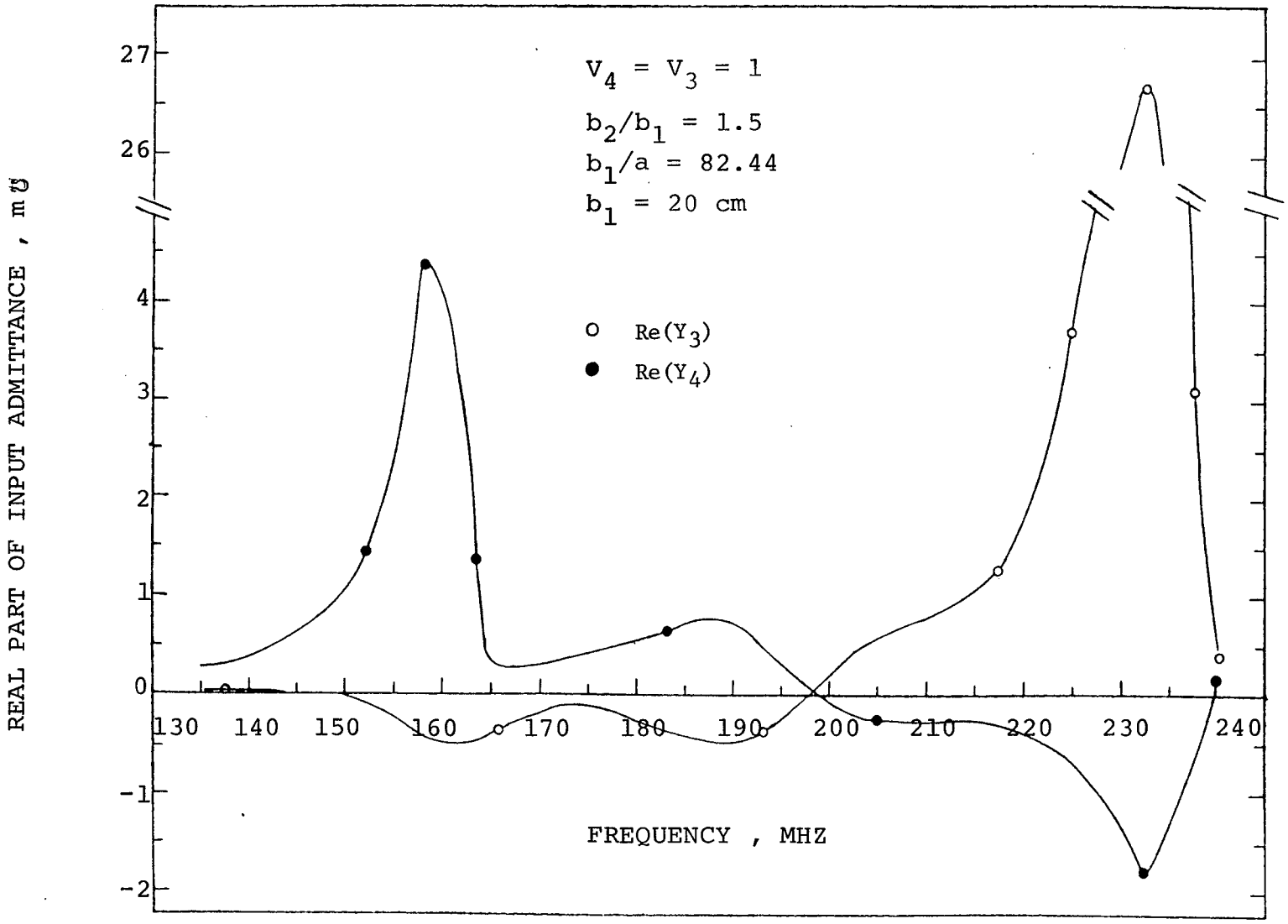

Fig. 6-4: Variation of the conductance of an 18-element Yagi array of concentric loops (9 cells) with frequency. Both inner (kb_3) and outer (kb_4) are excited. $b_2/b_1 = 1.5$, $b_1 = b_3 = \ldots\ldots b_{17} = 20$ cm, $d = 20$ cm, $b_1/a = 82.44$

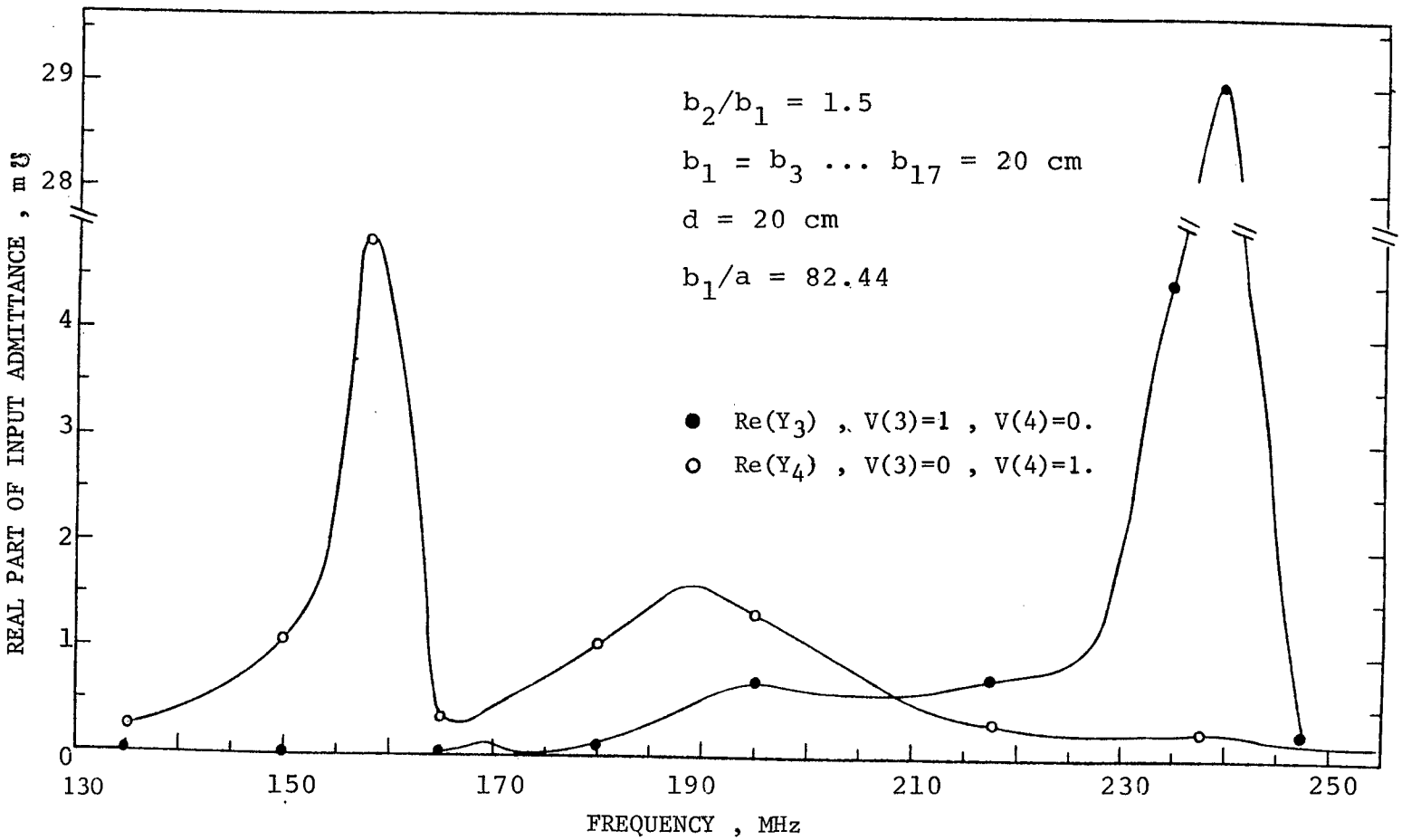

Fig. 6-5: Variation of the conductance of an 18-element Yagi array of concentric loops (9 cells) with frequency when the inner loop (kb_3) or the outer loop (kb_4) is excited. The geometry is the same as in figure (6-4)

becomes positive at f = 190 MHz and has a relatively high maximum at f = 230 MHz. These results indicate that within the first passband the outer loop is contributing to the radiation, but the inner loop absorbs the energy and does not radiate. On the other hand, the outer loop absorbs energy within the second passband and the inner loop radiates energy. Figure (6-5) shows the real part of the input admittance of the same array when either the inner or the outer loop is excited. When only the outer loop (kb_4) is excited, the real part of the input admittance has a maximum in the first passband and then decreases rapidly. It achieves a second maximum in the stopband and then remains almost constant within the second passband. When only the inner loop (kb_3) is excited the real part of the input admittance is so small within the first passband that it is difficult to show the results in the figure. It increases with increasing frequency and has a relatively high maximum in the second passband.

Figure (6-6) shows the directive gain of the array with three different methods of excitation. It is seen that the behaviour of the gain in the first passband when both sub-arrays are excited is similar to the behaviour when only the outer loop (kb_4) is excited. When only the inner loop is excited, the array has a poor directive gain in the positive z-direction and also a substantial portion of the first passband. All three methods of excitation have almost similar gain behaviour in the second passband. Figure (6-6) shows that the directive gain of the array when only the inner loop is

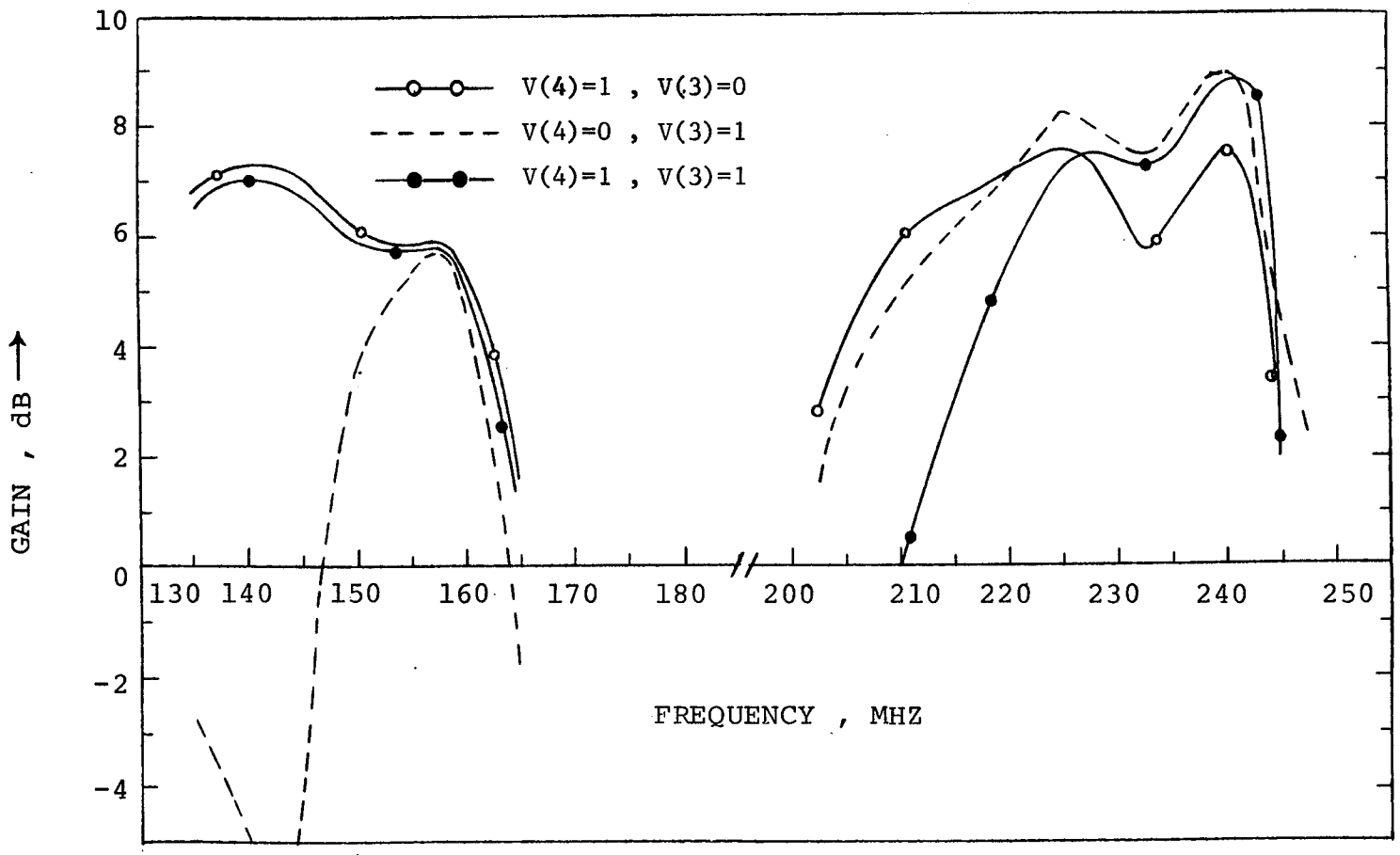

Fig. 6-6: Behaviour of the directive gain of an 18-element Yagi array of concentric loops (9 cells) with frequency for three different methods of excitation. The geometry is the same as in figure (6-4).

excited, is comparable with those of the other two cases within 155 - 160 MHz. However, figure (6-5) indicates that its radiation in this range is negligible.

From the results obtained it is clear that from a practical point of view, the excitation of only the outer sub-array seems to give the most superior gain and the input impedance behaviour. However, in an earlier investigation we have shown that [71] both the gain and the bandwidth of an isolated circular-loop Yagi arrays can be optimized by increasing the size of the reflector and the exciter (Appendix VI-A). A concentric loop Yagi array operates in a similar manner and the same conclusion must apply for this antenna as well. Thus, the reflector and the exciter size can be utilized to further improve the gain and bandwidth of concentric loop Yagi arrays. The far field radiation of the array is studied in the next section.

6.6 The Far Field Radiation Pattern

The H-plane far field radiation of an 18-element uniform Yagi array of concentric loops (9 cells) is shown in figure (6.7). The array is operating at $f = 146$ MHz which is in the first passband and, therefore, the outer loops are the major contributer to the far field radiation. Figure (6.7) compares the total radiated far field with the radiation from the inner elements. It is seen that the contribution of the inner loops to the total far field is very small. Figure (6.8) compares the H-plane radiation fields of parasitic outer elements with that of inner loops of the above

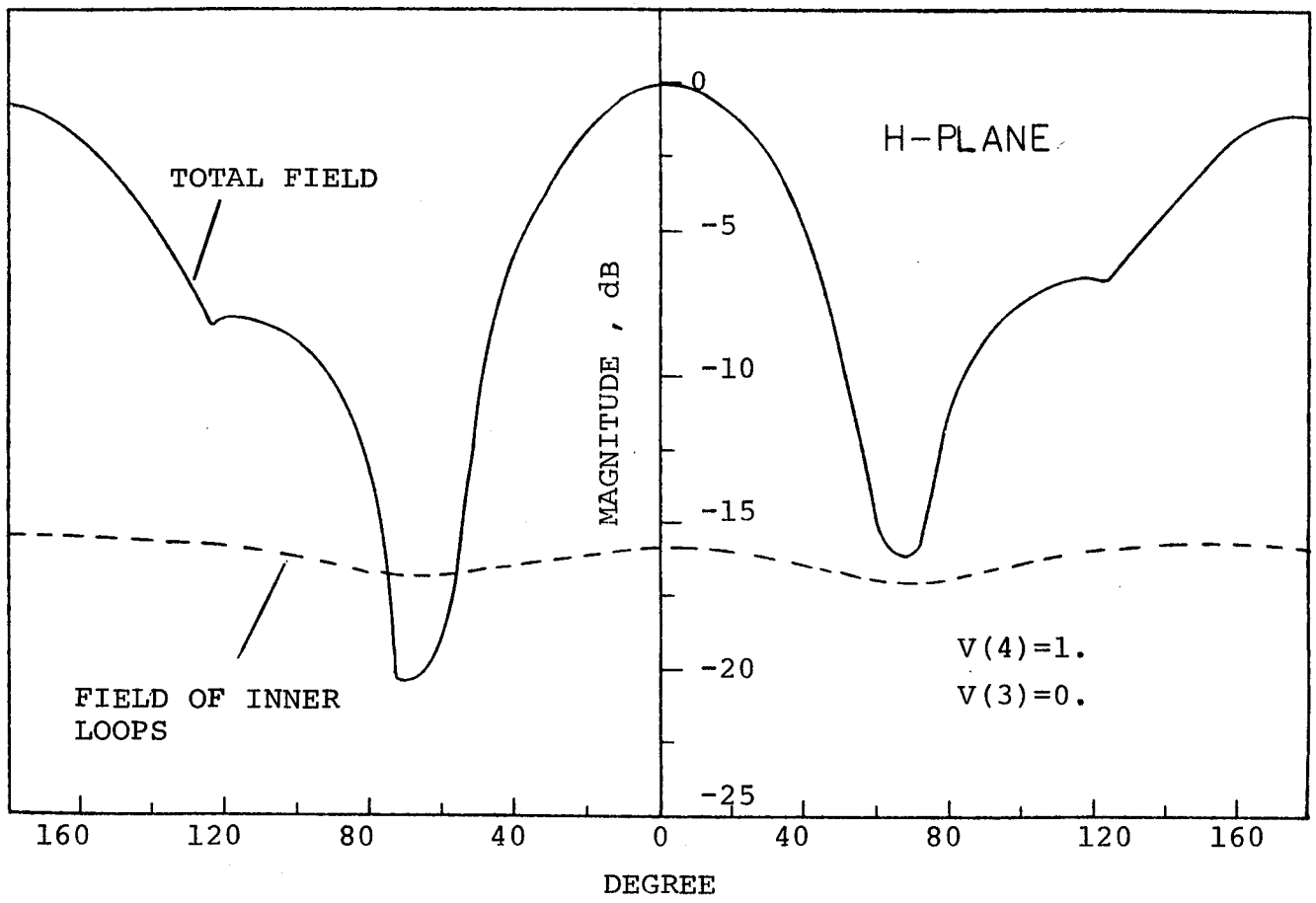

Fig. 6-7: Comparison of the total H-plane far field radiation of an 18-element Yagi array of concentric loops (9 cells) against that of the inner elements at f = 145 MHz. The geometry is the same as in figure (6-4) and only the outer loop (kb_4) is excited. Only kb_4 is excited.

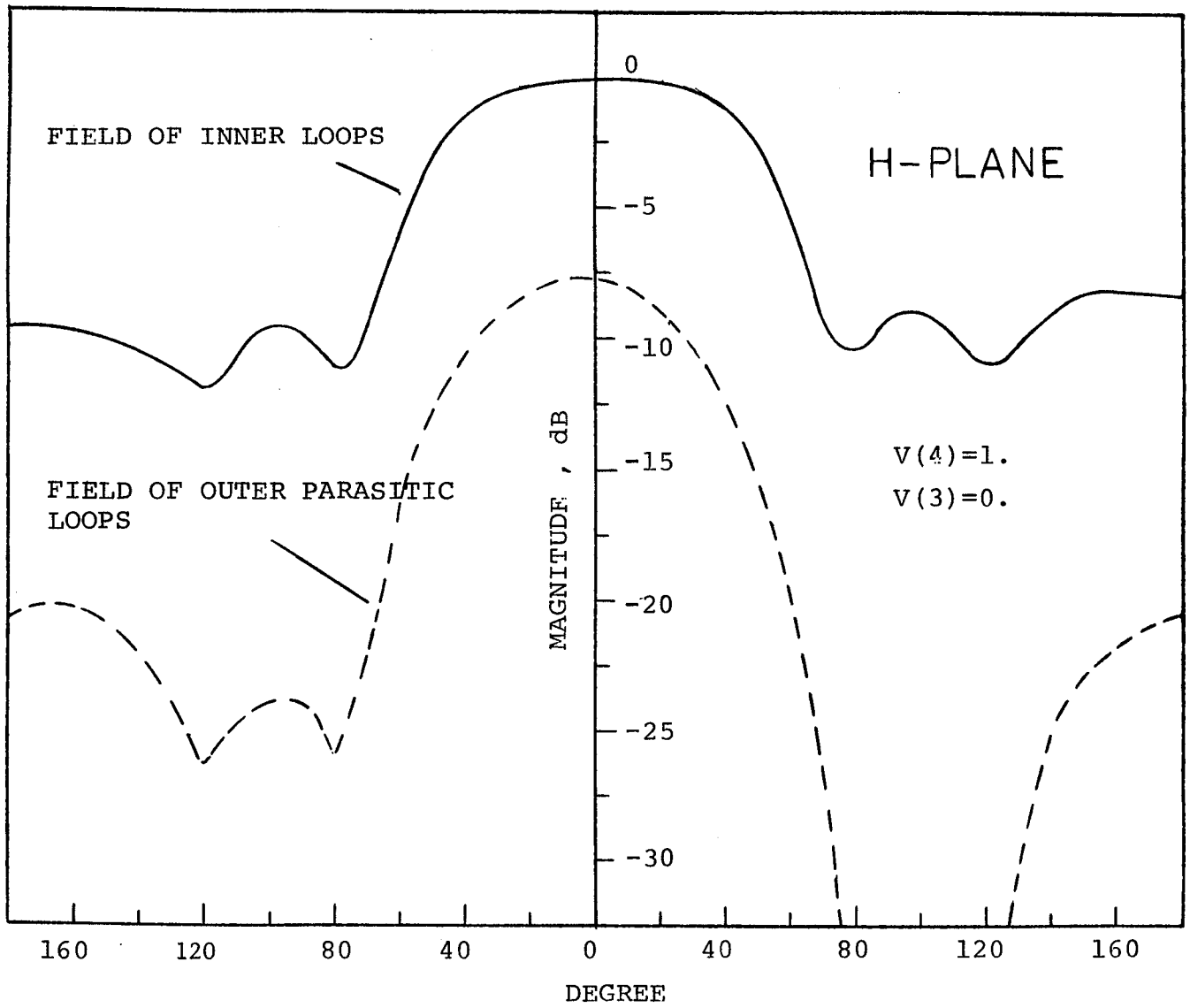

Fig. 6-8: Comparison of the H-plane far field radiation of the inner loops of an 18-element Yagi array of concentric loops (9 cells) with that of the outer parasitic loops at f = 225 MHz. The geometry is the same as in figure (6-4) and only the outer loop (kb_4) is excited

array at $f = 225$ MHz which is in the second passband. It is interesting to note that the radiation from the parasitic outer elements is not as negligible as the far field radiation from the inner elements shown in figure (6.7). From these figures one may conclude that in the first passband the current distributions on the outer loops must be significantly larger than the currents on the inner elements. This relationship reverses in the second passband where the currents on the inner loops become large but evidently by a smaller factor. To examine these current distributions in a more detailed manner, figures (6.9) and (6.10) are included which show the magnitude of the currents on each element at $\phi = 0$ and for $f = 145$ MHz and $f = 225$ MHz, respectively. Figure (6.9) shows that the currents on the outer loops are about ten times larger than the currents on the inner loops, when the array is operating in the first passband. In the second passband, the currents on the inner loops are only about three times larger than those of the outer elements. These results justify the radiated far field given in figures (6.7) and (6.8).

6.7 Summary

Loaded Yagi arrays of concentric loops were studied in this chapter. The circuit theory method developed in Chapter II was combined with the technique given for the co-planar array of Chapter IV to investigate the phase velocity on an infinite loaded concentric loop array. It was shown that by a proper selection of the reactive loading, the passbands and the stopband can be controlled. The computation revealed

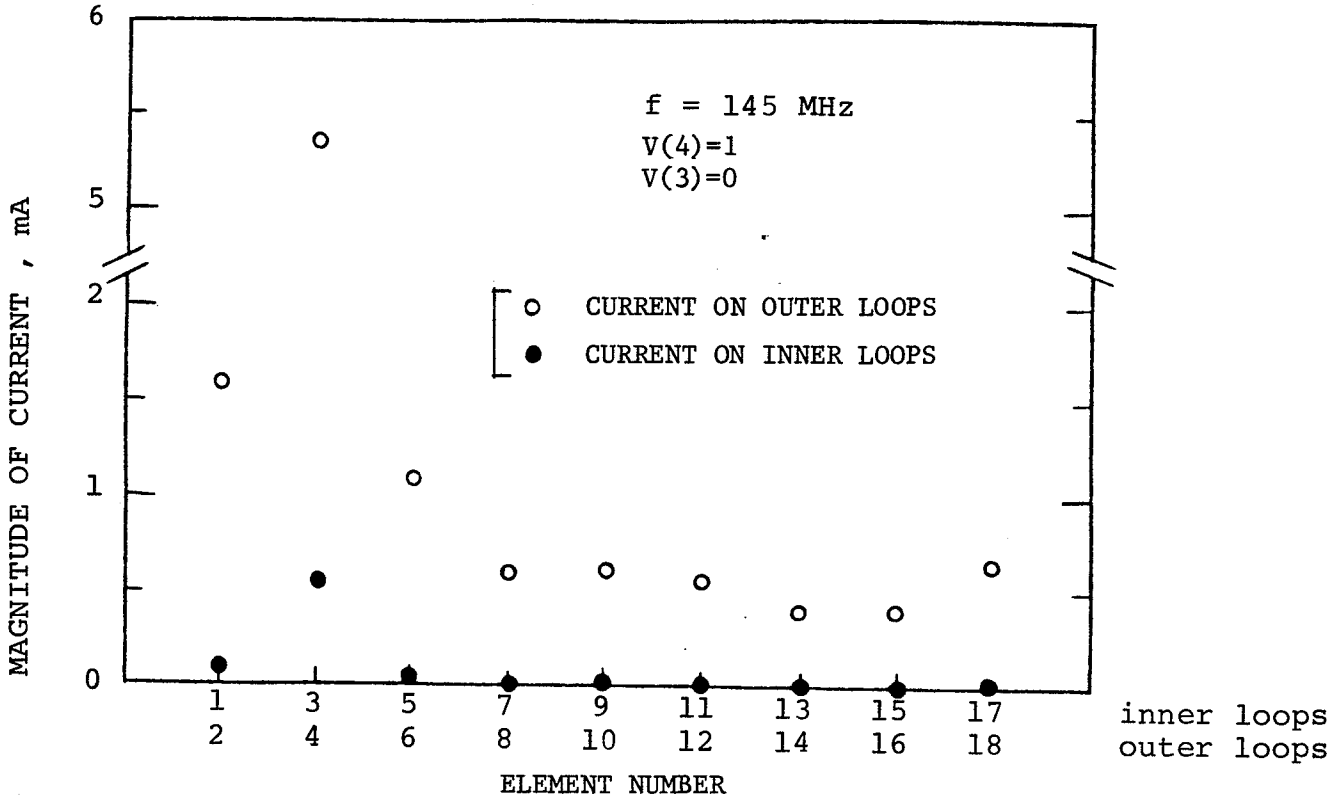

Fig. 6-9: Comparison of the magnitude of the current at $\phi = 0$ of the outer loops with that of the inner loops at f = 145 MHz. The geometry is the same as in figure (6-4)

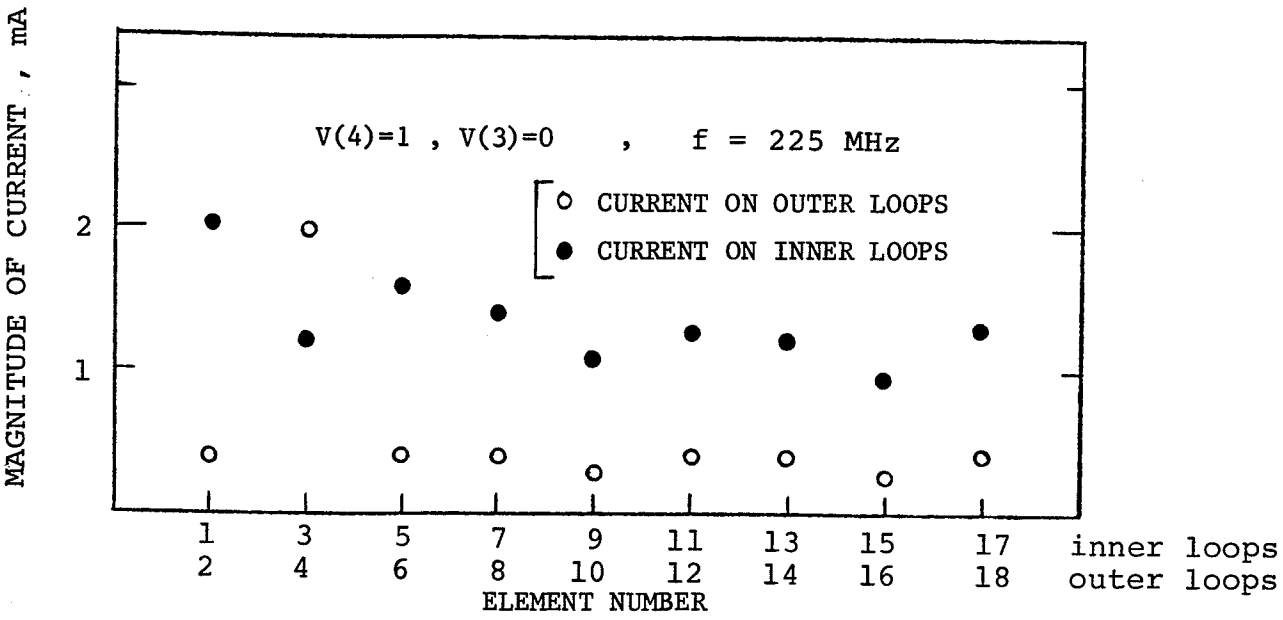

Fig. 6-10: Comparison of the magnitude of the current at $\phi = 0$ of the outer loops with that of the inner loops. The geometry is the same as in figure (6-4)

that a capacitive loading of the inner array increases both the separation of the passbands and the bandwidth of the second passband. The effect of the above loading on the first passband was, however, found to be negligible. This relative independence of the first passband from loading the inner loops is due to the fact that the mutual coupling between the inner and the outer arrays is rather weak.

The excitation of finite Yagi arrays of concentric loops was also studied in this chapter. Three different methods of excitation were considered; only the outer sub-array was excited, both sub-arrays were excited or, only the inner one was excited. It was found that generally the gain and the input impedance of the array depend strongly on the method of excitation from a practical point of view, the excitation of only the outer array seems to have the most superior gain and input impedance characteristics.

The far field radiation of a finite Yagi array of concentric loops was also investigated. It was shown that the radiation from the inner array is negligible when the array is operating in the first passband. In the second passband the radiation from the outer array was found to be small.

CHAPTER VII

DISCUSSION AND CONCLUSION

The problem of loading the circular loop array with lumped or distributed impedances was studied in this thesis. The impedance loading of elements was used to modify the current distributions on the array and consequently, its bandwidth and the radiation characteristics. Initially, the investigation was focused on an infinitely long array with loaded coaxial circular loops of equal size. The problem was then extended to two concentric arrays of loaded loops which operate at two pass-bands which are separated with a stop-band and controllable with the impedance loading. The thesis also presented a new type of antenna consisting of a coaxial planar loop array. Its properties were investigated and the application of this design to backfire antennas was discussed. The main objectives and the results which are obtained in the course of this investigation are summarized in the following paragraphs.

The travelling wave idea was applied on an infinitely long loaded circular loop array in order to obtain a relationship for the propagation constant along the structure. The analysis was based on the so-called "circuit theory" method and gave the dispersion relation in terms of the mutual impedances between the reference and the other elements in the array. In addition, Flouquet's theorem was used

to account for the periodicity of the structure. It was shown that capacitive loading increases the operating frequency range, for a given phase velocity of the travelling wave along the structure, and consequently, increases the bandwidth of the array. An inductive loading of the elements was found to have the opposite effect.

Similar results were also obtained for loaded arrays of two concentric loops, which operated in two pass-bands separated with a stop-band. It was found that a capacitive loading of the inner array increases both the separation of the pass-bands and the bandwidth of the second pass-band. The effect of the above loading on the first pass-band was, however, found to be negligible. The excitation of a finite array was also investigated. For two concentric loops the choice of the outer loop as the exciter was found to give the most superior gain and input impedance characteristics.

The question of a suitable kind of load for the reflector of a finite Yagi array of loops was investigated in detail. It was shown that the loading of the reflector has negligible effects on the high frequency cut off of the array, but affects the low frequency cut off significantly. An inductive loading of the reflector reduces the low frequency cut off and consequently, further increases the array bandwidth.

As an example of multiple loading, the case of the doubly loaded array was considered. The investigation was made possible by an application of the principle of super-

position. The study revealed that for a relatively smooth variation of the input admittance in a Yagi array, the exciter may be loaded resistively. Thus, to improve the overall characteristics of a Yagi loop array, it was recommended that the directors and the reflector be loaded by capacitive and inductive loads, respectively. The exciter, however, must be loaded resistively in order to reduce the variation of the input admittance with frequency.

Coaxial circular loop arrays with distributed impedance loading was also analyzed by a simple extension of the Fourier series solution for the perfectly conducting loops. It was shown that, in general, a broadband characteristic can be obtained by a distributed impedance loading. The constant resistive loading was studied in a more detailed manner since it can be fabricated readily. The introduction of a dissipative load resulted in a decrease of the efficiency, but it improved the broadband characteristics of the antenna.

The thesis has also dealt with the coaxial planar loop arrays and their application to backfire antennas. First, a general method was developed which enables one to study compact coaxial loop arrays and planar antennas. The technique was then used to investigate the radiation characteristics of planar arrays and backfire antennas constructed entirely with loops. The comparison between this type of backfire antenna and the conventional one with a solid reflector revealed that the optimum size of the reflector is approximately the same for both kinds of reflectors. In the

case of a backfire antenna with a peripheral rim, the length of the rim at optimum gain was also found to be about the same for both kinds of reflectors. However, the optimum gain of the solid reflector was about 1dB larger than that of the loop reflector. The investigation showed that as few as 6 loops are sufficient to construct the optimum size of the reflectors and almost the same number of loops are required to form the optimum peripheral rim. Not only does this new structure for the backfire antenna reduces the weight, windage, and obstruction of view which accompanies solid reflectors, but it also lends itself to exact analytical investigation.

7.1 Suggestions for Future Research

During the course of the present work, several topics have arisen of which a few will be suggested here as a way of motivation for future research in the general area of the coaxial circular loop arrays. The first and the most relevant problem is to investigate the phase velocity of the surface wave along two (or more) coupled parallel arrays. Since the relationships between the surface wave and the beamwidth or the gain are already known [71], the design of coupled parallel Yagi arrays becomes possible if the phase constant of the surface wave is obtained. The information on the phase constant is also useful when the structure is employed as millimeter waveguides. In this case the array can carry more power or divide a given power among several branches. The analytical approach to obtain the solution for the phase constant of the surface wave along a coupled parallel arrays of

circular loops is similar to those of Chapter II and VI.

A second interesting problem would be the investigation of ohmic loss per unit length on a periodic structure of circular loops. This ohmic loss attenuates the signal along the structure and therefore, becomes a significant parameter of the array when it is used as a surface waveguide in applications in railway traffic control, railway obstacle detection and telecommunications. The analysis given in Chapter IV for continuous resistive loading may be helpful in calculation of this parameter.

An important index of performance for a Yagi loop array is the gain or directivity. However, a survey of available literature indicates that so far no attempt has been made to develop a method to maximize the gain of a Yagi loop array. In general, the gain of any array can be maximized by using a purely numerical search method. However, it is exceedingly laborious to consider all possible combinations of the various parameters involved in order to obtain a true maximum. In this area, recently, a perturbation technique was used to simplify the optimization process and was utilized to optimize the gain of a dipole Yagi array [72],[73]. A preliminary investigation by the author on the space perturbation of a loop Yagi array revealed that it is possible to apply the above technique to loop arrays as well. However, a more detailed examination of the subject is required, so that its usefulness and in particular the convergence of the method when applied to loop arrays can be fully understood.

Gain optimization by impedance loading, side lobe reduction of the far field radiation pattern of loop Yagi arrays by tapering the lumped load impedance from element to element, reduction of scattering cross-section of single or an array of loops by lumped or continuous impedance loading, and characteristics of log periodic arrays of circular loops are other unresolved problems, which may be studied in the future. This thesis has considered some of the most relevant problems and during the course of their investigation methods of solution and results have been introduced which may become useful for future investigations.

APPENDIX (III-A)

In this appendix it is shown that loading a Yagi antenna at $\phi=0$ or $\phi=\pi$ has similar effects on the antenna characteristics. For simplicity we assume that the current distribution is of the form

$$I_i(\phi) = I_i^n \cos n\phi_i \qquad (3A\text{-}1)$$

That is we are assuming that all other modes are negligible in comparison with the dominant nth mode [15] (for the end fire array discussed in this thesis we have used n=1 mode). Substituting (3A-1) into equation (3-18) yields, (for n=1)

$$I_i(\phi) = \sum_{j=1}^{N} [y_{ij}^1 V_j^0 + (-1)y_{ij}^1 V_j^\pi] \cos \phi \qquad (3A\text{-}2)$$

For a Yagi array with only the second element excited at $\phi=0$ and the rest of the elements loaded at $\phi=\pi$, we have

$$I_i(\phi) = y_{i2}^1 V_2 \cos\phi + \sum_{\substack{j=1 \\ \neq 2}}^{N} y_{ij}^1 Z_{Lj}^\pi I_j^\pi(\pi) \qquad (3A\text{-}3)$$

From equation (3A-1) we have $I_i(\pi)=-I_i^1$. Substitution of $I_i(\pi)$ in (3A-3) gives

$$I_i^1 + \sum_{\substack{j=1 \\ \neq 2}}^{N} y_{ij}^1 Z_{Lj}^\pi I_j^1 = y_{i2}^1 V_2^0, \quad (i=1,2,\ldots N) \qquad (3A\text{-}4)$$

The above system of inhomogeneous equations gives the current distribution on each loop loaded at $\phi=\pi$.

Now assume that the array is loaded at $\phi=0$, instead of at $\phi=\pi$, and loads are replaced by short circuits at $\phi=\pi$. Equation (3A-2), therefore, changes to

$$I_i(\phi) = y^1_{i2} V^0_2 - \sum_{\substack{j=1 \\ \neq 2}}^{N} y^1_{ij} \, Z^0_{Lj} \, I_j(0), \quad i=1,2,\ldots,N \qquad \text{(3A-5)}$$

substitution of $I_i(0) = I^1_i$ in (3A-5) gives

$$I^1_i + \sum_{\substack{j=1 \\ \neq 2}}^{N} y^1_{ij} \, Z^0_{Lj} \, I^1_j = y^1_{i2} \, V^0_2 \qquad \text{(3A-6)}$$

The system of inhomogeneous equation (3A-6) gives the current distribution on each loaded element at $\phi=0$. It is obvious that the results of (3A-5) and (3A-6) will be the same if $Z^{\pi}_{Li} = Z^0_{Li}$ which verifies the results obtained in Chapter III.

APPENDIX IV-A

In deriving equation (4.5) it was assumed that

$$G = Z_{Li} b_i \sum_{n=0}^{\infty} I_i^n \int_{-\pi}^{\pi} \cos n\phi_i \, e^{jm\phi_i} \, U_i(\phi_i) \, d\phi_i \simeq 0$$

The validity of this assumption is examined in this appendix. Since $U_i(\phi_i)$ is equal to zero everywhere except inside the driving gap, we find

$$G = \sum_{n=0}^{\infty} G_{n,m} = Z_{Li} b_i \sum_{n=0}^{\infty} I_i^n \int_{-\delta\phi_i/2}^{\delta\phi_i/2} \cos n\phi_i \cos m\phi_i \, d\phi_i \tag{4A.1}$$

which for $n = m = 0$ gives

$$G_{0,0} = Z_{Li} b_i \, \delta\phi_i \, I_i^0 \tag{4A.2}$$

and for $n \neq m \neq 0$

$$G_{n,m} = Z_{Li} b_i \, I_i^n \, \frac{\sin(n \pm m)\delta\phi_i/2}{(n \pm m)} \tag{4A.3}$$

For a small driving gap $\delta\phi_i$, the above relation can be approximated to

$$G_{n,m} \simeq Z_{Li} b_i \, \delta\phi_i \, I_i^n / 2$$

and for $n = 0$ and $m \neq 0$ equation (4A.1) yields (for small $\delta\phi_i$)

$$G_{0,m} = \frac{2}{m} Z_{Li} b_i \, I_i^0 \sin(m \, \delta\phi_i/2) \simeq Z_{Li} b_i \, I_i^0 \, \delta\phi_i$$

Similarly for $n \neq 0$ and $m = 0$ we have

$$G_{n,0} = \frac{2}{n} Z_{Li} b_i \, I_i^n \sin(n \, \delta\phi_i/2) \simeq Z_{Li} b_i \, I_i^n \, \delta\phi_i$$

Hence, for any n or m the results of the integration is $\delta\phi_i$. Since $\delta\phi_i$ is small, and for a practical magnitude of Z_{Li}, the contribution of (4A.1) to equation (4.3) can be neglected.

APPENDIX IV-B

Another method to determine the efficiency of an array of circular coaxial loops with continuous impedance loading is given in this appendix. The approach given in Chapter IV is general and is applicable to any antenna type. The following method is only applicable to those antennas for which the real part of the input admittance is precisely known. The Fourier series solution for the currents of circular loop arrays provides the exact value of the input impedance. Therefore, the following method can be applied to circular loop antennas.

The efficiency of an antenna can be defined as

$$\text{efficiency} = \frac{P_r}{P_D + P_r} = \frac{P_{in} - P_D}{P_{in}} \tag{4B.1}$$

where P_D is the dissipated power given in (4.21) and P_{in} is the input power calculated from

$$P_{in} = \frac{1}{2} \sum_{i=1}^{N} \text{Re}(Y_i) \, |V_i|^2 \tag{4B.2}$$

where Y_i is the input admittance of the i^{th} element. A substitution of (4.21) and (4B.2) into (4B.1) gives the efficiency in the form

$$\text{efficiency} = 1 - \frac{\sum_{i=1}^{N} [b_i R_{Li} \pi \sum_{n=0} \varepsilon_n I_i^n]}{\sum_{i=1}^{N} \text{Re}(Y_i) \, |V_i|^2} \tag{4B.3}$$

APPENDIX (VI-A)

In this appendix it is shown that the reflector and exciter size can be used to improve both the gain and the bandwidth of circular-loop Yagi arrays. Based on the integral equation method, explained in Chapter I, a computer program is prepared to study the array characteristics. The program is used to study Yagi loop arrays with 14 directors of equal size and spacing. Figure (6A-1) shows the variation of the array gain with frequency. Curve a is for an array that has no reflector and has an exciter equal in size to its directors. Curve b is for the same array, but with a reflector equal in size and spacing to the other array elements. It is interesting to see that the gains of these arrays have a similar behaviour as a function of frequency and the gain of the array without a reflector is about 1 dB more than the gain of the array with a reflector. This suggests that the reflector in the array of curve b is not placed at an optimum location. However, by modifying the reflector spacing and with further examination of the array gain, it was found that the gain of the array does not change significantly with the reflector spacing. This seems to validate the assumption of Shen and Raffoul [15] that the reflector has a negligible effect on the forward radiation. This assumption is, however, only valid as long as the reflector size is equal to that of other array elements.

The reflector, generally, reflects part of the primary field of the driven element with a phase change which depends

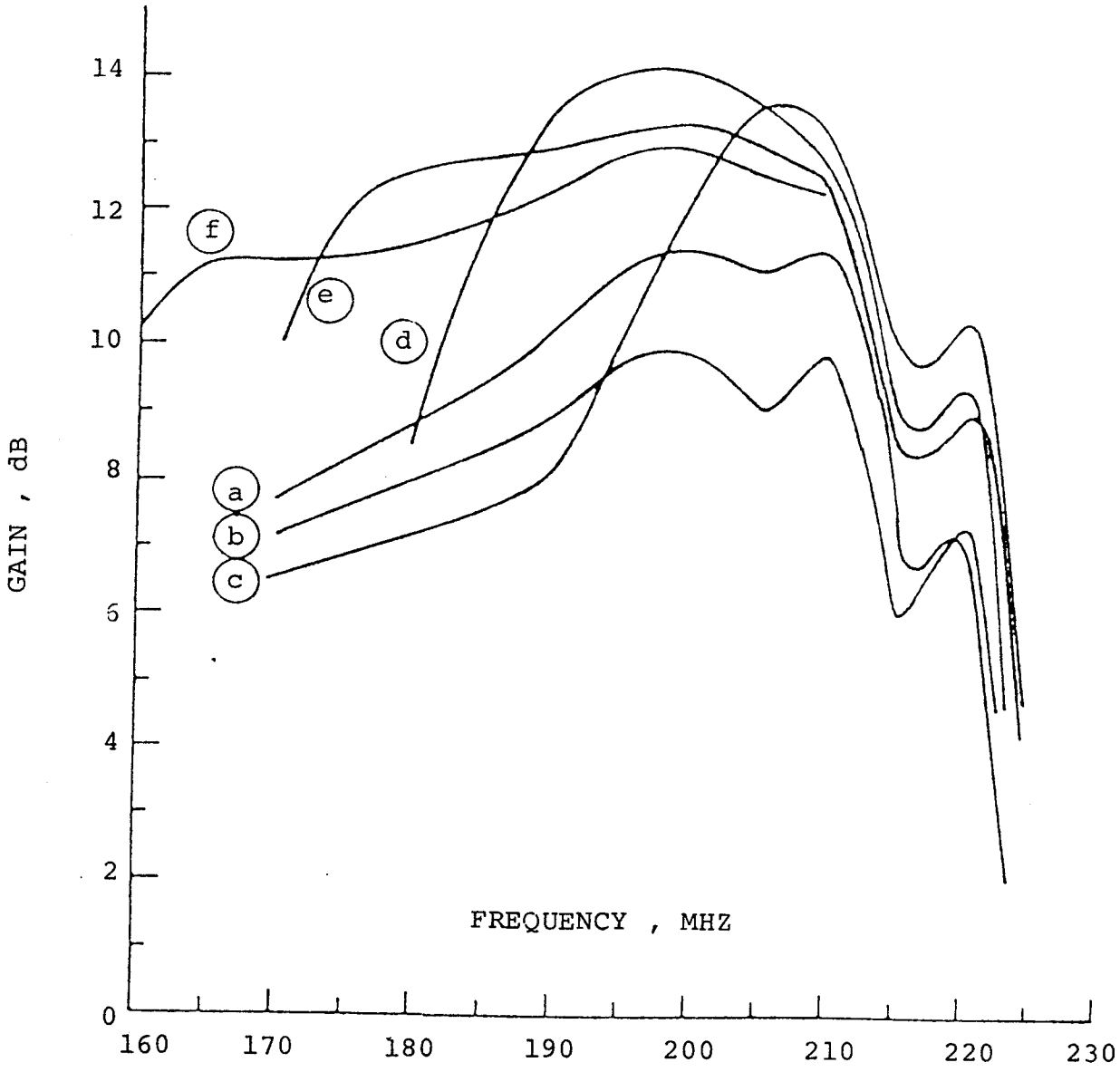

Fig. 6A-1: Variation of directive gain of 16-element array with frequency. Director radius = 21.45 cm, element spacing = 21.45 cm

on its size and spacing. Loop antennas with $kb \simeq 1$, where k and b are the propagation constant and the loop radius, exhibit inductive or capacitive impedances, depending whether kb is larger or smaller than unity. In addition, the array induction field also affects the phase distribution. One, therefore, expects that for reinforcement of the forward radiation field, the reflector should have a size larger than the directors. This expectation is verified by the remaining curves of figure 2. Curve c depicts the behaviour of the gain for the above arrays, when the reflector is larger than other elements by a factor of 1.1. It is seen that the array gain is increased by about 2.5 dB, but results in a corresponding bandwidth reduction. Using the above argument for the loop impedance one can expect that the array gain can also be improved by increasing the size of the exciter. This is verified in curve d, where the reflector and the exciter size are increased respectively to 1.2 and 1.1 times that of directors. Not only the gain is further increased, but also the bandwidth of the arrays is now comparable with those of curves a and b. It is interesting to note that the gain of this reflector and exciter combination is about 3 dB larger than that of the array without a reflector shown in curve a. This indicates that the reflector-exciter combination has almost optimum dimensions and a further increase of their size should reduce the array gain. Curves e and f illustrate this conclusion, as the array gain reduces continuously as the reflector size is increased. An additional interesting

result is the kink on all curves at about 215 MHz. A similar kink is also reported for dipole Yagi arrays [23] and is believed to be due to the same reason.

In summary, the gain and the bandwidth of any Yagi array can be improved by a proper selection of the reflector and exciter size. By an optimum reflector-exciter combination, which normally requires larger elements, as much as 3 dB improvement in the gain over that of an array without a reflector can be obtained. Since a concentric loop Yagi array operates in a similar manner, the reflector and the exciter size of this antenna can, therefore, be utilized to further improve its gain and bandwidth.

REFERENCES

[1]. ADACHI, S., MUSHIAKE, Y., "Theoretical formulation for circular loop antennas by integral equation method", Sci, Rep. Research Institutes of Tohoku University (RITU), B, 9, p. 9, 1957.

[2]. ADACHI, S., MUSHIAKE, "Studies of large circular loop antennas", Sci. Rep. Research Institutes of Tohoku University (RITU), B, 9, 2, pp. 79-103, 1957.

[3]. HALLEN, E., "Theoretical investigations into transmitting and receiving qualities of antennas", Nova Acta Regiac Soc. Sci. Upsal. (Series IV), Vol. 2, pp. 1-44, 1938.

[4]. STORER, J.E., "Impedance of thin-wire loop antennas", AIEE Trans. (Commun. Electron.), Vol. 75, pp. 606-619, Nov. 1956.

[5]. WU, T.T., "Theory of the thin circular loop antenna", J. Math. Phys., Vol. 3, pp. 1301-1304, Nov.-Dec. 1962.

[6]. KING, R.W.P., HARRISON, C.W., JR., TINGLEY, D.J., "The admittance of bare circular loop antennas in a dissipative medium", IEEE Trans. Antennas and Propagation, Vol. AP-12, pp. 434-438, July 1964.

[7]. INAGAKI, N., ITO, S., SEKIGUCHI, T., "A theory of a circular loop", J. Inst. Electron. Commun. Eng. In Japan, Vol. 53-B, pp. 135-142, Mar. 1970.

[8]. IIZUKA, K., KING, R.W.P., HARRISON, C.W., JR., "Self and mutual admittances of two identical circular loop antennas in a conducting medium and in air", IEEE Trans. Antennas and Propagation, Vol. AP-14, pp. 440-450, July 1966.

[9]. LINDSAY, J.E., JR., "A parasitic end-fire array of circular loop elements", IEEE Trans. on Antennas and Propagation (Commun.), Vol. AP-15, pp. 697-698, Sept. 1967.

[10]. APPEL-HANSEN, J., "The loop antenna with director arrays of loops and rods", IEEE Trans. Antennas and Propagation, Vol. AP-20, pp. 516-517, July 1972.

[11]. TAKATA, N., SEKIGUCHI, T., "Array antennas consisting of linear and loop elements", J. Inst. Electron. Commun. Eng. In Japan, Vol. 59-B, No. 5, pp. 61-67, 1976.

[12]. ITO, S., INAGAKI,N., SEKIGUCHI, R., "An investigation of the array of circular-loop antenna", IEEE Trans. Antennas and Propagation, Vol. AP-19, pp. 469-476, July 1971.

[13]. SHOAMANESH, A., SHAFAI, L., "Resonance effect in arrays of circular loop antennas", International Symposium on Antennas and Propagation, University of Illinois, AP-S, pp. 293-296, June 1975.

[14]. SHAFAI, L., SHOAMANESH, A., "An approximate method for investigation of large circular loop arrays", International Symposium on Large Engineering Systems, University of Manitoba, Aug. 1976.

[15]. SHEN, L.C., RAFFOUL, G.W., "Optimum design of Yagi arrays of loops", IEEE Trans. Antennas and Propagation, Vol. AP-22, pp. 829-830, Nov. 1974.

[16]. SHOAMANESH, A., SHAFAI, L., "Properties of coaxial loop arrays", IEEE Trans. Antennas and Propagation, Vol. AP-26, pp. 547-550, July 1978.

[17]. SHOAMANESH, A., "An investigation of coaxial Yagi loop arrays", Master Thesis, University of Manitoba, Oct. 1975.

[18]. SCHINDLER, J.K., MACK, R.B., BLACKSMITH, P., JR., "The control of electromagnetic scattering by impedance loading", Proc. IEEE, Vol. 53, pp. 993-1004, 1965.

[19]. ALTSHULER, E.E., "The travelling wave linear antenna", IEEE Trans., AP-9, pp. 324-329, 1961.

[20]. HARRISON, C.W., JR., "Monopole with inductive loading", IEEE Trans., AP-11, pp. 394-400, 1963.

[21]. WU, T.T., KING, R.W.P., "The cylindrical antenna with non-reflecting resistive loading", IEEE Trans., AP-13, pp. 369-373, 1965.

[22]. NYQUIST, D.P., CHEN, K.M., "The travelling-wave linear antenna with nondissipative loading", IEEE Trans., AP-16, pp. 121-131, 1968.

[23]. SETH, D.P.S., CHOW, Y.L., "On linear parasitic array of dipoles with reactive loading", IEEE Trans. AP-21, pp. 286-293, 1973.

[24]. IIZUKA, K., "The circular loop antenna multiloaded with positive and negative resistors", IEEE Trans. AP-13, pp. 7-20, 1965.

[25]. LIN, J.L., "The imperfectly conducting circular loop antennas", Rad. Sci., Vol. 8, pp. 251-257, March 1973.

[26]. SMITH, G.S., "A note on the imperfectly conducting circular-loop antenna", Rad. Sci., Vol. 9, pp. 35-41, January 1974.

[27]. SHEN, L.C., "Possible new applications of periodic linear arrays", IEEE Trans. on Antennas and Propagation, Vol. AP-18, pp. 698-699, September 1970.

[28]. SENGUPTA, D.L., "On the phase velocity of wave propagation along an infinite Yagi structure", IRE Trans., AP-7, pp. 234-239, 1959.

[29]. MAILLOUX, R.J., "Antenna and wave theories of infinite Yagi-Uda arrays", IEEE Trans., AP-13, pp. 499-506, 1965.

[30]. SHEFER, J., "Periodic cylinder arrays as transmission lines", IEEE Trans., MTT-11, pp. 55-61, 1963.

[31]. SMITH, R.A., "Aerials for metre and centimetre wavelengths", Cambridge University Press, Cambridge, England, pp. 150-151, 1950.

[32]. WATKINS, D.A., Topics in Electromagnetic Theory , New York, John Wiley & Sons, 1958.

[33]. SERRACCHIOLI, F., LEVIS, C.A., "The calculated phase velocity of long end-fire uniform dipole arrays", IRE Trans. on Antennas and Propagation, Vol. AP-7, pp. S424-S434, July 1959.

[34]. COLLIN, R.E., Field Theory of Guided Waves , McGraw-Hill Book Co., New York, pp. 579-580, 1960.

[35]. YOSHIMURA, K., TOKUMURA, S., "Calculated phase constant of coupled Yagi arrays", J. Inst. Electron. Commun. Eng. In Japan, Vol. 54-B, No. 10, pp. 135-142, October 1971.

[36]. SENGUPTA, D.L., "Travelling wave analysis of certain end-fire antennas", Ph.D. dissertation, University of Toronto, Canada, September 1958.

[37]. SHOAMANESH, A., SHAFAI, L., "Yagi arrays of coaxial circular loops with loaded elements", Archv. for Elect. and Comm., Vol. 33, pp. 244-249, June 1979.

[38]. SHOAMANESH, A., SHAFAI, L., "Multiply-Driven and loaded coaxial circular loop arrays", accepted for publication in IEEE Trans. Antennas and Propagations, Paper No. 2232-A.

[39]. SHOAMANESH, A., SHAFAI, L., "Broad-Band circular loop Yagi arrays", Antenna Applications Symposium, Allerton House, Monticello, Illinois, September 1978.

[40]. WU, T.T., KING, R.W.P., "The cylindrical antenna with non-reflecting resistive loading", IEEE Trans. Antennas and Propagation, Vol. AP-13, pp. 369-373, May 1965.

[41]. KING, R.W.P., WU, T.T., "The imperfectly conducting cylindrical transmitting antenna", IEEE Trans. Antennas and Propagation, Vol. AP-14, pp. 524-534, September 1966.

[42]. KING, R.W.P., HARRISON, C.W., JR., ARONSON, E.A., The imperfectly conducting cylindrical transmitting antenna: numerical results", IEEE Trans. Antenna and Propagation, Vol. AP-14, pp. 535-542, September 1966.

[43]. SHEN, L.C., WU, T.T., "Cylindrical antennas with tapered resistive loading", Radio Science, Vol. 2 (New Series), No. 2., pp. 191-201, February 1967.

[44]. KING, R.W.P., Fundamental Electromagnetic Theory , Second Edition, New York, Dover Publication, pp. 346-348, 1960.

[45]. SHOAMANESH, A., SHAFAI, L., "Design data for coaxial Yagi array of circular loops", Accepted for publication in IEEE Trans. Antennas and Propagation, Vol. AP-27, 1979.

[46]. RAO, B.L.J., FERRIS, J.E., ZIMMERMAN, W.E., "Broadband characteristics of cylindrical antennas with exponentially tapered capacitive loading", IEEE Trans. Antennas and Propagation, Vol. AP-17, pp. 145-151, March 1969.

[47]. KENNEDY, P.A., "Loop antenna measurements", IRE Trans. Antennas and Propagation, Vol. AP-4, pp. 610-618, October 1956.

[48]. BLOCH, A., MEDHURST, R.G., POOL, S.D., "A new approach to the design of Super-Directive aerial", Proc. Inst. Elec. Engrs. 100, Part III, pp. 303-314, 1953.

[49]. ABRAMOWITZ, M., STEGUN, I.A., Handbook of Mathematical Functions , (Applied Mathematics Series 55), Washington, D.C., NBC, pp. 589-615, 1964.

[50]. SHOAMANESH, A., SHAFAI, L., "An efficient method for investigation of compact coaxial loop-arrays", Antenna Applications Symposium, Allerton House, Monticello, Illinois, September 1978.

[51]. EHRENSPEK, H.W., "The backfire antenna, a new type of directional line source", Proc. IRE (correspondence), Vol. 48, pp. 109-110, Jan. 1960.

[52]. EHRENSPEK, H.W., "The backfire antenna: new results", Proc. IEEE (correspondence), Vol. 53, pp. 639-641, June 1965.

[53]. DOD, L.R., "Experimental measurements of the short backfire antenna", Tech. Rept. X-525-66-480, Goddard Space Flight Center, Green Belt, Md., Oct. 1966.

[54]. DOD, L.R., "Backfire Yagi antenna measurements", Tech. Rept. X-525-67-604, Goddard Space Flight Center, Green Belt, Md., Dec. 1967.

[55]. STORM, J.A., EHRENSPECK, H.W., "Backfire antennas for SHF, UHF and VHF bands", Research Rept. AFCRL-63-114, Electromagnetic Radiation Lab., Air Force Cambridge Research Lab., L.G. Hanscom Field, Mass., April 1963.

[56]. CHEN, K.M., NYQUIST, D.P., LIN, J.L., "Radiation fields of the short backfire antenna", IEEE Trans. Antennas and Propagation, AP-16, pp. 596-597, Sept. 1968.

[57]. EHRENSPECK, H.W., "The short-backfire antenna", Proc. IEE (correspondence), Vol. 53, pp. 1138-1140, Aug. 1965.

[58]. ZUCKER, F.J., "The backfire antenna: A qualitative approach to its design", Proc. IEEE (correspondence), Vol. 53, pp. 746-747, July 1965.

[59]. NIELSEN, E.D., PONTOPPIDAN, K., "Backfire antennas with dipole elements", IEEE Trans. Antennas and Propagation, Vol. AP-18, pp. 367-374, May 1970.

[60]. PATEL, D.C., "Directivity of short backfire antenna", Proc. IEE, Vol. 118, No. 11, pp. 1550-1552, Nov. 1971.

[61]. KING, R.W.P., SANDLER, S.S., "A modified backfire antenna", IEEE Trans. Antennas and Propagation Vol. AP-22, pp. 349-352, March 1974.

[62]. EHRENSPECK, H.W., "A new class of medium-size high efficiency reflector antennas", IEEE Trans. Antennas and Propagation, Vol. AP-22, pp. 329-332, March 1974.

[63]. ROJARAYANONT, B., SEKIGUCHI, T., "One-element loop antenna with finite reflector", J. Inst. Electron. Commun. Eng. In Japan, Vol. 59-B, pp. 68-74, May 1976.

[64]. KRAUS, J.D., Antennas , McGraw-Hill Book Co., New York, pp. 324-327, 1950.

[65]. KOSUGI, M., ET AL., "Design of an array of circular-loop antennas with optimum directivity", J. Inst. Electron. Commun. Eng. Japan, Vol.54-B,pp.67-76, May 1976

[66]. BOWMAN, J.J., ET AL., Electromagnetic and Acoustic Scattering by Simple Shapes , John Wiley & Sons, Inc. - New York, pp. 503-588, 1969.

[67]. RYDAHL, O., "Scattering from small bodies of revolution", M.Sc. Thesis, Electromagnetics Institute, Tech. University of Denmark, Lyngby, September 1974.

[68]. RYDAHL, O., "A numerical technique to predict scattering from bodies of revolution (User's Guide for the Computer Program)", Electromagnetics Institute, Report R150, Lyngby, Denmark, December 1975.

[69]. JASIK, H., Antenna Engineering Handbook , First Edition, McGraw-Hill Book Co., New York, 1961.

[70]. RAFFOUL, G.W., SHEN, L.C., "The Yagi array of concentric loops", Electronic Letters, Vol. 14, No. 6, pp. 168-170, March 1978.

[71]. SHOAMANESH, A., SHAFAI, L., "Effect of reflector and exciter size on the radiation of circular-loop Yagi arrays", Electronic Letters, Vol. 15, No. 4, pp. 103-105, February 1979.

[72]. CHENG, D.K., CHEN, C.A., "Optimum element spacing for Yagi-Uda arrays", IEEE Trans. Antennas and Propagation, Vol. AP-21, pp. 615-623, September 1973.

[73]. CHEN, C.A., CHENG, D.K., "Optimum element lengths for Yagi-Uda arrays", IEEE Trans. Antennas and Propagation, Vol. AP-23, pp. 8-15, January 1975.

[74] APPEL-HANSEN, J., "Directive loop array antenna", International Symposium on Antennas and Propagation, Sendai, Japan September 1971.